



UNIVERSIDADE FEDERAL DE SANTA CATARINA
CENTRO TECNOLÓGICO
PROGRAMA DE PÓS-GRADUAÇÃO EM ENGENHARIA MECÂNICA

JOB ANGEL LEDEZMA PÉREZ

**FORCE CONTROL ON HYDRAULIC ACTUATORS THROUGH ADDITIONAL
HYDRAULIC COMPLIANCE**

Florianópolis, SC

2019

Job Angel Ledezma Pérez

**FORCE CONTROL ON HYDRAULIC ACTUATORS THROUGH ADDITIONAL
HYDRAULIC COMPLIANCE**

Tese submetida ao Programa de Pós-Graduação em Engenharia Mecânica da Universidade Federal de Santa Catarina para a obtenção do título de Doutor em Engenharia Mecânica.

Orientador: Prof. D.Eng. Victor Juliano De Negri

Coorientador: D.Eng. Victor Barasuol.

Florianopolis, SC

2019

Ficha de identificação da obra elaborada pelo autor,
através do Programa de Geração Automática da Biblioteca Universitária da UFSC.

Ledezma, Job Angel

Force control on hydraulic actuators through additional hydraulic compliance / Job Angel Ledezma ; orientador, Victor Juliano De Negri, coorientador, Victor Barasuol, 2019.

147 p.

Tese (doutorado) - Universidade Federal de Santa Catarina, Centro Tecnológico, Programa de Pós-Graduação em Engenharia Mecânica, Florianópolis, 2018.

Inclui referências.

1. Engenharia Mecânica. 2. Controle de força em sistemas hidráulicos. 3. Impedância mecânica. 4. Flexibilidade hidráulica. I. De Negri, Victor Juliano. II. Barasuol, Victor. III. Universidade Federal de Santa Catarina. Programa de Pós-Graduação em Engenharia Mecânica. IV. Título.

Job Angel Ledezma Pérez

Force control on hydraulic actuators through additional hydraulic compliance

O presente trabalho em nível de doutorado foi avaliado e aprovado por banca examinadora composta pelos seguintes membros:

Prof. Eduardo André Perondi, Dr. Eng.
Universidade Federal do Rio Grande do Sul

Prof. Antônio Carlos Valdiero, Dr. Eng.
Universidade Regional do Noroeste do Estado do Rio Grande do Sul

Prof. Eugênio de Bona Castelan Neto, Dr. Eng.
Universidade Federal de Santa Catarina

Prof. Henrique Simas, Dr. Eng.
Universidade Federal de Santa Catarina

Prof. Jonny Carlos da Silva, Dr. Eng.
Universidade Federal de Santa Catarina

Certificamos que esta é a **versão original e final** do trabalho de conclusão que foi julgado adequado para obtenção do título de Doutor em Engenharia Mecânica.

┌

Prof. Jonny Carlos da Silva, Dr. Eng.

Coordenador do Programa de Pós-graduação em Engenharia Mecânica - POSMEC

┌

Prof. Victor Juliano De Negri, Dr. Eng.
Orientador

Florianópolis - SC, 18 de maio de 2018

Este trabalho vai dedicado à minha família, aos meus amigos e professores, sem cujo apoio não teria sido possível conseguir esta meta.

ACKNOWLEDGEMENTS

This thesis should not be possible without the support and encouragement of several people including my professors, friends, and family. I would like to express my gratitude to all of them and beg for the forgiveness of those whom I have possibly forgotten.

I would like to express my sincere gratitude to my advisor, Professor Victor Juliano De Negri, for his patience, great teachings, and friendship among all these years working at the lab. I really appreciate all of his effort to advise me, always trying to obtain the better of me. Thank you very much “Fessor”.

In the same way, I would like to thank to my co-advisor, Dr. Eng. Victor Barasuol. His sympathy, friendship, willingness to help and sharing knowledge were essential in my development. Thanks for that Vitorinho.

I would like to thank the Dynamic Legged Systems Lab at the Advanced Robotics Department of the Italian Institute of Technology (IIT), headed by Dr. Claudio Semini, for the opportunity to work with the HyQ team and the nice reception during my stay in Italy. Many thanks to all the colleagues who work in that powerful team. Many thanks Claudio and all of the HyQ team.

I have no words to express my gratitude to the lashipian guys. All of them, old and new generations, made the postgraduate life livelier and pleasantly bearable with their great camaraderie and friendship. You are awesome guys.

I need to give a special thanks to Ivan Mantovani, who help me a lot with the experimental tests, which results are shown in this thesis. Thank you very much Ivan.

I would also like to thanks very much to Vinicius Vígolo, Guilherme Pagatini and Rafael Goularte for their friendship, support, and willingness to help in the most critical time. Many thanks guys.

I would like to thank the Brazilian National Council for Scientific and Technological Development (in Portuguese: Conselho Nacional de Desenvolvimento Científico e Tecnológico - CNPq) for the financial support provided during my doctoral studies.

Finally, I would like to express my gratitude to my beloved family for their eternal support and love. This thesis is dedicated to all of them.

RESUMO

A força é o resultado da interação entre dois sistemas mecânicos. Toda vez que ocorre uma interação mecânica, o sistema de atuação troca energia com o meio externo. A dinâmica da interação mecânica pode ser caracterizada por uma impedância mecânica, a qual está intimamente relacionada à elasticidade nas transmissões mecânicas. O incremento da elasticidade é uma maneira de superar os problemas de estabilidade inerentes ao controle de força. Por outro lado, o controle de força é um dos assuntos mais estudados em várias áreas, especialmente na robótica, onde é usado para descrever a interação entre um robô e um entorno desconhecido. Um atuador com transmissão elástica terá uma impedância mecânica menor no porto de interação e, portanto, uma melhor capacidade de reduzir as forças de interação ao encontrar um objeto imprevisível, sendo uma boa opção para sistemas de controle de força. A maioria dos pesquisadores usa elementos mecanicamente flexíveis, como uma mola ou um amortecedor, em série com o atuador a fim de obter a flexibilidade necessária para as suas aplicações. A flexibilidade do sistema pode ser modificada de forma ativa ou passiva. A flexibilidade ativa é alcançada pelo controle realimentado baseado nas medições de força, e a flexibilidade passiva é alcançada inserindo componentes mecânicos flexíveis na transmissão do sistema de atuação. No entanto, nos sistemas de controle de força hidráulica, o comportamento flexível dos componentes mecânicos também pode ser ajustado usando apenas componentes hidráulicos equivalentes. Nesse sentido, o caso hidráulico tem algumas vantagens em comparação com o caso eletromecânico, pois nenhum componente adicional é inserido em série com o atuador. Sendo assim, nenhum espaço adicional é necessário, seja no eixo longitudinal, no caso de atuadores lineares, ou axial, no caso de atuadores rotativos, para incorporar um componente mecânico flexível, reduzindo o espaço necessário para o sistema de atuação. Esta tese visa a mostrar a possibilidade de garantir a flexibilidade requerida usando apenas componentes hidráulicos, fornecendo uma análise matemática que fundamenta a necessidade de adicionar componentes hidráulicos flexíveis e estabelecendo um procedimento de seleção e dimensionamento dos mesmos. Além disso, uma técnica de controle robusta no domínio da frequência é avaliada considerando os problemas intrínsecos do controle de força, tais como variações de parâmetros internos do sistema, incertezas de comportamento dinâmico do entorno, entre outros.

Palavras-chave: Controle de força em sistemas hidráulicos. Impedância mecânica. Flexibilidade hidráulica.

ABSTRACT

Force is the result of the interaction between two mechanical systems, and every time that a mechanical interaction occurs, the actuation system and the environment exchange power. Mechanical interaction dynamics may be characterized by mechanical impedance, which is intimately related with compliance in mechanical transmissions. Increasing the compliance is a way to overcome the inherent stability problems associated with force control. On the other hand, force control is one of the most studied topics in diverse areas, especially in robotics where it is used to describe the interaction between a robot and an unknown environment. An actuator with compliant transmission will have a lower mechanical impedance at the interaction port and, therefore, a better capability to reduce interaction forces when it encounters an unpredicted object, being a good choice for force control systems. Most of researchers use mechanical compliant elements in series with the actuator, such as springs or dampers, in order to achieve a required compliance for their applications. System compliance can be controlled or modified in active or passive ways. Active compliance is obtained by force-based feedback control, and passive compliance is typically obtained by introducing mechanical compliant components in the transmission of the actuation system. Nevertheless, in hydraulic force control systems, the compliant behavior of the mechanical components can also be obtained and shaped using only equivalent hydraulic components. In this sense, the hydraulic case has some advantages compared with the electromechanical case, because no additional components are inserted in series with the actuator. Therefore, no additional space is required, either in the longitudinal axis, in case of linear actuators, or axial, in case of rotational actuators, to incorporate a mechanical compliant component, reducing the space required for the actuation system. This thesis aims to show the possibility of ensuring a required compliance in hydraulic actuators using only hydraulic components, giving a mathematical background to substantiate the need for additional hydraulic compliant components, and establishing a procedure for selecting and sizing them. Additionally, a robust control technique in frequency-domain is evaluated considering the intrinsic force control problems, such as the variations of internal parameters of the system, uncertain dynamic behavior of the environment, among others.

Keywords: Force control in hydraulic systems. Mechanical impedance. Hydraulic compliance.

RESUMO EXPANDIDO

Introdução

O controle de força é um tópico de estudo bastante difundido na área de robótica e se iniciou entre as décadas de 1950 e 1960. Já no final de 1960 e início de 1970 foi implementado o primeiro controlador de força usando computadores. O principal objetivo dos computadores era resolver problemas de estabilidade, os quais surgiram ao mesmo tempo que as aplicações de controle de força. No decorrer do tempo, diversas técnicas e abordagens de controle de força foram estudadas e implementadas visando atingir melhores resultados de desempenho e estabilidade.

A força é o resultado da interação entre dois sistemas mecânicos e, conseqüentemente, toda vez que se produz uma interação mecânica entre o sistema de atuação e o entorno, existe uma troca de energia através de um ponto denominado porto de interação. Transmissões rígidas garantem bom desempenho nas tarefas de posicionamento devido a largura de banda que está intrinsecamente ligada à propriedade de rigidez. Por outro lado, transmissões flexíveis produzem um comportamento de tipo mola, podendo conduzir a problemas de estabilidade nos sistemas de posicionamento, pois o controlador de posição requer a aplicação de maiores esforços de controle a fim de garantir que se cumpram os requisitos de desempenho. Esta situação não acontece com o controle de força, onde componentes flexíveis são usados para limitar a taxa de variação da força aplicada sobre a carga. Com isto, garante-se a obtenção de esquemas de controle de força práticos e robustos. O uso de acoplamentos flexíveis, a fim de obter um certo grau de isolamento entre o sistema de atuação hidráulico e o movimento da carga ou o entorno, ajuda a manter a estabilidade no controle de força aplicado.

O fluido hidráulico presente nas câmaras de um cilindro possui um efeito similar ao de uma mola. Este efeito está diretamente relacionado com a transmissão hidráulica (rigidez) e poderia ser modificável acoplando componentes capacitivos hidráulicos às câmaras do cilindro para elevar a flexibilidade do sistema de atuação. Sistemas de atuação hidráulicos com acumuladores acoplados às câmaras podem ser encontrados em diversas patentes e artigos científicos. Porém, na literatura consultada, não foi encontrado um procedimento formal de dimensionamento e seleção de componentes hidráulicos que adicionem uma flexibilidade controlada a um sistema de controle de força hidráulico. A flexibilidade passiva em sistemas de controle de força é bastante relacionada com a impedância de saída do atuador que, por sua vez, pode ser alterada passivamente modificando a transmissão hidráulica com a inserção de componentes hidráulicos de natureza capacitiva e resistiva.

Objetivos

O objetivo principal desta tese é apresentar um procedimento de seleção de componentes hidráulicos que garantam a uma flexibilidade controlada no atuador do sistema de controle de força hidráulico. Assim também, pretende-se apresentar um novo tipo de atuador hidráulico denominado Atuador Elástico Puramente Hidráulico (*Pure Hydraulic Elastic Actuator – PHEA*) cuja principal característica é a de possuir uma elasticidade controlada e adaptada para aplicações de controle de força.

Entre os objetivos específicos pode-se citar os seguintes: (a) realização dos modelos lineares e não lineares do sistema hidráulico de controle de força, que incluem um modelo da mangueira de alta expansão volumétrica; (b) proposta de uma nova equação matemática que define a curva de vazamento interno da válvula; (c) validação experimental do PHEA; e, finalmente, (d) aplicação de um controlador baseado na Teoria de Realimentação Quantitativa (*Quantitative*

Feedback Theory – QFT). A QFT é uma técnica de controle robusto que oferece a possibilidade de obter um controlador com estrutura de baixa ordem e ganhos fixos que satisfaçam os requerimentos de desempenho ainda sob a influência das variações paramétricas internas da planta ou de perturbações externas.

Metodologia

A presente tese baseia-se numa pesquisa bibliográfica a fim de coletar informações relevantes que fundamentam o assunto exposto e dissertado, além de testes experimentais realizados para demonstrar a aplicabilidade dos modelos matemáticos desenvolvidos. Dado o caráter tanto qualitativo como quantitativo da pesquisa, após a fundamentação teórica, são realizados diversos testes experimentais que validem os modelos matemáticos propostos neste estudo. Adicionalmente, é realizado e analisado um caso de estudo de laboratório como exemplo de aplicação do procedimento de seleção de componentes hidráulicos proposto como objetivo da tese. Para a implementação e simulação do modelo dinâmico do sistema de controle de força hidráulico é usado o software Matlab/Simulink.

Resultados e discussões

Dois tipos de modelos matemáticos são desenvolvidos no presente estudo: um modelo linear, usado para o projeto de controle, e um modelo não linear, usado para as simulações dinâmicas. A modelagem matemática é baseada num circuito hidráulico genérico que inclui uma servoválvula, mangueiras e um cilindro. Cabe ressaltar que a unidade de potência hidráulica não é considerada no modelo apresentado, considerando-se que o suprimento de fluido hidráulico é constante. A bancada hidráulica usada para a validação experimental é denominada de Ybitú e pertence ao Laboratório de Sistemas Hidráulicos e Pneumáticos (LASHIP) do Departamento de Engenharia Mecânica da Universidade Federal de Santa Catarina (UFSC). Considerando que a servoválvula é um dos componentes mais críticos para o controle de força hidráulico, a tese apresenta uma análise detalhada tanto da elaboração do modelo matemático como da validação experimental baseada na norma ISSO 10770. A servoválvula considerada para o presente estudo é uma válvula 4/3 simétrica de tipo bocal-defletor com centro fechado e de duplo estágio acionado por motor-torque. Devido à elevada rigidez intrínseca que possuem os atuadores hidráulicos, variações bem pequenas de posição do atuador produzem variações grandes de força. Sendo que variações pequenas da posição do atuador se produzem, principalmente, quando o movimento do carretel fica ao redor da origem, ou ponto nulo, da válvula. Desta forma, faz-se necessário analisar, detalhadamente, tanto as vazões como os vazamentos internos ao redor desse ponto. Neste sentido, apresenta-se uma equação matemática que permite modelar o comportamento do vazamento interno ao redor do ponto nulo e que se adiciona às equações que representam as vazões dentro da válvula com a finalidade de ter um modelo matemático mais próximo à realidade. Com o objetivo de validar o modelo proposto, se realizam dois testes experimentais: teste de vazamento interno, baseado na norma ISO 10770-1, item 8.1.3, que permite obter a curva de vazamento interno na válvula; e o teste de medição de vazão, baseado na norma ISO 10770-1, item 8.1.4, que é utilizado para obter a curva de ganho de vazão. Os resultados experimentais obtidos permitem validar o modelo matemático proposto da servoválvula. Os resultados comparativos entre o comportamento dinâmico experimental da válvula e o do modelo matemático são apresentados no documento, destacando-se a semelhança entre eles.

Por outro lado, o modelo da mangueira é baseado no modelo dinâmico no domínio de tempo proposto por Johnston (2006) que, por sua vez, baseia-se no Método de modelagem por Linhas de Transmissão (*Transmission Line Method* – TLM).

Tendo em vista que o objetivo principal da presente tese se refere ao estabelecimento de um procedimento de seleção de componentes hidráulicos que adicionem uma flexibilidade controlada ao sistema de controle de força, o presente estudo é focado no uso de mangueiras como elementos capacitivos hidráulicos a serem dimensionados, selecionados e implementados no PHEA. O tipo de mangueira a ser analisado tem uma característica especial pois são de alta expansão volumétrica. Sendo assim, estas mangueiras especiais possuem uma maior capacitância hidráulica em comparação com as mangueiras hidráulicas industriais comumente usadas. No capítulo relacionado com o PHEA, apresentam-se as equações que permitem o dimensionamento de mangueiras de alta expansão volumétrica, considerando um valor de rigidez hidráulica desejada. Por sua vez, apresenta-se uma análise sobre a forma de calcular a rigidez hidráulica necessária para uma aplicação de controle de força, de acordo a requerimentos dinâmicos de desempenho e rejeição às perturbações externas. Com isto, garante-se que o componente selecionado permitirá ao sistema de controle de força atuar da forma desejada. Durante o desenvolvimento das equações que permitem o cálculo da rigidez desejada, percebe-se que o modelo dinâmico linear completo do sistema de controle de força hidráulico pode ser descomposto em três dinâmicas essenciais: uma dinâmica eletromagnética relacionada ao primeiro estágio da válvula; uma dinâmica hidráulica, que descreve o comportamento do fluido hidráulico na válvula, nas linhas de pressão e no cilindro; e uma dinâmica mecânica relacionada ao movimento do pistão. Esta decomposição não resulta ser exata, mas sim aproximada. Uma comparação entre as respostas em frequência do modelo linear completo do sistema e do modelo decomposto mostra que a aproximação é válida. Adicionalmente, encontra-se viável, inclusive, simplificar o modelo e considerar apenas a dinâmica hidráulica como a característica dominante no comportamento dinâmico do sistema. Esta situação é validada numericamente e, finalmente, a determinação do valor da rigidez desejada se resume a uma equação que depende das características físicas da válvula e do cilindro, assim como dos requisitos de desempenho e de um ganho proporcional.

Por outro lado, a equação resultante que permite dimensionar o comprimento de mangueira requerido está em função das características físicas do cilindro (área útil do êmbolo e curso do cilindro), do valor de rigidez desejada, definido anteriormente, assim como das características físicas da própria mangueira (diâmetro comercial e a sua capacidade de expansão volumétrica). Um fluxograma é apresentado a fim de mostrar o procedimento de seleção de mangueiras comerciais com foco em aplicações de controle de força. Após a aplicação do procedimento de seleção de mangueira para um caso de estudo realizado no LASHIP, os resultados experimentais e de simulação demonstram a aplicabilidade do procedimento proposto.

Em relação ao projeto de controle, a técnica QFT é selecionada devido à capacidade que a mesma possui para controlar sistemas que possuem variações paramétricas internas. Como o sistema sob estudo da presente tese tem parâmetros variantes no tempo tais como a rigidez hidráulica, que varia dependendo da posição do êmbolo do cilindro, assim como os ganhos de vazão e o coeficiente de vazão-pressão da válvula, que variam dependendo da posição de abertura da válvula, a técnica QFT vê-se propícia para o projeto de controle. O projeto de controlador baseado na técnica QFT dá a possibilidade de incluir restrições tanto na estabilidade robusta, assim como na capacidade de rejeição de perturbações e de seguimento de trajetória de força. Contudo, o controlador obtido apresenta uma estrutura de baixa ordem e com ganhos fixos, que é uma particularidade da técnica e os resultados experimentais confirmam a possibilidade de aplicar este tipo de controlador num sistema de controle de força hidráulico.

Considerações finais

A presente tese desenvolve um estudo sobre o controle de força em atuadores hidráulicos através da adição de flexibilidade hidráulica. A flexibilidade em um sistema de controle de força pode ser adicionada de forma ativa ou passiva, e o foco da tese é na adição passiva puramente hidráulica. Isto se deve ao fato de que desta forma se reduz o esforço de controle e simplifica-se a implementação prática. Adicionalmente, o comprimento do sistema de atuação linear hidráulico é reduzido em comparação, por exemplo, com o Atuador Elástico em Serie (*Series Elastic Actuator* – SEA) de tipo hidráulico proposto por Robinson (2000), que propõe a adição de uma mola entre a carga e o atuador hidráulico. Considerando-se, portanto, o objetivo principal da tese, conclui-se que o procedimento de seleção proposto cumpre com o desejado. Os resultados experimentais demonstram a aplicabilidade prática do método de seleção de mangueiras de alta expansão volumétrica como componentes capacitivos a serem adicionados num sistema de controle de força hidráulico.

Com relação às equações apresentadas como parte da modelagem matemática na tese, conclui-se que algumas delas podem constituir um aporte importante para aprimorar trabalhos futuros que pretendam continuar com a mesma linha de pesquisa. Dentro dos aportes matemáticos inovadores apresentados na tese, destacam-se, por exemplo, a equação que modela a curva de vazamento interno da válvula, assim como também o modelo linear simplificado, que resulta da decomposição do modelo linear completo de um sistema hidráulico. Com este modelo decomposto, torna-se simples identificar qual das dinâmicas internas do sistema tem maior efeito sobre o comportamento dinâmico geral de um sistema de controle de força hidráulico. Adicionalmente, as equações que visam o cálculo e dimensionamento das mangueiras integram tanto características intrínsecas hidráulicas que dependem dos componentes associados, tais como a válvula, mangueiras e o cilindro, assim como características de desempenho dinâmico, tais como constantes de tempo e um ganho proporcional.

A respeito do sistema de controle, a técnica proposta de controle robusto proposta possui características que se acomodam bem ao caso do sistema hidráulico. A técnica QFT leva em consideração a possibilidade de incluir faixas de incertezas paramétricas durante a etapa de projeto do controlador além da inclusão de restrições relacionadas à estabilidade, rejeição às perturbações e seguimento a trajetória. Contudo, o resultado final obtido é um controlador feito sob medida com uma estrutura de baixa ordem com ganhos constantes que consegue atender os requisitos de desempenho definidos pelo projetista. De acordo com os resultados experimentais apresentados, percebe-se que o controlador projetado através da técnica proposta consegue atender bem os requisitos de desempenho desejados.

Finalmente, é concluído que existem ainda vários campos, dentro dos sistemas de controle de força hidráulica, a serem explorados como produto desta tese. Têm-se, por exemplo, a possibilidade de adicionar outro tipo de componentes capacitivos tais como os acumuladores, mas também o uso de componentes dissipativos hidráulicos tal como restrições reguláveis. Modificações na forma dos atuadores lineares também poderiam influenciar em uma mudança controlada da rigidez hidráulica. Adicionalmente, modificações dinâmicas da rigidez hidráulica através, por exemplo, de acumuladores variáveis permitiriam um controle de força muito mais avançado que possa mudar de acordo ao tipo de carga que manipula. Sem dúvidas, ainda há muito a ser explorado nesta linha de pesquisa e a presente tese pode representar um aporte base para tais pesquisas.

Palavras-chave: Controle de força em sistemas hidráulicos. Impedância mecânica. Flexibilidade hidráulica.

LIST OF FIGURES

Figure 2.1 – Meaning of the causal links: (a) the effort leaves A and enters B (Impedance); the flow leaves B and enters A (Admittance); and (b) the effort leaves B and enters A (Impedance); the flow leaves A and enters B (Admittance).....	50
Figure 2.2 – Passive and active compliance methods classification.....	53
Figure 2.3 – Schematic of the SEA.....	55
Figure 2.4 – (a) Series elastic actuator and (b) Series damping actuator.....	57
Figure 2.5 – Schematic design of the Hydro-elastic Actuator proposed by Robinson and Pratt (2000).....	58
Figure 2.6 – Schematic design of a hydraulic remote manipulator.	59
Figure 2.7 – Model of double-acting hydraulic actuator with accumulators coupled to the chambers.	59
Figure 3.1 – QFT Methodology.	62
Figure 3.2 – Two degree-of-freedom (2-DOF) canonical control system.	63
Figure 3.3 – Example of templates, including the location of the nominal plant, calculated at frequencies of interest and plotted in Nichols diagram.	65
Figure 3.4 – Unit-step response curve showing rise time (t_r), peak time (t_p), maximum overshoot (M_p), and settling time (t_s).....	66
Figure 3.5 – Upper ($B_U(t)$) and lower ($B_L(t)$) bounds of the time-domain performance specification defining a region of acceptable system responses.....	68
Figure 3.6 – (a) Ideal approximation case considering a second-order behavior in both of upper ($ B_U(j\omega) $) and lower ($ B_L(j\omega) $) bounds; and, (b) Augmented case with the addition of a zero and a pole in high frequencies.	68
Figure 3.7 – Example of stability bounds calculated at $\omega \in \Omega_1 = [0.1, 5, 10, 100]$ rad/s; disturbance bounds calculate at $\omega \in \Omega_2 = [0.1, 5, 10]$ rad/s; and tracking bounds calculated at $\omega \in \Omega_3 = [0.1, 5, 10]$ rad/s	72
Figure 3.8 – Example of bounds union based on Figure 3.7.	73
Figure 3.9 – Example of bound intersection process at every frequency of interest.	74
Figure 3.10 – Final result of bounds intersection process, including the location of the loop transmission function ($L(j\omega)$).	74
Figure 3.11 – Example of loop-shaping in order to synthesize the controller function.	75

Figure 3.12 – Example of QFT prefilter synthesis: (a) initial condition with a unitary gain prefilter $ P(j\omega) =1$, and (b) final condition of the system with the upper and lower limits within the acceptable range after the addition of control elements ensuring the system traceability.	77
Figure 4.1 – Diagram of a generic hydraulic circuit showing the parts to be modelled.....	79
Figure 4.2 – Nozzle flapper torque motor servovalve description (first stage).	80
Figure 4.3 – Second stage parts description at null position.	81
Figure 4.4 – Flow rates during a positive displacement of the spool ($U_{Csp} \geq 0$).	82
Figure 4.5 – Flow rates during a negative displacement of the spool ($U_{Csp} < 0$).	83
Figure 4.6 – Internal leakage flow around the null position.....	85
Figure 4.7 – Detail of flowrates and pressures inside the cylinder.....	88
Figure 4.8 – Typical static friction model with different phenomena, such as Coulomb friction, static friction, viscous friction and Stribeck effect.....	90
Figure 4.9 – LuGre model assumption of the friction interface between two surfaces considering it as the contact between bristles.	91
Figure 4.10 – Generic layers found in a braided hose.	93
Figure 5.1 – Schematic of the data acquisition system of the test rig Ybitú.	99
Figure 5.2 – Picture of the hydraulic test rig Ybitú used for the study.	100
Figure 5.3 – (a) Hydraulic circuit and (b) test rig arrangement used for internal leakage test.	101
Figure 5.4 – Internal leakage test measurements using WEBTEC LT5 flowmeter. (a) Temperature of the oil, (b) normalized control signal sent to the servovalve, (c) normalized internal leakage flowrates, and (d) normalized pressures.	102
Figure 5.5 – Internal leakage curves in positive and negative spool directions.	103
Figure 5.6 – (a) Hydraulic circuit and (b) test rig arrangement used for metering test.....	104
Figure 5.7 – Metering test measurements using WEBTEC CT60 flowmeter. (a) oil temperature, (b) normalized control signal sent to the servovalve, (c) normalized internal leakage flowrates, and (d) normalized pressures.	105
Figure 5.8 – Metering test measurements using WEBTEC LT5 flowmeter. (a) Oil temperature, (b) normalized control signal sent to the servovalve, (c) normalized internal leakage flowrates, and (d) normalized pressures.	106
Figure 5.9 – (a) Normalized control flowrate measurements using flowmeters CT60 and LT5, and (b) Normalized control flowrate vs normalized control signal.	107

Figure 5.10 – Zoom-in of area remarked in Figure 5.9(b).....	108
Figure 5.11 – Comparison of experimental and simulation results for (a) normalized internal leakage flowrates and (b) normalized pressures during a negative displacement of the spool.....	110
Figure 5.12 – Comparison of experimental and simulation results for (a) normalized internal leakage flowrates and (b) normalized pressures during a positive displacement of the spool.....	110
Figure 6.1 – Hydraulic force control system using: (a) mechanical compliant component (SEA) and (b) hydraulic compliant components.....	114
Figure 6.2 – Schematic representation of the hydraulic stiffness of each cylinder chamber.	115
Figure 6.3 – Schematic representation of the hydraulic cylinder in the mechanical domain.	115
Figure 6.4 – Hydraulic stiffness in function of the piston position considering a symmetrical cylinder. The blue line is an example of the initial hydraulic stiffness values depending on the piston position. The red dashed line and the black dashed line with dots represent how the hydraulic stiffness changes as the compliance increases.....	116
Figure 6.5 – Rough characterization of a hydro-elastic actuator impedance proposed by Robinson (2000), showing that the impedance is equal to an equivalent mass at low frequencies, and it tends to acts as a spring with a stiffness equal to the load cell stiffness at high frequencies.....	122
Figure 6.6 – Frequency response comparison between a complete linear model (Equation (6.7)) and a quasi-exact approximated linear model (Equation (6.12)).....	124
Figure 6.7 – Zero-pole map of the approximated linear model shown in Equation (6.12)....	125
Figure 6.8 – Constitutive layers of Synflex 3130 hoses provided by the manufacturer EATON.	127
Figure 6.9 – Volumetric expansion data of Synflex 3130 hose model provided by the manufacturer EATON.	129
Figure 6.10 – High volumetric expansion hose sizing and selection flowchart.	131
Figure 6.11 – Example of defining a feasible group of hose commercial diameters.....	132
Figure 6.12 – Internal description of the commercial hose diameter selection subprocess...	133
Figure 6.13 – Hydraulic circuit considered for the case of study of a PHEA.....	135
Figure 6.14 – Upper and lower limits of performance specifications described in (a) time-domain and, posteriorly translated to, (b) frequency-domain.....	138
Figure 6.15 – Loop shaping of the QFT-based controller.....	140

Figure 6.16 – Comparison between experimental and simulation force tracking responses based on a step force references using HVE hoses.	141
Figure 6.17 – Enlarged plot of the region marked in Figure 6.16, including: (a) control signal sent to the valve, (b) chamber pressures, (c) hydraulic force, and (d) measured force in the same range of time.	142
Figure 6.18 – Comparison between force responses using pipes or HVE hoses.	143
Figure 7.1 – Hydraulic force control system using accumulators.	147
Figure 7.2 – Hydraulic force control system using a flow control valve between chambers.	147

LIST OF TABLES

Table 2.1 – Example of effort and flow variables according to the physical domain.	49
Table 2.2 – Laplace-transformed impedance and admittance functions of common mechanical elements.....	51
Table 2.3 – Comparison between the two types of compliance used in force control systems.	54
Table 3.1 – Performance specification models (QFT margins).	70
Table 5.1 – Valve coefficients obtained using a nonlinear optimization algorithm and based on experimental test results.	109
Table 6.1 – Pole locations for different values of K_H	125
Table 6.2 – Combinations of K_p , K_H , and L_{ho} to obtain the required dynamic performance assuming the HVE hose model EATON Synflex ® 3130-08.....	137
Table 6.3 – Parameter uncertainties of the plant.....	139
Table A.1 – Nominal parameters values of the components used for experimental tests based on manufacturer’s catalog data.	159

LIST OF SYMBOLS

CHAPTER 2

$F(t)$	Force component	[N]
$\tau(t)$	Torque component	[Nm]
$p(t)$	Fluid pressure, gas pressure	[Pa]
$U(t)$	Voltage	[V]
$v(t)$	Velocity component	[m/s]
$\omega(t)$	Angular velocity component	[rad/s]
$q_v(t)$	Volumetric flowrate	[m ³ /s]
$q_m(t)$	Mass flowrate	[Kg]
$i(t)$	Current	[A]
$F(s)$	Laplace transform of force	
$X(s)$	Laplace transform of position	
$Z(s)$	Impedance transfer function	
$Y(s)$	Admittance transfer function	
K	Stiffness at the contact point	[N/m]
F_{ref}	Force reference	[N]
F_{load}	Load force	[N]

CHAPTER 3

$G(s)$	Controller transfer function	
$F(s)$	Pre-filter transfer function	
$P(s)$	Plant transfer function	
$H(s)$	Sensor dynamics transfer function	
$R(s)$	Laplace transform of the reference	
$Y(s)$	Laplace transform of the system output	
$D_1(s)$	Laplace transform of the external disturbance before the plant	
$D_2(s)$	Laplace transform of the external disturbance after the plant	
$N(s)$	Laplace transform of the sensor noise input	
$U(s)$	Laplace transform of the controller output	
$E(s)$	Laplace transform of the error signal	
\mathcal{P}	Set of plants	

$L(s)$	Transmission function	
$P(j\omega_i)$	All possible variations of the plant P at every frequency ω_i	
ω_i	Frequencies under analysis	[rad/s]
Ω_k	Set of frequencies of interest	[rad/s]
ω_n	Undamped natural frequency of the system	[rad/s]
ζ	Damping ratio	
t_r	Rise time	[s]
t_p	Peak time	[s]
t_s	Settling time	[s]
M_p	Maximum peak in time-domain	
σ	Attenuation	
ω_d	Damped natural frequency	[rad/s]
$B_U(t)$	Upper performance specifications in time-domain	
$B_L(t)$	Lower performance specifications in time-domain	
M_m	Maximum peak in magnitude in frequency-domain	[dB]
ω_{hf}	Frequency that denotes the high frequency region	[rad/s]
$\delta_r(\omega_i)$	Difference in magnitude between the upper and lower limit at the frequency of analysis	[dB]
$H(j\omega)$	Sensor dynamics in frequency-domain	
$\delta_1(\omega)$	Robust stability margin	
$\delta_2(\omega)$	Sensitivity margin	
$\delta_3(\omega)$	Disturbance rejection margin	
$\delta_4(\omega)$	Effort control margin	
$\delta_{5U}(\omega)$	Upper tracking margin	
$\delta_{5L}(\omega)$	Lower tracking margin	
$B_U(j\omega)$	Upper performance specifications in frequency-domain	
$B_L(j\omega)$	Lower performance specifications in frequency-domain	
$L(j\omega)$	Transmission function in frequency-domain	
$G(j\omega)$	Controller function in frequency-domain	
$P(j\omega)$	Plant function in frequency-domain	
$U(j\omega)$	Controller output in frequency-domain	
$N(j\omega)$	Sensor noise input in frequency-domain	
$T_{rU}(j\omega)$	Maximum limits of the system closed-loop function in frequency-domain	
$T_{rL}(j\omega)$	Minimum limits of the system closed-loop function in frequency-domain	

CHAPTER 4

U_C	Input control signal	[V]
U_{Csp}	Equivalent voltage	[V]
ω_{nv}	Natural frequency of the valve	[rad/s]
ξ_v	Damping ratio of the valve	
p_A	Pressures in line A	[Pa]
p_B	Pressures in line B	[Pa]
p_S	Supply pressure	[Pa]
p_T	Reservoir pressure	[Pa]
U_{Cn}	Nominal control voltage	[V]
q_{vi}	Flowrate through port number $i = 3$ to 6	[m ³ /s]
K_{vi}	Partial flow coefficient of the valve at port number $i = 3$ to 6	[m ³ /(s·Pa ^{0.5})]
K_{vp}	Partial flow coefficient of the valve	[m ³ /(s·Pa ^{0.5})]
$K_{vin\ i}$	Internal partial leakage coefficient at port number $i = 3$ to 6	[m ³ /(s·Pa ^{0.5})]
K_{vinp}	Internal partial leakage coefficient	[m ³ /(s·Pa ^{0.5})]
q_{vA}	Flowrate at port A	[m ³ /s]
q_{vB}	Flowrate at port B	[m ³ /s]
q_{vn}	Nominal flowrate at the maximum valve opening	[m ³ /s]
Δp_{tn}	Nominal total valve pressure drop	[Pa]
q_{vin}	Nominal internal leakage flowrate	[m ³ /s]
p_{in}	Internal pilot pressure	[Pa]
q_{vinT}	Total internal leakage flowrate	[m ³ /s]
q_{tare}	Tare flow	[m ³ /s]
λ	Curve-shape coefficient	
q_{vC}	Control flowrate	[m ³ /s]
p_L	Load pressure	[Pa]
K_{qUi}	Flow-voltage gain at operating point i	[m ³ /s·V]
K_{ci}	Flow-pressure coefficient at operating point i	[m ³ /s·Pa]
V_A	Volume inside the chamber A	[m ³]
V_B	Volume inside the chamber B	[m ³]
x_p	Rod position	[m]
β_e	Effective bulk modulus of the system	[Pa]

V_{A0}	Dead volumes coupled to cylinder chamber A	[m ³]
V_{B0}	Dead volumes coupled to cylinder chamber B	[m ³]
L	Cylinder stroke	[m]
A_A	Area of side A of the piston	[m ²]
A_B	Area of side B of the piston	[m ²]
A_u	Useful piston area	[m ²]
M_t	Total mass displaced by the piston	[Kg]
F_{fr}	Friction forces	[N]
F_e	Measured force or the applied force	[N]
z	Average deflection of the bristles	[m]
v	Relative velocity between the surfaces	[m/s]
F_C	Coulomb friction	[N]
F_S	Stiction	[N]
v_S	Stribeck velocity	[m/s]
α	Coefficient that defines the Stribeck curve	
σ_0	Stiffness of the bristles	[N/m]
σ_1	Bristle's damping coefficient	[Ns/m]
σ_2	Viscous friction coefficient	[Ns/m]
$g(v)$	LuGre function	
F_{frSS}	Steady-state friction force	[N]
$Q_{vC}(s)$	Laplace transform of control flowrate	
V_T	Total volume of the cylinder	[m ³]
B	Viscous friction coefficient	[Ns/m]
$P_L(s)$	Laplace transform of load pressure	
$F_e(s)$	Laplace transform of force applied	
p_{dw}	Hose downstream pressure	[Pa]
q_{up}	Upstream flowrate	[m ³ /s]
p_{up}	Hose upstream pressure	[Pa]
q_{dw}	Downstream flowrate	[m ³ /s]
Z_i	Hose characteristic impedance	[kg/m ² s]
ρ	Fluid density	[kg/m ³]
c_i	Speed of wave i	[m/s]
A_{ho}	Cross-sectional area of the fluid passageway in the hose	[m ²]
N_i	Modal ratio between the wall and fluid velocity for wave i	

f_i	Wave travelling in the forward direction	
g_i	Wave travelling in the reverse direction	
$f_1'(t)$	Delayed and attenuate wave in the forward direction	
$g_1'(t)$	Delayed and attenuate wave in the reverse direction	
$h_1'(t)$	Function that represents the functions $f_1'(t)$ or $g_1'(t)$	
N	Number of exponential weighting functions	
T_i	Time delay	[s]
$w_{i,n}$	Auxiliary function	
$a_{i,n}$	coefficient a calculated from non-dimensional values	
$b_{i,n}$	coefficient b calculated from non-dimensional values	
$X_L(s)$	Laplace transform of load position	
$X_P(s)$	Laplace transform of piston position	
K_S	Load cell stiffness	[N/m]

CHAPTER 5

T_A	Oil temperature at chamber A	[°C]
T_B	Oil temperature at chamber B	[°C]
T_S	Oil temperature at supply point	[°C]

CHAPTER 6

K_{HA}	Internal stiffness related to chamber A	[N/m]
K_{HB}	Internal stiffness related to chamber B	[N/m]
K_H	Hydraulic stiffness	[N/m]
V_0	Dead volume coupled to each cylinder chamber ($V_{A0} = V_{B0} = V_0$)	[m ³]
V	Uncertain parameter of volume such that ($V_A = V_B = V$)	[m ³]
F_{eSS}	Steady-state value of the force	[N]
K_{eq}	Equivalent stiffness	[N/m]
K_S	Load cell stiffness	[N/m]
K_{SS}	Steady state gain	
τ_d	Desired time constant	[s]
K_p	Proportional gain	
q_{max}	Maximum flowrate	[m ³ /s]

v_{oil}	Oil velocity inside the hose	[m/s]
K_{Hmax}	Maximum hydraulic stiffness	[N/m]
K_{Hmin}	Minimum hydraulic stiffness	[N/m]
β_0	Fluid	[Pa]
β_{ho}	Hose bulk modulus	[Pa]
β_{hoSS}	Steady state hose bulk modulus	[Pa]
r_{β}	Dynamic hardening ratio	
ΔV_{ho}	Change in the hose volume	[m ³]
V_{ho}	Volume of oil trapped in the hose coupled to each cylinder chamber	[m ³]
E	Volumetric expansion	[m ³ /m]
L_{ho}	Hose free length	[m]
ε	Expansion slope of the hoses	[m ³ /m·Pa]
V_{0ho}	Initial volume of the hose	[m ³]
p	Working pressure	[Pa]

SUMMARY

ACKNOWLEDGEMENTS	21
RESUMO	22
ABSTRACT	23
RESUMO EXPANDIDO	24
LIST OF FIGURES	28
LIST OF TABLES	32
LIST OF SYMBOLS	33
SUMMARY	39
1 INTRODUCTION	43
1.1 MOTIVATION	46
1.2 CONTRIBUTIONS.....	47
1.3 THESIS OUTLINE	48
2 RELATED WORKS	49
2.1 MECHANICAL INTERACTION AND CAUSALITY	49
2.2 PASSIVITY.....	51
2.3 COMPLIANCE.....	52
2.4 PASSIVE COMPLIANT ACTUATORS	55
2.4.1 Series elastic actuators	55
2.4.2 Series damping actuators	56
2.4.3 Variable stiffness actuators	57
2.4.4 Hydro-elastic actuators	58
2.5 CHAPTER CONCLUSIONS.....	60
3 QUANTITATIVE FEEDBACK THEORY	61
3.1 FUNDAMENTALS OF THE QUANTITATIVE FEEDBACK THEORY	63
3.1.1 Templates generation	63

3.1.2	Performance specifications	66
3.1.3	QFT bounds calculation	69
3.1.4	Loop-shaping	73
3.1.5	Prefilter synthesis.....	76
3.1.6	Simulation and design validation	77
3.2	CHAPTER CONCLUSIONS	78
4	MATHEMATICAL MODELING OF HYDRAULIC ACTUATION SYSTEM	
	79	
4.1	SERVOVALVE.....	80
4.1.1	Nonlinear model.....	81
4.1.2	Linear model	86
4.2	CYLINDER	88
4.2.1	Nonlinear model.....	88
4.2.1.1	Friction force model.....	89
4.2.2	Linear model	92
4.3	HOSE	92
4.4	FORCE SENSOR	97
4.5	CHAPTER CONCLUSIONS	97
5	TEST RIG AND MODEL VALIDATION	99
5.1	DESCRIPTION OF TEST RIG	99
5.2	EXPERIMENTAL TESTS	100
5.2.1	Internal leakage test.....	100
5.2.2	Metering test.....	103
5.3	MODEL VALIDATION	108
5.4	CHAPTER CONCLUSIONS	111
6	PURE HYDROELASTIC ACTUATOR	113
6.1	DESCRIPTION	113

6.2	INCREASING PASSIVE COMPLIANCE THROUGH HYDRAULIC STIFFNESS VALUE	114
6.2.1	Modifications in the linear model of the system	117
6.2.2	Disturbance rejection based on the output impedance	120
6.2.3	Performance based on the desired tracking control ratio	123
6.3	SIZING AND SELECTION OF HIGH VOLUMETRIC EXPANSION HOSES	126
6.3.1	Mathematical background for HVE hose sizing and selection	127
6.3.1.1	Hose diameter calculation	127
6.3.1.2	Hose length calculation	127
6.3.1.3	Hydraulic stiffness calculation based on hose length and diameter	130
6.3.2	High volumetric expansion hose selection flowchart	130
6.4	SIZING HVE HOSES AND DESIGNING A QFT-BASED CONTROLLER FOR PHEA: CASE OF STUDY	135
6.4.1	High volumetric expansion hose selection	135
6.4.2	QFT-based controller design for PHEA	137
6.5	SIMULATION AND EXPERIMENTAL RESULT ANALYSIS	141
6.6	CHAPTER CONCLUSIONS	144
7	DISCUSSION AND CONCLUSIONS	145
7.1	FUTURE WORKS	146
	REFERÊNCIAS	149
	APPENDICES	159
	A TECHNICAL DATA OF HYDRAULIC COMPONENTS USED FOR EXPERIMENTAL TESTS	159

1 INTRODUCTION

One of the main advantages of hydraulic systems is related to the high power/weight ratio mainly due to the simple conversion mechanism of hydraulic to mechanical energy. Therefore, the high-power density of hydraulic systems allows to have the same force capacity with smaller actuators than their electromagnetic counterpart at the same power level. Additionally, hydraulic systems can maintain their carrying capacity indefinitely, which is something that would normally cause excessive heat generation in electrical components. These reasons made them a good choice for applications that need high forces and have small spaces for installation as in aeronautics and robotics. However, their main disadvantages are related to the presence of several nonlinearities and parameters uncertainty that increase the complexity of the controllers (MERRIT, 1967; TOTTEN AND DE NEGRI, 2012; VON LISINGEN, 2013).

This thesis deals with hydraulic force control and its applications. In general, force control is one of the most studied topics in robotics used to describe the interaction between a robot and an unknown environment. Its study began in the 1950s and 1960s with remote manipulators and artificial arm control. However, stability issues appeared at the same time and, in the late 1960s and 1970s, the first feedback force controller using computers was implemented trying to solve these problems (WHITNEY, 1985). From that time until now, several techniques and force control approaches were studied and implemented aiming to achieve better stability and performance. Considering the above-mentioned facts, this thesis will use the force control principles studied in robotics and will focus specifically on hydraulic force control systems.

Force is the result of the interaction between two mechanical systems. Therefore, every time that a mechanical interaction occurs, the actuation system and the environment exchange power. The point where this power exchange occurs is called interaction port (HOGAN AND BUERGUER, 2005). According to Hogan (1985a), mechanical interaction dynamics may be characterized by mechanical impedance, which is intimately related with compliance in mechanical transmissions.

Positioning systems are usually made up of rigid transmissions to avoid undermining the stability and also to maximize the system bandwidth. A rigid transmission allows to have a good performance in positioning tasks because the system bandwidth is directly related to this stiffness property. On the other hand, compliant transmission produces a spring-like behavior,

which can lead to stability problems because the position controller need to apply greater control efforts to meet the performance requirements.

However, Pratt et al. (1997) affirmed that this traditional design of actuators with stiff transmissions does not apply for force control applications. They sustained that, depending on the application, actuators to load interfaces (output impedances) should be more compliant trying to reproduce performance characteristics more suited to the natural world. An actuator with compliant transmission will have a lower mechanical impedance at the interaction port and, therefore, a better capability to reduce interaction forces when it encounters an unpredicted object, being a good choice for force control systems.

Another fact to be accounted in force control comes from an intrinsic loop resultant from the mechanical interaction. Dyke et al. (1995) demonstrated that the poles of the structure (environment) appear as zeros of the transfer function during the mechanical interaction between a hydraulic cylinder and a structure. This fact occurs because the existence of an intrinsic loop called natural velocity feedback. The main effect of the natural velocity feedback is to greatly limit the bandwidth of the coupled system. Dimig et al. (1999) and Shield et al. (2001) supported the conclusions drawn by Dyke et al. (1995) and proposed the creation of an additional feedback loop to compensate the natural velocity feedback of the actuator. Considering this force control problem, Alleyne and Liu (1999) affirmed that using a simple PID controller can be problematic, arguing that a more advanced control algorithm is not just a luxury, but a necessity.

Boaventura et al. (2012) concluded that the natural velocity feedback exists in any interaction between an actuator and a load, regardless of actuator type and load characteristics. Likewise, they highlighted the necessity of a compensator of this velocity feedback. However, a major limitation of this approach is that it is model-based, being susceptible to parameter uncertainties. Plummer (2007) proposed a force control method which also needs the load motion measurement to be included in the control loop but the load dynamics itself does not need to be accounted (modelled). The author also argued about the necessity of including a spring (flexible link) between the actuator and the load, which provides a degree of mechanical isolation. With this arrangement, according to the author, it is possible to design a high bandwidth force controller that does not depend on the load dynamics, with good performance in tracking responses and disturbance rejection. In fact, the introduction of the spring in between the actuator turns the transmission more compliant and, in consequence, it reduces the output impedance of the system.

As can be noted, a way to cope with the difficulties related to force control systems is making the actuation more compliant. This task can be attained by an active or a passive approach:

- **active compliance** is obtained by software through force-based feedback control and allows greater flexibility to change the dynamic characteristics of the system without the need of physical components (HOGAN, 1985a; WHITNEY, 1985). Notwithstanding, it requires additional measuring and data processing devices and is not energy efficient in the sense of energy storage and consumption, i.e. active systems are always consuming energy during their operation;
- on the other hand, **passive compliance** approach uses hardware, introducing mechanical compliant components in order to reduce the transmission stiffness and, consequently, the output impedance of the system. It is usually cheaper compared with active compliance, enables to store mechanical energy (in case of using springs), but requires a mechanical design focused on space reduction (BOAVENTURA, 2013).

The Series Elastic Actuator (SEA) is a known example of a compliant actuation systems that can be found in the literature (WILLIAMSON, 1995; ROBINSON, 2000). The SEA uses a spring between the actuator and the load in order to obtain good force fidelity, low output impedance, and shock tolerance capability. However, the bandwidth of the system is reduced due to the use of that compliant element (ROBINSON, 2000). This kind of actuator has been applied in robotics and biomechanics due to its simplicity and good performance in force control (LEE et al., 2016; LOSEY et al., 2016). Another well-known example of compliant actuator is the Series Damping Actuator (SDA), which is common as well as SEA (CHEW et al., 2004). Compared with the SEA, the SDA uses a series damper to the actuator that allows it to have an inherent shock absorption capability. In recent years, the use of semi-active dampers, which take advantage of Magneto-Rheological (MR) fluids for realizing compliant actuation, has received increasing attention in force control applications, mainly in robotics (FOCCHI, 2013; LI, 2014). The main advantage of this kind of actuators, in contrast with others compliant actuators such as the SEA, is the possibility of controlling the force with a wider bandwidth.

1.1 MOTIVATION

Plummer (2007) and Lamming et al. (2010) emphasize the importance of using a flexible coupling to ensure a certain degree of isolation for the hydraulic system in relation to the load motion, helping to maintain stability in the applied force control. Compliant components limit the rate of force change applied to the load and using them allows to obtain a practical and robust force control scheme.

A spring effect is expected if the fluid compressibility in hydraulic actuators is taken into account. Theoretically, this spring effect is directly related to the hydraulic transmission (stiffness) and, in consequence, it can be shaped by adding hydraulic capacitive components obtaining an elastic actuator. Actuation systems using accumulators coupled to each cylinder chambers can be found in conference papers and patents trying to apply this kind of actuators in simple force control systems (WELLS et al., 1990; PETERSEN, 2002; ZOPPI, 2013). However, a formal procedure to determine the required hydraulic compliance for achieving the force control requirements as well as for the hydraulic component selection has not been found in literature. Moreover, a damping effect can be obtained hydraulically when there is an interconnection between the two-cylinder chambers. If this interconnection is controlled, then the damping can also be controllable. In the same way that the case mentioned before where accumulators are used, there is no specific research related to sizing hydraulic components in order to ensure a precise damping necessary for force control application.

As can be seen, the passive compliance in force control systems is closely related with the output impedance of the actuator, which can be shaped passively modifying the hydraulic transmission using capacitive and resistive components. Most of researchers use mechanical compliant elements in series with the actuator, such as springs or dampers, in order to achieve a required compliance for their applications (XU et al., 1995; NIKSEFAT AND SEPEHRI, 1999; ALLEYNE AND LIU, 2000; PLUMMER, 2007; AHN, K. K. et al., 2008; SIVASELVAN et al., 2008; NAKKARAT AND KUNTANAPREEDA, 2009; LAMMING et al., 2010; KARPENKO AND SEPEHRI, 2012). Nevertheless, in hydraulic force control systems, the compliant behavior of the mechanical components can also be obtained using only hydraulic components. In this sense, the hydraulic case has some advantages compared with the electromechanical case, because no additional components are inserted in series with the actuator. Therefore, no additional space is required, either in the longitudinal axis, in case of linear actuators, or axial, in case of rotational actuators, to incorporate a mechanical compliant component, reducing the space required for the actuation system.

Following the aforementioned line of reasoning, one of the main motivation of this thesis is to show the possibility of ensuring a required compliance in hydraulic actuators using only hydraulic components. The mathematical analysis to be carried out in thesis will focus on the linear actuator case, but its extension to the rotational case is almost straightforward.

The second main motivation is related to the control technique to be used in these kinds of hydraulic force control systems. Due to the variations of internal parameters of the system and uncertain external disturbances, the main control technique proposed to be used in this thesis is the Quantitative Feedback Theory (QFT) technique (HOROWITZ, 1988; HOUPIS AND RASMUSSEN, 1999).

1.2 CONTRIBUTIONS

The main contributions of this thesis in the fluid power community are listed below:

- *Summary of mathematical nonlinear and linear models describing a hydraulic system:* it is important to highlight that this thesis itself is a compendium of the nonlinear and linear models of a generic hydraulic system composed by a servovalve, a cylinder, and the capacitive elements between them (pipes or hoses). New equations are also presented aiming to obtain a more representative nonlinear model of the hydraulic system during its experimental validation. In case of the linear modeling, some modifications are assumed for using during the control design process. Such modifications consider the presence of parameter uncertainties aiming to not only analyze around an operating point but include all possible variations of the most essential parameters.
- *Proposing new equations to define the curve shape of the internal leakage flowrate:* a new equation based on hyperbolic function is used to reproduce a realistic behavior of the internal leakage near to the null position of a servovalve. Its applicability is demonstrated during the experimental validation process.
- *Presentation of the Pure Hydroelastic Actuator (PHEA):* this actuator is based on the use of hydraulic compliant components as required from the force control application. The hydraulic compliant components are sized in a controlled way through an analytical procedure. During the initial study, a first approach of the

PHEA was presented (LEDEZMA et al., 2015). However, after some refinements in the process, the mathematical background was strengthened and a new procedure was formulated (LEDEZMA et al., 2017; LEDEZMA et al., 2018).

- *Development of a mathematical background demonstrating the possibility to add controlled compliance to a hydraulic system:* the mathematical background, that supports the ideas applied in this thesis, is presented and described in detail. Some simplifications and considerations are described, aiming to demonstrate that it is possible to add hydraulic compliant components in a controlled way. This mathematical foundation is the base of the sizing and selection procedure of the hydraulic compliant components. Doing that, this thesis fills some of the gaps in the actual scientific literature related to the analysis of hydraulic passive compliance and its influence in force control applications.
- *Definition of a procedure for sizing hydraulic passive compliant components:* sizing and selection procedure of hydraulic compliant components. This procedure is a key element in the design of the PHEA.
- *Application of a robust control technique for controller design:* The Quantitative Feedback Theory, which is a robust control technique based on the frequency-domain, is selected, described, and applied in this thesis. The applicability and reliability of this technique is demonstrated through experimental results.

1.3 THESIS OUTLINE

The organization of this document is as follows: Chapter 2 explains the basic concepts of causality, passivity, compliance, and some reviews related to hydroelastic actuators. Chapter 3 describes the force control technique used in this thesis. Chapter 4 shows the mathematical modeling of the hydraulic system. Chapter 5 presents the test rig used for the experiments and explain the experimental tests used to calculate the valve coefficients. Chapter 6 introduces the Pure Hydroelastic Actuator and proposes a procedure for sizing and selection of compliant hydraulic components based on a detailed mathematical background. Additionally, it explains the QFT-based controller designed for the test rig using high expansion volumetric hoses. Finally, Chapter 7 presents the conclusions of this thesis.

2 RELATED WORKS

Before starting to describe the force control system applications, some concepts related to force control systems need to be reviewed.

2.1 MECHANICAL INTERACTION AND CAUSALITY

Mechanical interaction with loads or with an external environment is one of the most relevant activities of robotic manipulation. Its dynamics may be characterized by mechanical impedance, consequently for compliant robotics manipulators, a low mechanical impedance is required (HOGAN AND BUERGUER, 2005). Low mechanical impedances reduce the forces of interaction with unknown external environment, protecting manipulator and load. Moreover, high impedances help to obtain a more precise positioning, since the rigid transmissions offer greater stability and disturbance rejection against external disturbances (IYER, 2012; BOAVENTURA, 2013).

When two subsystems or components interact, there is a power flow between them that can be defined as the product of two power variables: effort and flow (PAYNTER, 1961; KARNOPP et al., 2012). Depending on the domain, the effort and flow variables can define several types of power interchange as can be seen in Table 2.1.

Table 2.1 – Example of effort and flow variables according to the physical domain.

Domain	Effort, $e(t)$	Flow, $f(t)$
Mechanical translation	Force component, $F(t)$	Velocity component, $v(t)$
Mechanical rotation	Torque component, $\tau(t)$	Angular velocity component, $\omega(t)$
Hydraulic	Fluid pressure, $p(t)$	Volumetric flowrate, $q_v(t)$
Pneumatic	Gas pressure, $p(t)$	Mass flowrate, $q_m(t)$
Electric	Voltage, $U(t)$	Current, $i(t)$

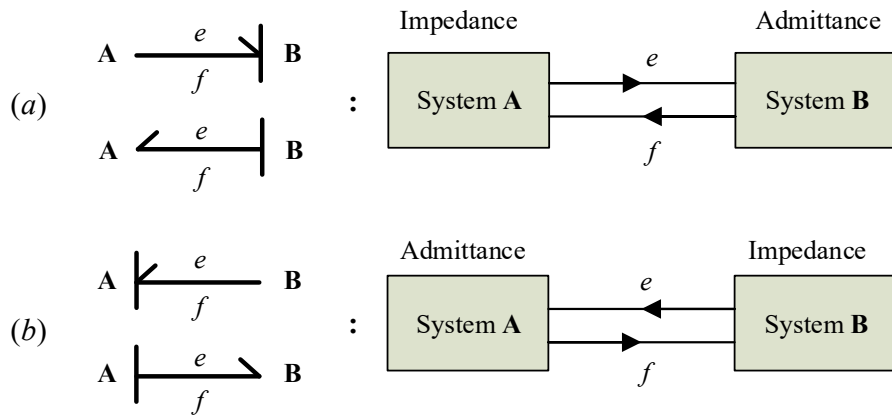
Source: Adapted from Karnopp et al. (2012).

According to Hogan (1985a), physical systems can be classified into two basic forms: admittances, which accept effort as input (e.g. force) and produce flow as output (e.g. velocity); and impedances, which accept flow as input (e.g. flowrate) and produce effort as output (e.g.

pressure). In addition, one of the most important facts related to the dynamic interaction between physical systems is that an isolated system cannot independently control effort and flow variables at the same time, i.e. it cannot apply force and set the position simultaneously (HOGAN, 1985a). The causality, therefore, defines the relation between the input and output variable of a physical system which, in turn, depends on the type of nature it possesses, which may be an admittance or an impedance (PAYNTER, 1961).

Figure 2.1 shows two basic examples of bond graphs representation during a dynamic interaction between systems A and B. The causal bar indicates the direction of the effort variable and, consequently, which system acts as an admission. The middle arrow indicates the direction of the energy flow.

Figure 2.1 – Meaning of the causal links: (a) the effort leaves A and enters B (Impedance); the flow leaves B and enters A (Admittance); and (b) the effort leaves B and enters A (Impedance); the flow leaves A and enters B (Admittance).



Source: Adapted from Karnopp et al. (2012).

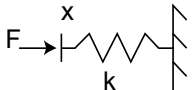
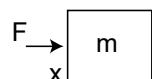
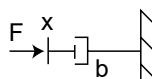
The mechanical impedance is equivalent to the electrical impedance and can be defined as the dynamic operator (Z) that determines the force output as a function of a velocity input in the same interaction port. In contrast, mechanical admittance is defined as the dynamic operator (Y) that determines the velocity output as a function of a force input in the same interaction port.

In the case of linear systems, the admittance is an inverse function of the impedance, so both can be represented as transfer functions (see Table 2.2). In the nonlinear case, both impedance and admittance can be represented by state equations (HOGAN, 1985a).

For most manipulation tasks, the external environment usually contains inertial elements and kinematic constraints. Therefore, from the manipulator point of view, this external

environment acts as an admittance, since it accepts inputs of force and produce a displacement motion in response.

Table 2.2 – Laplace-transformed impedance and admittance functions of common mechanical elements.

Scheme	Impedance $Z(s) = \frac{F(s)}{sX(s)}$	Admittance $Y(s) = \frac{sX(s)}{F(s)}$
	$Z(s) = \frac{k}{s}$	$Y(s) = \frac{s}{k}$
	$Z(s) = ms$	$Y(s) = \frac{1}{ms}$
	$Z(s) = b$	$Y(s) = \frac{1}{b}$

Source: Adapted from Hogan and Buerguer (2005).

Note: F represents an applied force; x , displacement; m , mass; b , viscous friction coefficient; and k is the stiffness.

To avoid causal conflicts during the analysis of an actuator that, for example, displaces an inertial element when applying a force on it, it is possible to consider that there is an impedance element between the actuator and the external environment (HOGAN, 1985a). The impedance control is based on this fact and aims to provide a controller that allows manipulating the impedance of the system in the iteration port. Thus, a desired impedance can be imposed through the controller, to control the dynamic interaction as needed (HOGAN, 1985a; b; c).

Manipulators that require an interaction with the external environment or with humans by applying controlled forces in a secure manner necessarily need low impedance at the interaction point. This means having more compliant actuators that allow more stable and safe force control.

2.2 PASSIVITY

Mechanical interaction affects the controlled variable introducing errors that can not only degrade the performance but also the stability of the entire coupled system. Therefore, a

system and an environment which are stable in isolation can become unstable when coupled, and need to be analyzed together (HOGAN AND BUERGUER, 2005).

Coupled stability is an additional specification necessary for any actuator or manipulator which is interacting with the environment. Colgate (1988) has shown that a necessary and sufficient condition to maintain stability during a dynamic interaction between a physical system and the environment is that both systems need to be passive. By ensuring passivity, the coupled system is stable, regardless of the magnitude of flow and effort variables in the interaction port.

There are several concepts regarding passivity, however explained in a simplified manner, a system is considered passive when it cannot, for any time period, output more energy than the amount of energy received at the same interaction port (HOGAN AND BUERGUER, 2005). Mathematically, the passivity of a linear physical system can be proved by fulfilling the following basic conditions (COLGATE, 1988; HOGAN AND BUERGUER, 2005):

1. the $Z(s)$ function has no poles in the right half-plane;
2. any imaginary poles of $Z(s)$ are simple, and have positive real residues;
3. $\text{Re}(Z(j\omega)) \geq 0$.

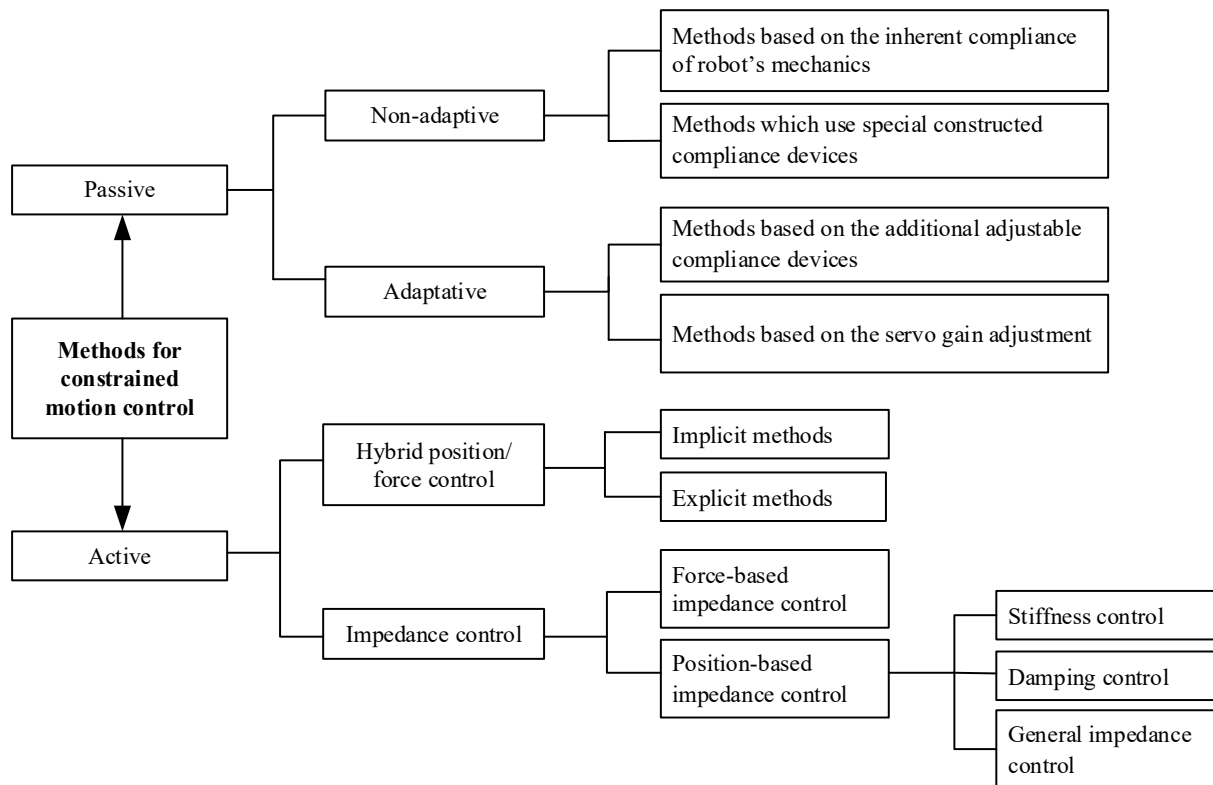
Another important observation to note is that any combination of passive elements is also considered a passive set (HOGAN AND BUERGUER, 2005). In this sense, it is impossible for an actuator or manipulator that interacts with any passive environment to become unstable if such actuator does not become unstable when coupled to a simple mass or a spring. It is observed that, according to Table 2.2, both an ideal spring and an ideal mass acting as admittance (external environment), modify the phase of the coupled system at $+90^\circ$ or -90° . Consequently, if the actuator is not passive and its phase exceeds, at some frequency, the value of -90° or $+90^\circ$, it is possible that the coupled system exceeds -180° or $+180^\circ$ in the phase, becoming unstable. On the other hand, due to its dissipative properties, a damper could not destabilize the coupled system since it is considered a strictly passive element and has no phase input.

2.3 COMPLIANCE

In the literature related to force control, the term compliance is commonly used to describe a system behavior when the dynamic interaction between the actuator, with rigid

transmission, and the load is controlled via software (VUKOBRATOVIĆ AND TUNESKI, 1994). However, the concept of compliance is more comprehensive and related with the impedance at the interaction port, which can be shaped through passive or active methods (WHITNEY, 1985). Figure 2.2 shows a classification of the compliance methods used in force control (VUKOBRATOVIĆ AND TUNESKI, 1994).

Figure 2.2 – Passive and active compliance methods classification.



Source: Adapted from Vukobratović and Tuneski (1994).

The passive compliance methods are based on the incorporation of mechanical elements in the system in order to passively manage the events produced during a dynamic interaction. This behavior is considered the most energy efficient (BOAVENTURA, 2013). In active compliance methods, force control is performed directly through the controller, where the force signal is measured by a sensor and feedback to close the control loop.

Hybrid position/force control is an active force control used in robotics, which aims to simultaneous and independently define the trajectories of force and position introducing natural and artificial constraints (MASON, 1981). The difference between explicit and implicit methods in hybrid position/force control is that in the first case (explicit method) the control method

consists in two complementary and parallel sets of feedback loops with separate and independent sensor systems. On the other hand, the implicit method is based on the identification of the contact stiffness (damping) using the force feedback, and the computation of the position (velocity) equivalent to the desired force. Therefore, the main advantage of the implicit method, compared with the explicit method, is its reliability and disturbance rejection (VUKOBRATOVIĆ AND TUNESKI, 1994).

Table 2.3 shows a brief comparison between passive and active control methods (BOAVENTURA, 2013).

Table 2.3 – Comparison between the two types of compliance used in force control systems.

Passive compliance	Active compliance
Obtained by hardware	Obtained by software
Added inertia to the structure	No weight added to the structure
Unlimited range of passive impedances	Limited range of passive impedances
Unlimited bandwidth	Bandwidth limited by closed-loop force control
Possible to vary the stiffness (with Variable Stiffness Actuators), but still slow	Fast change of apparent stiffness
It is possible to store energy	Only consume energy
Hard to physically realize complex impedances profiles	Any programmable impedance can be easily realized
Usually cheap	Usually expensive

Source: Adapted from Boaventura (2013).

Lawrence (1989) analyzed the influence of the actuator torque/speed capability on the ability of an active force control. A case of study of a DC permanent magnet electric motor was selected for his study and it was shown that the closed loop impedance is a linear combination of two extreme impedances: one related to the open loop impedance (physical actuator impedance), and the other, with the designed closed loop impedance (virtual impedance). An interesting result was the fact that when the actuator was in presence of a small external disturbance torque, the impedance specified by the controller was achieved. However, as the disturbance torques increase, the actuator impedance dominates the overall behavior and, consequently, the transmission may worsen the effects (LAWRENCE, 1989; HURST et al., 2004). According to De Schutter (1987), all active force control methods require a comparable degree of passive compliances in order to yield comparable performance and disturbance rejection

capabilities. Therefore, the more compliance added to the actuation system, the better the force control will be for a given bandwidth, considering that the force error due unforeseen motion disturbances is inversely proportional to $1/K$, where K is the stiffness at the contact point (HURST et al., 2004).

This thesis will focus on the passive compliance method, aiming to increase the hydraulic compliance of the actuator in order to achieve stable dynamic interactions with the environment.

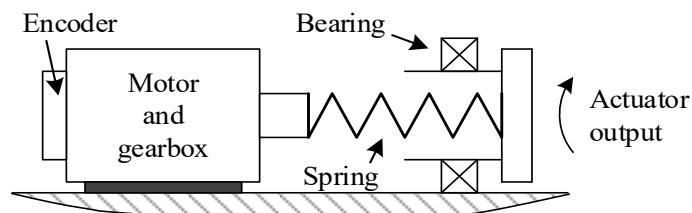
2.4 PASSIVE COMPLIANT ACTUATORS

2.4.1 Series elastic actuators

The Series Elastic Actuator (SEA) was originally proposed by Williamson (1995) and developed at the Massachusetts Institute of Technology (MIT). It is the passive elastic actuator most cited in the area of force control in robotic manipulators. Subsequently, this type of actuator became known as the MIT-SEA by its origin.

Basically, the SEA is an actuator with a spring in series used as flexible or elastic transmission. The spring inserted inside the system can modify the impedance of the actuator at the interaction port, reducing it in order to facilitate the force control, allowing to increase the stability during a dynamic interaction, being able to store energy and absorb shock impacts from the external environment (see Figure 2.3).

Figure 2.3 – Schematic of the SEA.



Source: Adapted from Williamson (1995).

The main characteristics of this type of actuator are (Hurst et al., 2004):

- an energy storage capacity,
- the force control problem turns in a position control problem,

- the risk of transmission damage is reduced,
- a low damping,
- a moderate level of stiffness.

It is known that the more elastic the spring is inserted, the greater the mechanical energy that can be stored. However, this considerably reduces the system impedance, and this is even more significant at high frequencies, clearly affecting the bandwidth of the system.

In the SEA, the force applied is calculated indirectly considering the spring stiffness value and its deflection, which is measured by a position sensor. Therefore, selecting a spring with appropriate stiffness and acceptable working length is essential in case of using a SEA in force control applications.

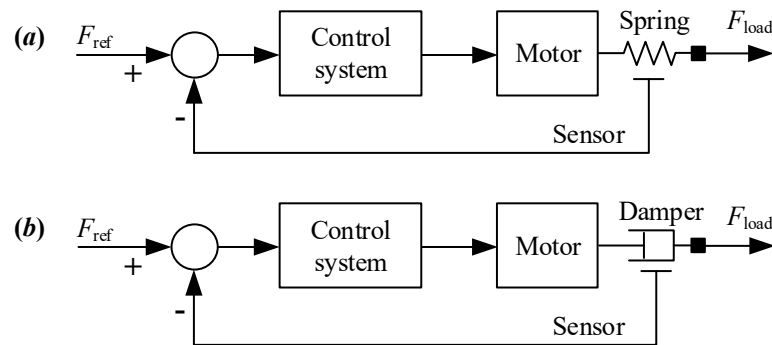
Williamson (1995) established the basic rules for selecting an appropriate spring for the SEA due to the lack of previous guidelines related to this topic. Few years later, Robinson (2000) developed a spring selection procedure based on generalized minimum actuator models and dimensional analysis. These models allowed to analyze the main advantages and disadvantages of using springs as compliant elements. However, in addition to the high conservative force responses, one of the major drawbacks of using mechanical spring as a compliant additive element is the need of more physical space in order to introduce it in series with the actuator. In order to solve this issue, some research projects propose new structural arrangements, such as placing the springs, of different sizes, in a concentric manner to reduce the space occupied (AHN, KYOUNG KWAN et al., 2008; PAINE AND SENTIS, 2012).

2.4.2 Series damping actuators

Force control solutions using Series Damping Actuators (SDA) are as common as SEA (CHEW et al., 2004). In comparison to the SEA, the SDA uses a standard shock absorber for the actuator, which allows it to have an intrinsic shock absorption capability (see Figure 2.4).

In this type of actuators, the damping coefficient can be variable using shock absorbers with magneto-rheological fluid (MR), and it is possible to increase the range of forces that can be applied to the environment. Unlike the SEA, where the applied force is controlled by position variations, the SDA relates the velocity changes with the force to be applied. However, the main disadvantage of this type of actuator is that it is not energy efficient since it only dissipates energy.

Figure 2.4 – (a) Series elastic actuator and (b) Series damping actuator.



Source: Adapted from Chew et al. (2004).

Note: F_{ref} and F_{load} represent the reference force and load force, respectively.

2.4.3 Variable stiffness actuators

This type of actuator has the ability to vary its passive compliance in order to ensure greater adaptability according to the variations of the external environment. Passive compliance, unlike the active compliance, is the most natural way to represent or imitate the animal force control process, allowing to store energy and being intrinsically safer in the interaction with the external environment. The animals store energy in the tendons during the stance phase, and then, this energy is released during knee extension, pushing the body upward and forward at the lift off (ALEXANDER, 1990; FOCCHI, 2013).

The actuator that presents dynamic adaptation characteristic is called Variable Stiffness Actuator (VSA) (VANDERBORGHT et al., 2009). The VSAs can be divided into four groups (HAM et al., 2009):

1. *equilibrium-controlled stiffness*, which can vary its stiffness, dynamically adjusting the position of equilibrium of the spring, e. g. Series Elastic Actuator (SEA);
2. *antagonistic-controlled stiffness*, which is based on two actuators working in parallel in an antagonistic setup. Both actuators have fixed compliance and non-linear force-displacement characteristics;
3. *structure-controlled stiffness*, which is based on the modulation of the effective physical structure to perform the change in stiffness in a staggered form with fixed values;

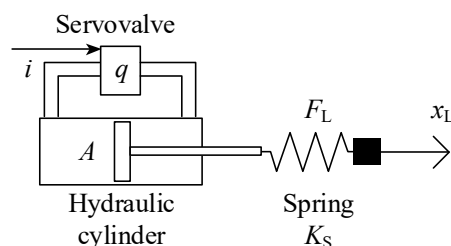
4. *mechanically controlled stiffness*, which is quite similar to the previously case, but can dynamically vary its stiffness.

It is important to highlight that variable stiffness actuators need for a second actuator to perform the change of the main actuator stiffness. Consequently, it is necessary to consume energy to accomplish this task, weakening the main characteristic of passive elasticity systems to be energy efficient. Currently, the main focus of researches related to variable stiffness actuators is to optimize the energy consumption during the stiffness variation of the main actuator, as well as their size (TSAGARAKIS et al., 2011; JAFARI et al., 2013).

2.4.4 Hydro-elastic actuators

Robinson and Pratt (2000) present two study cases using two different linear actuators: one electromechanical and one hydraulic. Both cases use a spring in series as an element that adds passive compliance to the system. The Hydro-elastic Actuator (see Figure 2.5), proposed by Robinson (2000), uses a hydraulic actuator in series with a mechanical spring. However, the name intended for this actuator is, in some way, misleading since it implies that it has a hydro-elastic characteristic, i.e. that the compliance variation is performed using solely hydraulic components, a fact that does not happen in the hydro-elastic actuator proposed by Robinson (2000).

Figure 2.5 – Schematic design of the Hydro-elastic Actuator proposed by Robinson and Pratt (2000).



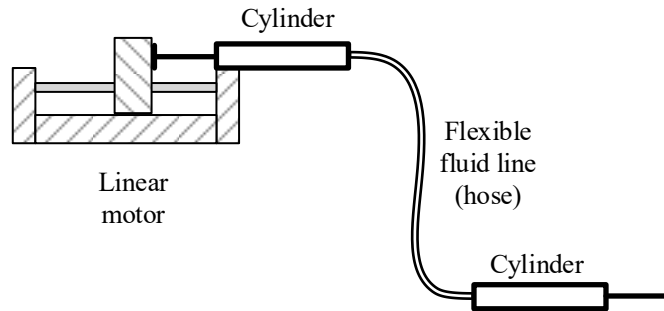
Source: Adapted from Robinson and Pratt (2000).

Note: i represents a current signal; q , the flow rate through the valve; A , the useful area of the piston; F_L , the load force; K_S , the load cell stiffness; and x_L , the load position.

Buerguer (2005) proposed the implementation of a hydraulic transmission in series between a linear actuator and the environment (see Figure 2.6). The researcher aimed to reduce the impedance at the interaction port in order to have a light and compact manipulator with

compliant characteristics. The hydraulic transmission can be considered as an impedance shaper that allows a more compliant behavior through hydraulic means. However, the main disadvantage is the need to estimate the value of hydraulic stiffness through practical tests, given the lack of a validated theoretical procedure that allows its calculation.

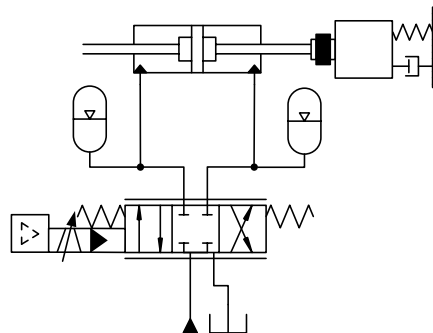
Figure 2.6 – Schematic design of a hydraulic remote manipulator.



Source: Adapted from Buerguer (2005).

There are few studies found in the literature regarding the influence of the incorporation of capacitive elements within a hydraulic actuation system. Wells et al. (1990) analyzed the effects of intrinsic compliance addition in hydraulic systems using accumulators coupled to the cylinder chambers (see Figure 2.7).

Figure 2.7 – Model of double-acting hydraulic actuator with accumulators coupled to the chambers.



Source: Personal collection.

They concluded that the intrinsic compliance affects the settling time during the positioning control and causes the responses to be less damped. Therefore, compliance addition

is detrimental for the performance in hydraulic positioning systems. However, this added compliance is helpful in force control applications.

It should be noted that although the authors studied the harmful effects of adding hydraulic compliance on position control systems, they did not expand the study for the case of force control, which is the main subject of study of this thesis.

2.5 CHAPTER CONCLUSIONS

This chapter presented some concepts related to force control system such as mechanical interaction, causality, passivity and compliance.

While two mechanical system interact, there is a power flow between them that can be described as the product of two power variables which are effort and flow. The nature of each mechanical system defines the causality of the interaction or the relation between the input and output power variable. The passivity analysis is used to verify the stability of the coupled system whenever a mechanical interaction occurs. Finally, the compliance is related to the output impedance at the interaction port and can be shaped through passive and active methods.

This chapter ends describing some passive compliant actuators as an overview of the passive methods used in force control systems.

The following chapter will discuss the force control technique to be used in this thesis.

3 QUANTITATIVE FEEDBACK THEORY

The Quantitative Feedback Theory (QFT) is an engineering method created by Isaac M. Horowitz in the 1960s and characterized by its emphasis on use feedback to satisfy performance specifications, even in the presence of uncertainties in the plant model and unknown disturbances (GARCÍA-SANZ AND HOUPIS, 2007). Uncertain plant does not always mean that it is unknown and, in the practice, parameter uncertainties of the plant model can be limited within known ranges of values (SIDI, 2001). This idea supports the term quantitative used in QFT. Furthermore, both model and disturbance uncertainties as well as performance requirements are managed quantitatively.

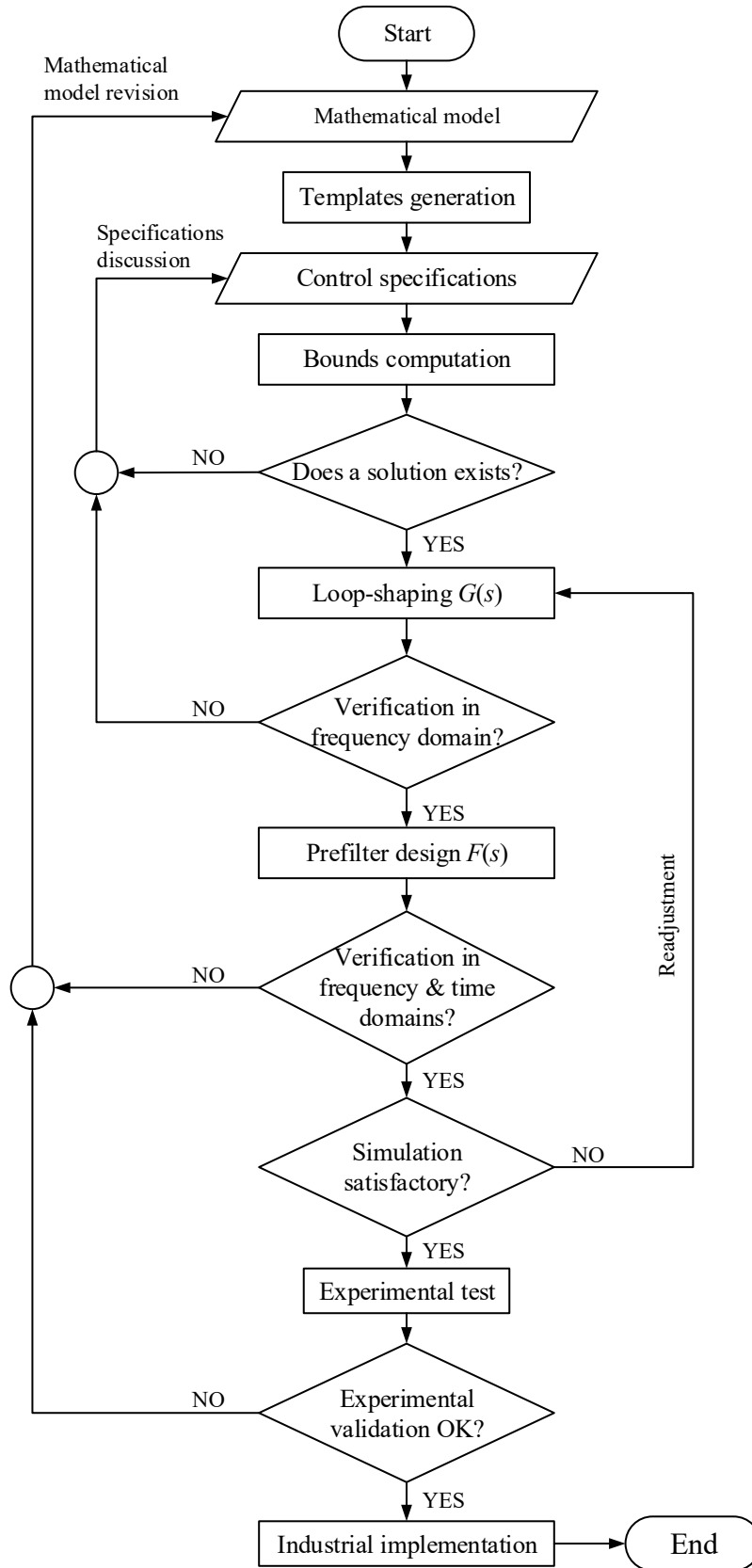
The main objective of this method is to design a controller ($G(s)$) and a prefilter ($F(s)$) with a low-order structure and a minimum bandwidth, satisfying all the performance specifications and disturbance rejection margins for any plant ($P(s)$) under the influence of parametric uncertainties and disturbance inputs (HOUPIS AND RASMUSSEN, 1999; YANIV, 1999; SIDI, 2001).

The performance and disturbance rejection specifications are usually defined in the time domain. However, since QFT works in the frequency domain, all of the specifications must be brought to that domain. The performance specifications describe the expected behavior of the system in front of a given reference input. On the other hand, disturbance rejection margins describe the rejection behavior that the system must have in the front of internal parametric variations and external disturbance inputs within a certain range (YANG AND LEVINE, 1999).

The greatest advantage of the QFT technique is the ability to work with linear or nonlinear plants that have parametric uncertainties within their model and be able to provide low order controllers with fixed and robust gains against various types of disturbances. The literature related to the QFT affirms that the applicability of this technique was demonstrated in several plant types (linear, nonlinear, minimal and non-minimal, variant and time invariant, among others), being an alternative choice when a control technique is needed for a specific application (HOUPIS AND PACHTER, 1997; HOUPIS, 2002).

Figure 3.1 summarizes the QFT methodology for controller design. The technique also allows to go back to any of the previous steps when some modifications are required.

Figure 3.1 – QFT Methodology.



Source: Adapted from García-Sanz (2006).

3.1 FUNDAMENTALS OF THE QUANTITATIVE FEEDBACK THEORY

The QFT methodology is simple and transparent, and several trade-offs can be evaluated in order to achieve the closed-loop system specifications. It is important to highlight that the methodology to be explained in this section represents the classical linear approach of the technique, where the specifications established by the project designer are according to his/her criterion (HOUPIS AND RASMUSSEN, 1999). All the plots shown in the following sections were obtained using the QFT Frequency Domain Control Design Toolbox for Matlab (BORGHESANI et al., 2003).

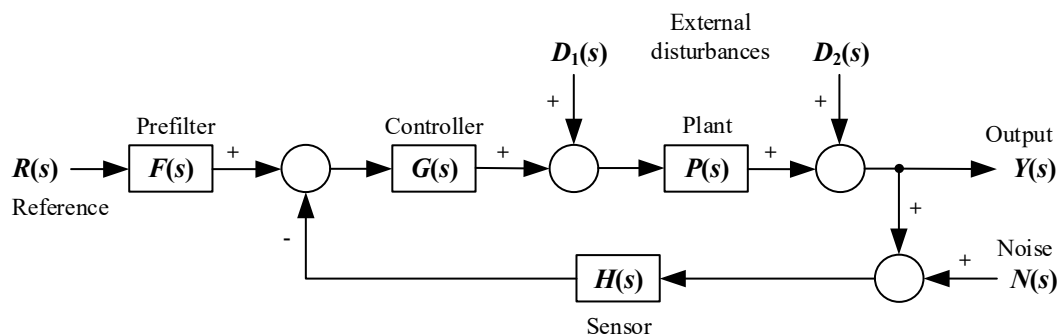
The QFT methodology is composed by some basic steps (HOUPIS AND RASMUSSEN, 1999; YANIV, 1999; GARCÍA-SANZ, 2006), which are:

- templates generation based on a plant model with parameter uncertainties;
- performance specifications in the frequency domain;
- QFT bounds calculation;
- controller design via loop-shaping;
- prefilter synthesis; and
- simulation and design validation.

3.1.1 Templates generation

The QFT technique is based on a two degree-of-freedom (2-DOF) control structure as shown in Figure 3.2.

Figure 3.2 – Two degree-of-freedom (2-DOF) canonical control system.



Source: Adapted from García-Sanz (2005).

Considering Figure 3.2, the QFT-based control design is based on the assumption of the existence of a plant $P(s)$ with parametric uncertainties that belong to a set of plants \mathcal{P} , such that $P \in \mathcal{P}$. Thus, the QFT methodology aims to obtain output responses that are within an acceptable range of values. In order to accomplish the task, the transmission function ($L(s)$) is used as the main design tool, which is defined as:

$$L(s) = G(s)P(s)H(s) \quad (3.1)$$

the relationships shown in equations (3.2) to (3.4) can be extracted. For space reasons, every letter represents a transfer function in the Laplace domain.

$$Y = \frac{GP}{1+GPH}FR + \frac{P}{1+GPH}D_1 + \frac{1}{1+GPH}D_2 - \frac{GPH}{1+GPH}N, \quad (3.2)$$

$$U = \frac{G}{1+GPH}FR - \frac{GH}{1+GPH}(N + PD_1 + D_2), \quad (3.3)$$

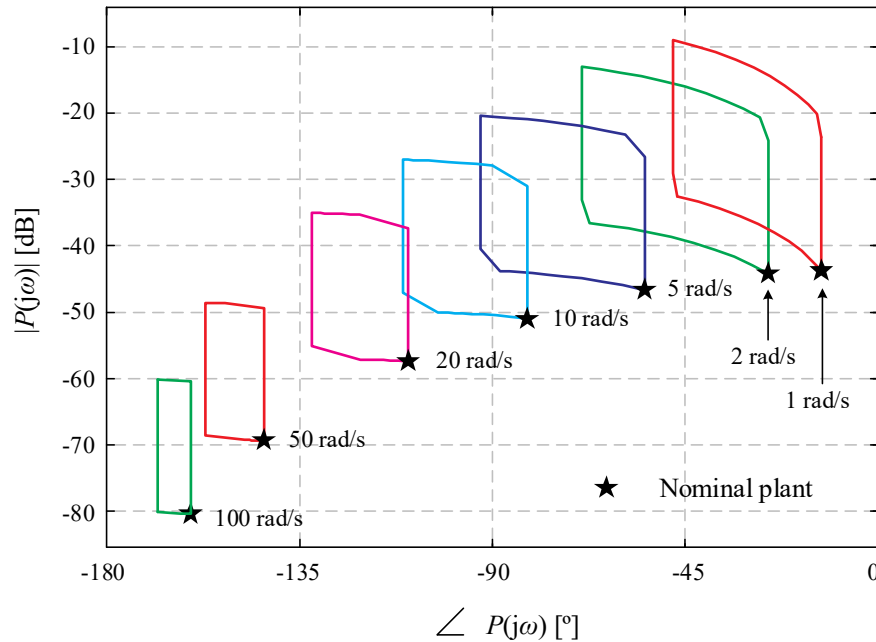
$$E = \frac{1}{1+GPH}FR + \frac{PH}{1+GPH}D_1 - \frac{H}{1+GPH}D_2 - \frac{H}{1+GPH}N, \quad (3.4)$$

where $Y(s)$ is the system output; $G(s)$ represents the controller; $P(s)$, the plant model; $F(s)$, the prefilter; $H(s)$, the sensor dynamics; $R(s)$, the reference input; $D_1(s)$ and $D_2(s)$, the external disturbance inputs; $U(s)$, the controller output; $E(s)$, the error signal; and, $N(s)$, the sensor noise input.

According to García-Sanz (2006), the plant model can be described in frequency response data, or by linear or nonlinear functions, which include the parametric uncertainties. In order to analyze all possible variations of the plant $P(j\omega_i)$ at every frequency $\omega_i \in \Omega_k$, the QFT methodology uses the so-called templates. The Nichols diagram is used to show these regions, being the main graphical tool used by the QFT methodology.

As can be seen in the example shown in Figure 3.3, each template represents a region in the frequency-domain where all possible variations of a plant $P(j\omega)$ are located. The templates also include the nominal plant location, which is marked with a star symbol. All of templates are calculated at specific frequencies $\omega_i \in \Omega_k$, where Ω_k represents the set of frequencies of interest. This set is usually defined considering a frequency range where the system will operate, including the most extreme cases. To establish this frequency range and specify which frequencies will be analyzed via QFT, the project designer should have a basic understanding of the process dynamics.

Figure 3.3 – Example of templates, including the location of the nominal plant, calculated at frequencies of interest and plotted in Nichols diagram.



Source: Personal collection.

All the frequencies under analysis (ω_i) can be equally distributed or divided within Ω_k or can be concentrated around some frequencies of greater interest. This versatility in the selection of frequencies of interest is another advantage of the QFT technique.

In the example shown in Figure 3.3, the set of frequencies of interest is $\Omega = [1, 2, 5, 10, 20, 50, 100]$ rad/s.

The templates calculation can be made using special toolboxes for Matlab (BORGHESANI et al., 2003; DÍAZ et al., 2006). As can be seen in Figure 3.3, the templates area shown as contours. According to the QFT literature, only the template's contour matters for the QFT bounds calculation (MARTÍN-ROMERO et al., 2007). However, this is not automatically performed by the toolboxes, where the templates are calculated considering every variation of the plant as a point located in Nichols diagram, creating a cloud of points. Therefore, this task increases the computational cost during the QFT bounds calculation.

For this reason, the templates calculation (as a contour) is also a topic of some researches focused on improving the computational cost (BAILEY AND HUI, 1989; DÍAZ et al., 2007; MARTÍN-ROMERO et al., 2007).

3.1.2 Performance specifications

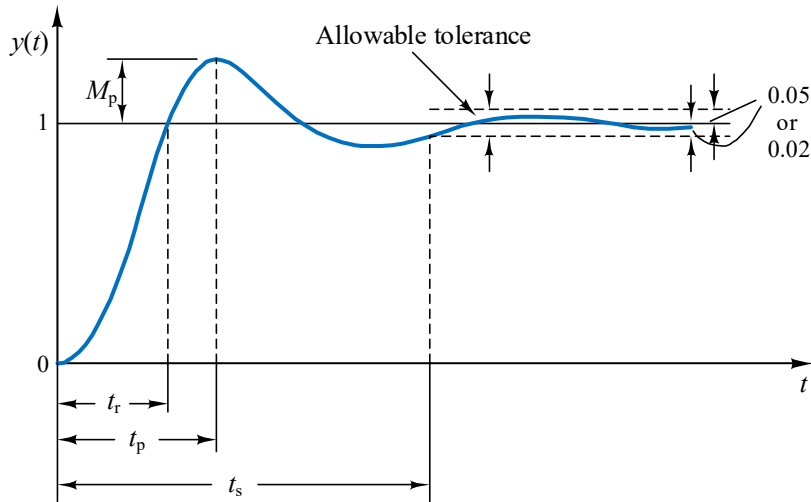
Performance specifications are commonly described in the time-domain and based on a unit-step response of a second-order system (Figure 3.4).

A second-order standard system is defined as:

$$\frac{Y(s)}{R(s)} = \frac{\omega_n^2}{s^2 + 2\xi\omega_n s + \omega_n^2}, \quad (3.5)$$

where ω_n is the undamped natural frequency of the system, and ξ , its damping ratio.

Figure 3.4 – Unit-step response curve showing rise time (t_r), peak time (t_p), maximum overshoot (M_p), and settling time (t_s).



Source: Adapted from Ogata (2010).

Because there is no exact mathematical relationship to do a direct translation from time-domain to frequency-domain, the following empirical relationships are used (OGATA, 2010; NISE, 2011):

$$t_p = \frac{\pi}{\omega_d} \quad \left| \quad \omega_d = \omega_n \sqrt{1 - \xi^2} \right., \quad (3.6)$$

$$t_r = \frac{1}{\omega_d} \tan^{-1} \left(-\frac{\omega_d}{\sigma} \right) \quad \left| \quad \sigma = \xi \omega_n \right., \quad (3.7)$$

$$M_p = 100e^{-\pi(\sigma/\omega_d)}, \quad (3.8)$$

$$\xi = \frac{-\ln(M_p / 100)}{\sqrt{\pi^2 - \ln^2(M_p / 100)}}, \quad (3.9)$$

where t_p represents the peak time; t_r , the rise time; σ , the attenuation, ω_d , the damped natural frequency; and M_p , the maximum overshoot value in percentage. On the other hand, the settling time (t_s) can be defined according to the kind of damping and the percentage error criterion desired (allowable tolerance):

- for undamped case ($0.4 < \xi < 0.8$):

$$t_{s\ 5\%} = \frac{3}{\xi \omega_n}, \quad (3.10)$$

$$t_{s\ 2\%} = \frac{4}{\xi \omega_n}, \quad (3.11)$$

$$t_{s\ 1\%} = \frac{5}{\xi \omega_n}, \quad (3.12)$$

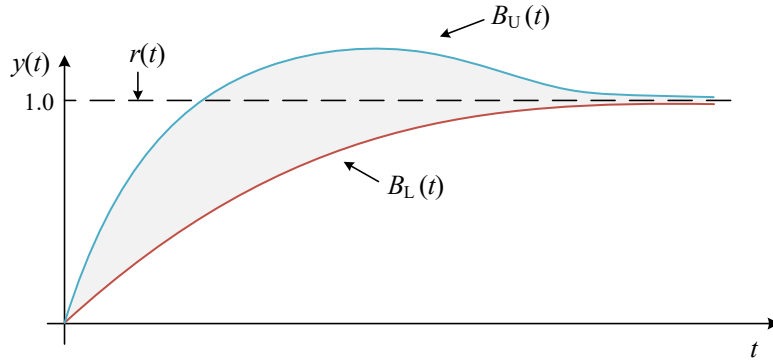
- for critically damped case ($\xi=1$):

$$t_{s\ 2\%} = \frac{6}{\xi \omega_n}. \quad (3.13)$$

Figure 3.5 show the upper and lower performance specifications in time-domain, $B_U(t)$ and $B_L(t)$, respectively, which define a region where the system response can be considered acceptable.

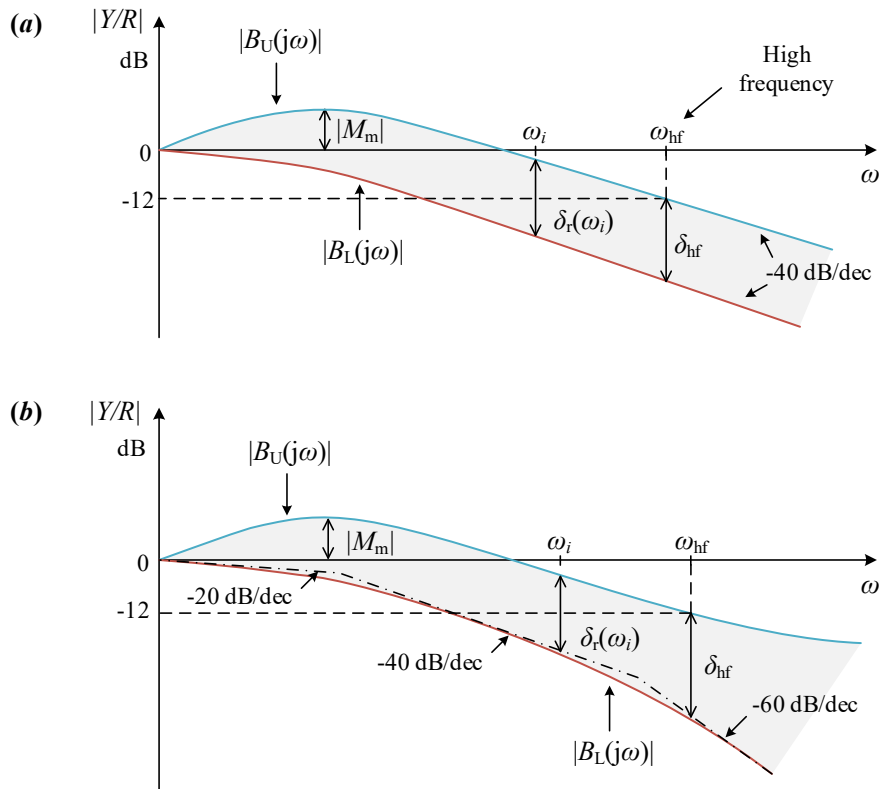
An ideal approximation case will result in two bounds with the same slope of -40 dB/dec, as can be seen in Figure 3.6(a). However, in order to allow to have different order in the controller function, additional zeros and poles can be added to open the acceptable region in high frequencies. Figure 3.6(b) shows an example of an augmented case, with one zero added to the upper bound and one pole added to the lower bound.

Figure 3.5 – Upper ($B_U(t)$) and lower ($B_L(t)$) bounds of the time-domain performance specification defining a region of acceptable system responses.



Source: Adapted from Houpis and Rasmussen (1999).

Figure 3.6 – (a) Ideal approximation case considering a second-order behavior in both of upper ($|B_U(j\omega)|$) and lower ($|B_L(j\omega)|$) bounds; and, (b) Augmented case with the addition of a zero and a pole in high frequencies.



Source: Adapted from Houpis and Rasmussen (1999).

Besides the upper and lower bounds, observing Figure 3.6(a), it is possible to notice the following parameters:

- the maximum peak in magnitude ($|M_m|$), which is closely related with the maximum peak in time-domain (M_p);
- the frequency under analysis ω_i ;
- the frequency that denotes the high frequency region ω_{hf} ;
- the difference in magnitude between the upper and lower limit at the frequency of analysis $\delta_i(\omega_i)$;
- and the difference in magnitude between the upper and lower limit at high frequencies δ_{hf} .

3.1.3 QFT bounds calculation

The QFT bounds are calculated based on frequency specifications called margins. Considering a unitary feedback ($|H(j\omega)| = 1$), the most used margins are explained below (HOUPIS AND RASMUSSEN, 1999; YANIV, 1999; GARCÍA-SANZ, 2005):

- **robust stability margin ($\delta_1(\omega)$)**, which is a constraint used to limit the magnitude of the closed-loop system within a specific Ω_1 set, and is directly related to the gain margin (GM) or the phase margin (PM) of the system (SIDI, 2001);
- **sensitivity margin ($\delta_2(\omega)$)**, related to the disturbance rejection at the plant output. It restricts the magnitude of the sensitivity function ($1/(1+L(j\omega))$) based on a frequencies of interest set (Ω_2), and can be specified using disturbance rejection models (D'AZZO et al., 2003);
- **disturbance rejection margin ($\delta_3(\omega)$)** at the plant input, which constrains the maximum influence of external disturbances at the input of the plant within a Ω_3 set;
- **effort control margin ($\delta_4(\omega)$)**, which is related to the constraint on the control signal, aiming to prevent its saturation, and with Ω_4 as the set of frequencies of interest selected for this margin;

- finally, **tracking margin** ($\delta_{5U}(\omega)$ and $\delta_{5L}(\omega)$) establish the upper and lower limits for tracking, which are based on performance specifications $|B_U(j\omega)|$ and $|B_L(j\omega)|$, and considering a set of frequencies of interest (Ω_5).

Table 3.1 shows the list of equations that describe every margin explained before:

Table 3.1 – Performance specification models (QFT margins).

δ_i	Transfer function based on Figure 3.2	Eq.
$\delta_1(\omega)$	$ T_1(j\omega) = \left \frac{Y(j\omega)}{R(j\omega)F(j\omega)} \right = \left \frac{U(j\omega)}{D_1(j\omega)} \right = \left \frac{Y(j\omega)}{N(j\omega)} \right =$ $= \left \frac{P(j\omega)G(j\omega)}{1+P(j\omega)G(j\omega)} \right = \left \frac{L(j\omega)}{1+L(j\omega)} \right \leq \delta_1(\omega), \quad \omega \in \Omega_1$	(3.14)
$\delta_2(\omega)$	$ T_2(j\omega) = \left \frac{Y(j\omega)}{D_2(j\omega)} \right = \left \frac{1}{1+L(j\omega)} \right \leq \delta_2(\omega), \quad \omega \in \Omega_2$	(3.15)
$\delta_3(\omega)$	$ T_3(j\omega) = \left \frac{Y(j\omega)}{D_1(j\omega)} \right = \left \frac{P(j\omega)}{1+L(j\omega)} \right \leq \delta_3(\omega), \quad \omega \in \Omega_3$	(3.16)
$\delta_4(\omega)$	$ T_4(j\omega) = \left \frac{U(j\omega)}{D_2(j\omega)} \right = \left \frac{U(j\omega)}{N(j\omega)} \right = \left \frac{U(j\omega)}{R(j\omega)F(j\omega)} \right =$ $= \left \frac{G(j\omega)}{1+P(j\omega)G(j\omega)} \right = \left \frac{G(j\omega)}{1+L(j\omega)} \right \leq \delta_4(\omega), \quad \omega \in \Omega_4$	(3.17)
$\delta_{5inf}(\omega)$ and $\delta_{5sup}(\omega)$	$\delta_{5L}(\omega) \leq \left F(j\omega) \frac{L(j\omega)}{1+L(j\omega)} \right = \left \frac{Y(j\omega)}{R(j\omega)} \right \leq \delta_{5U}(\omega), \quad \omega \in \Omega_5$ $\delta_{5L}(\omega) = B_L(j\omega) $ $\delta_{5U}(\omega) = B_U(j\omega) $	(3.18)

Source: Personal collection.

Considering equations (3.14) to (3.18), every QFT margin can be specified by a transfer function or by a constant value. The use of a transfer function implies that the margin is dynamic, so its magnitude varies according to the frequency. On the other hand, a constant value implies that the margin magnitude is maintained along the frequency spectrum.

The QFT margins $\delta_2(\omega)$, $\delta_3(\omega)$ and $\delta_5(\omega)$ are related to the disturbance rejection of the system because as the controller gain increases, the sensitivity of the plant decreases. Therefore, increasing controller gain helps to increase the system disturbance rejection at low frequencies, having a higher bandwidth. However, the sensor noise is amplified at high frequencies only by the controller proportional gain, affecting the system stability. This assertion is demonstrated below.

Assumption 3.1. $|L(j\omega)| = |G(j\omega)P(j\omega)| \gg 1$ at low frequencies.

Assumption 3.2. $|L(j\omega)| = |G(j\omega)P(j\omega)| \ll 1$ at high frequencies.

Proposition 3.1. *If a unitary feedback is considered ($|H(j\omega)| = 1$), the relationship between the control signal and the sensor noise ($U(j\omega)/N(j\omega)$) is filtered by the plant function ($P(j\omega)$) at low frequencies and only affected by the controller gain ($G(j\omega)$) at high frequencies (HOROWITZ, 1988; 2001).*

Proof. Considering the relationship between $U(j\omega)$ and $N(j\omega)$ (Equation (3.3)), we have:

$$\frac{U(j\omega)}{N(j\omega)} = \frac{G(j\omega)}{1 + L(j\omega)}. \quad (3.19)$$

Thus, under the Assumption 3.1, Equation (3.19) becomes:

$$\frac{U(j\omega)}{N(j\omega)} = \frac{1}{P(j\omega)}, \quad (3.20)$$

at low frequencies, having a natural filtering of the sensor noise through the plant itself.

On the other hand, under the Assumption 3.2, Equation (3.19) is simplified to:

$$\frac{U(j\omega)}{N(j\omega)} = G(j\omega). \quad (3.21)$$

Therefore, as the frequency increases ($\omega \rightarrow \infty$) the sensor noise is amplified only by the controller proportional gain, demonstrating this proposition.

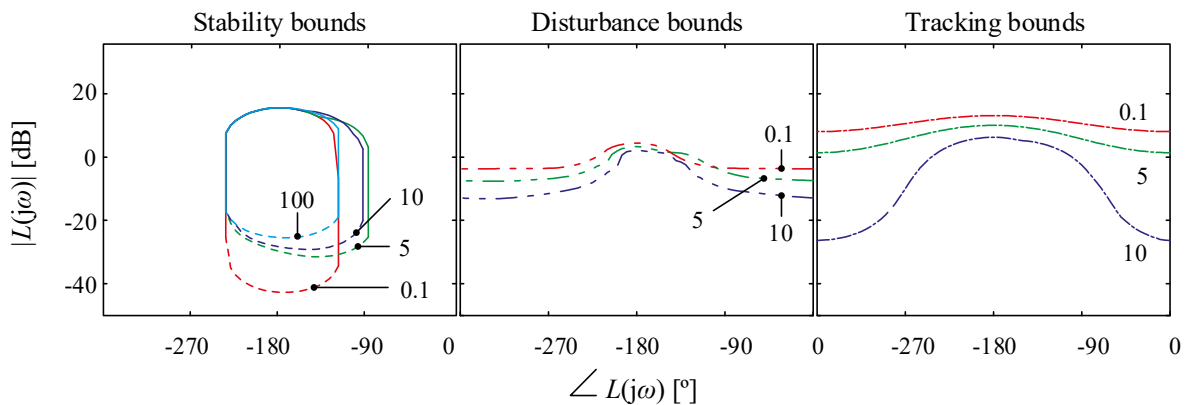
□

Another important consideration is related with the order of the controller. It is important to highlight that a low-order controller may have a higher bandwidth, which allows

the system to have a good reference tracking but considering the Proposition 3.1, it can also be affected by the sensor noise. On the other hand, a high-order controller increases the system robustness, making the system more conservative. However, this approach reduces the tracking capability of the system. Furthermore, the higher the order of the controller, the longer the induced delay time when the controller is discretized for practical implementation. Consequently, exist another trade-off between low-order and high-order controllers (HOUPIS AND PACTER, 1997; YANIV, 1999; HOROWITZ, 2001).

The QFT bounds, for all specifications shown in Table 3.1, can be calculated using some of the QFT toolbox available for Matlab (BORGHESANI et al., 2003; DÍAZ et al., 2005), which have an internal algorithm to make these calculations at every frequency of interest required. As an example of these bounds calculation, Figure 3.7 shows three different kind of bounds calculated at predefined frequencies of interest. Namely, it is the stability bounds based on robust stability margin ($\delta_1(\omega)$) and calculated at $\omega \in \Omega_1 = [0.1, 5, 10, 100]$ rad/s; the disturbance bounds based on sensitivity margin ($\delta_2(\omega)$) and calculated at $\omega \in \Omega_2 = [0.1, 5, 10]$ rad/s; and finally, the tracking bounds based on tracking margins ($\delta_{5L}(\omega)$ and $\delta_{5U}(\omega)$) and calculated at $\omega \in \Omega_5 = [0.1, 5, 10]$ rad/s.

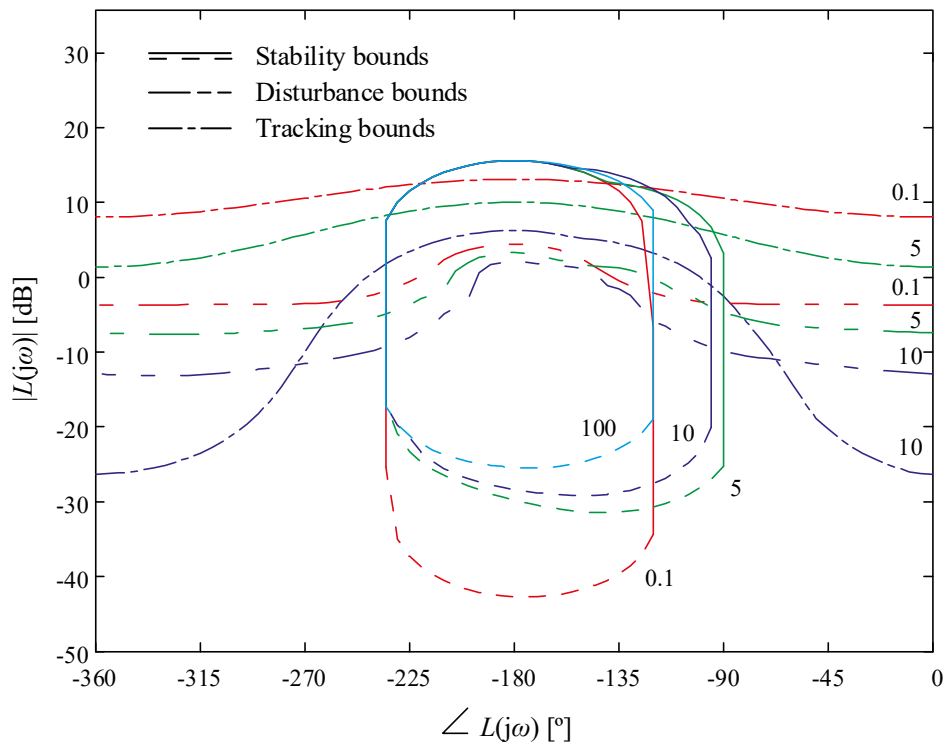
Figure 3.7 – Example of stability bounds calculated at $\omega \in \Omega_1 = [0.1, 5, 10, 100]$ rad/s; disturbance bounds calculate at $\omega \in \Omega_2 = [0.1, 5, 10]$ rad/s; and tracking bounds calculated at $\omega \in \Omega_5 = [0.1, 5, 10]$ rad/s



Source: Personal collection.

Once the bounds were computed, they are grouped (bounds union), and the most restrictive case at every phase is then selected (bounds intersection). This bounds intersection process results in a unique bound that is used for controller design (loop-shaping). Next subsection will explain the loop-shaping process.

Figure 3.8 – Example of bounds union based on Figure 3.7.



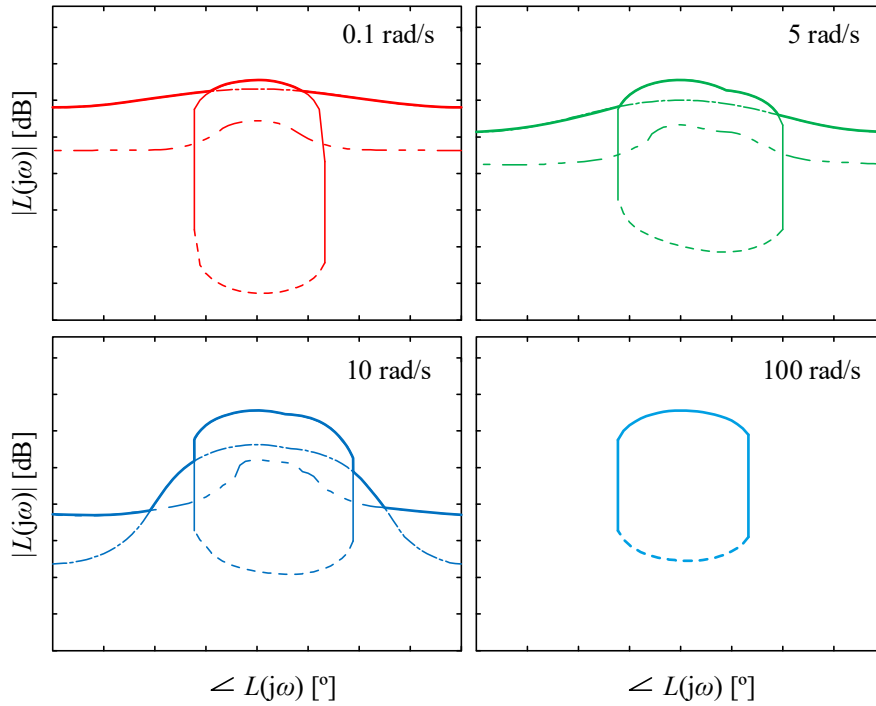
Source: Personal collection.

3.1.4 Loop-shaping

It is already known that each QFT bound is calculated at specific frequencies, which were defined during the performance specifications step. Based on Figure 3.8 and analyzing, separately, all bounds of the same frequency of interest at every phase value, it is possible to see that one of the QFT bounds will always have some regions with greater magnitudes than the others (Figure 3.9). Therefore, if these regions were selected, the result will be a new bound that considers only the most critical case for a particular frequency.

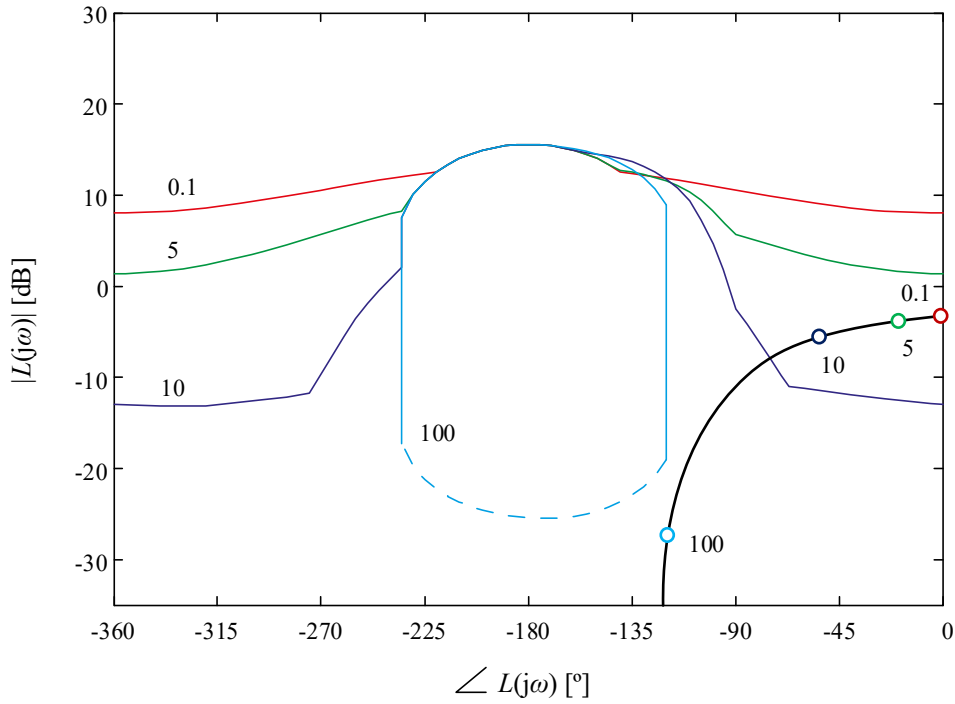
This process is called bounds intersection and the results are shown in Figure 3.9 and 3.10. Based on the bounds intersection results, it is possible to conclude that depending on the frequency under analysis, some performance specifications are more critical than others in some phase regions. Therefore, if the controller ensures that this critical bound is satisfied at that specific frequency, the system will meet all other performance specifications at the same time.

Figure 3.9 – Example of bound intersection process at every frequency of interest.



Source: Personal collection.

Figure 3.10 – Final result of bounds intersection process, including the location of the loop transmission function ($L(j\omega)$).



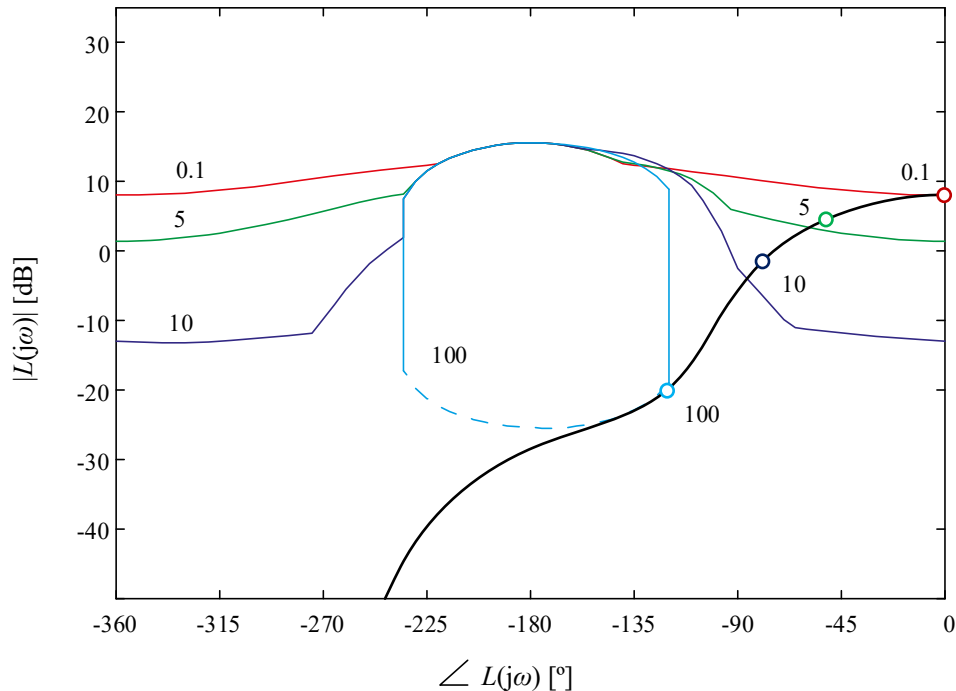
Source: Personal collection.

Figure 3.10 also shows the initial location of the loop transmission function ($L(j\omega)$). Every point of $L(j\omega)$ is calculated at a frequency value, which varies continuously from a very low value to a higher value. Usually this range is selected to be greater than the range specified for Ω , in order to conform a well-defined curve shape. However, each frequency of interest is highlighted, to represent the location of the loop transmission function at that particular frequency. It is also noteworthy that in order to calculate the initial location of $L(j\omega)$ the nominal values of plant parameters are used, and also a unitary gain controller ($|G(j\omega)| = 1$) is assumed. The loop-shaping step starts at this point.

This step is so-called loop-shaping because it comes from the fact that the shape of the loop transmission function changes as the control elements are included.

The objective of the loop-shaping is to synthesize a controller function, which is automatically obtained during the loop-shaping process because it is the product of every control element added until $|L(j\omega)|$ calculated at every $\omega_i \in \Omega$ is greater than the magnitude of the critical bound calculated at the same frequency (Figure 3.11).

Figure 3.11 – Example of loop-shaping in order to synthesize the controller function.



Source: Personal collection.

Since $L(j\omega)$ is function of $P(j\omega)$ and $G(j\omega)$, and as long as a control element is added, the shape will change because $L(j\omega)$ will have new values in magnitude and phase at different

frequencies. The control elements are generic and can be: gains, poles, zeros, complex poles, complex zeros, derivatives, integrators, and its combinations.

3.1.5 Prefilter synthesis

The process of the prefilter synthesis is only necessary when the feedback system need to have tracking capabilities. The mission of the controller is to deal with the disturbance rejection of the system (stability and disturbance rejection). On the other hand, the prefilter is dedicated to deal with the performance (tracking).

Therefore, based on the performance specifications limits ($B_U(j\omega)$ and $B_L(j\omega)$), and considering the maximum and minimum limits of the system closed-loop function ($T_{rU}(j\omega)$ and $T_{rL}(j\omega)$), which are defined as:

$$|T_{rU}(j\omega)| = \max \left| \frac{GPF}{1+GP} \right|, \quad (3.22)$$

$$|T_{rL}(j\omega)| = \min \left| \frac{GPF}{1+GP} \right|, \quad (3.23)$$

the objective of the prefilter synthesis step is to maintain the difference between $|T_U(j\omega)|$ and $|T_L(j\omega)|$ within the acceptable region defined by the difference between $|B_U(j\omega)|$ and $|B_L(j\omega)|$:

$$\Delta |T_r(j\omega)| = |T_{rU}(j\omega)| - |T_{rL}(j\omega)| \leq \delta_r(\omega), \quad (3.24)$$

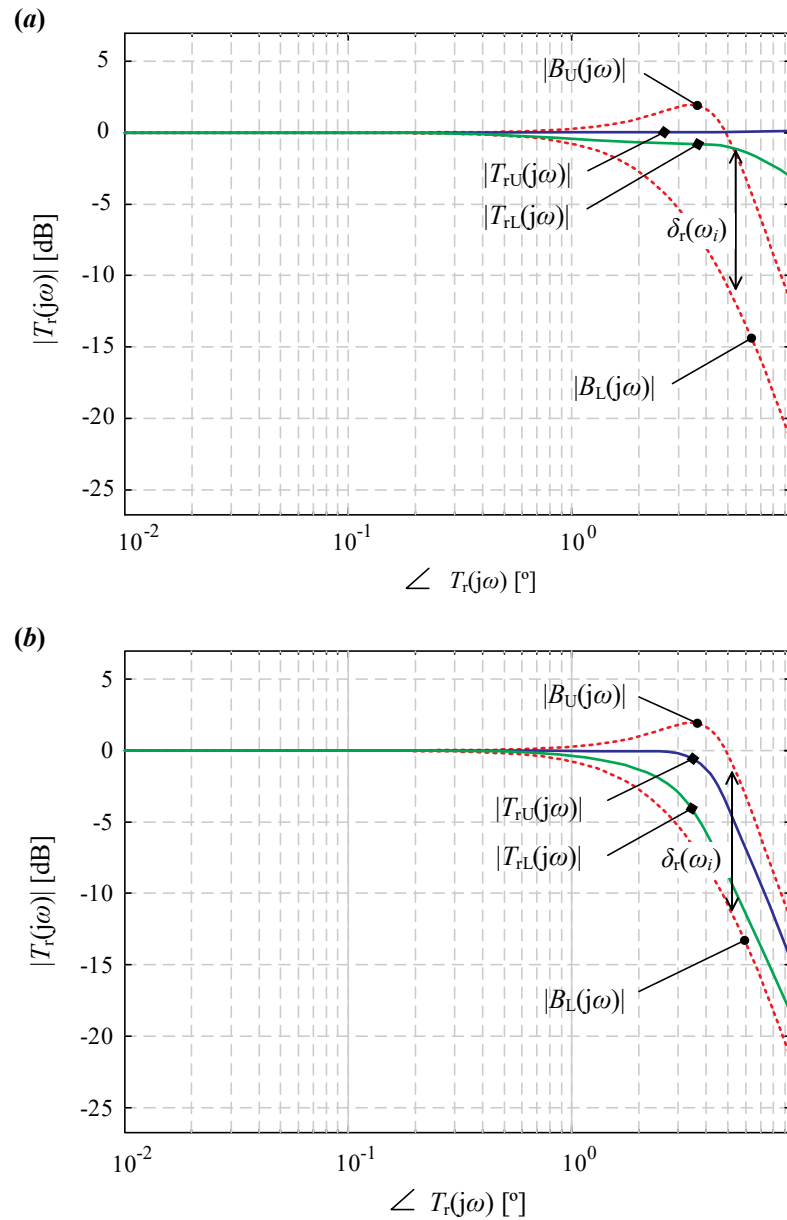
where:

$$\delta_r(\omega) = |B_U(j\omega)| - |B_L(j\omega)|. \quad (3.25)$$

The prefilter synthesis is performed in a similar way of the previous case. However, instead of plotting and modifying the transmission function, in this case the modifications are made on the closed-loop transfer function $|T_r(j\omega)|$.

Therefore, based on an initial condition, where the prefilter acts as unitary gain prefilter $|P(j\omega)|=1$ (Figure 3.12(a)), control elements can be added to the prefilter function in order to modify the final behavior of the system until the difference between $|T_U(j\omega)|$ and $|T_L(j\omega)|$ be within the predefined range.

Figure 3.12 – Example of QFT prefilter synthesis: (a) initial condition with a unitary gain prefilter $|P(j\omega)|=1$, and (b) final condition of the system with the upper and lower limits within the acceptable range after the addition of control elements ensuring the system traceability.



Source: Personal collection.

3.1.6 Simulation and design validation

After the loop-shaping and prefilter synthesis are concluded, it is necessary to analyze the behavior of the system based on simulations. Several tests considering all of the possible variations need to be carried out, especial attention need to be gave to the worst-case scenarios.

If the controller and prefilter successfully meet the performance requirements in all of cases, then they can be tested experimentally in order to validate the results.

3.2 CHAPTER CONCLUSIONS

This chapter shown the fundamentals of the Quantitative Feedback Theory. The QFT is a control technique based on a 2-DOF control structure, where the performance and robustness specifications are managed quantitatively in the frequency domain. Additionally, the QFT methodology was described in this chapter, step by step, as well as the advantages of using this control technique.

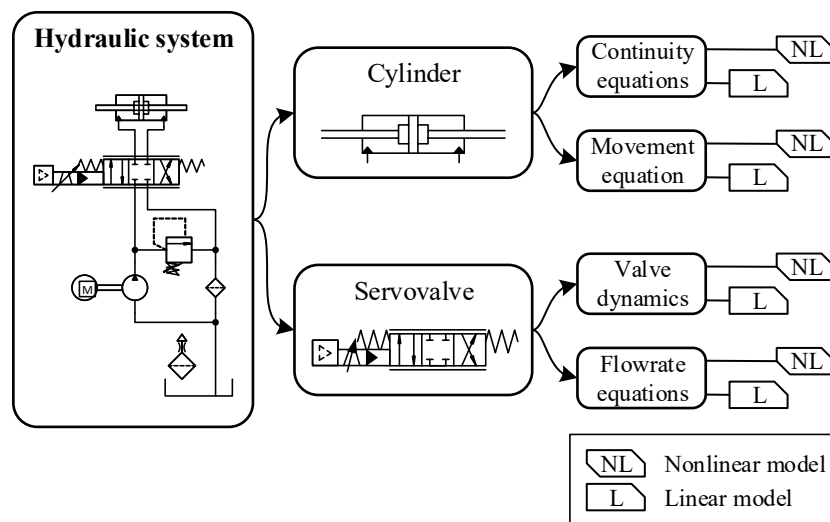
Since the QFT technique can manage nonlinear plants with parametric uncertainties, it was considered useful for controlling a nonlinear system such as the hydraulic force control system.

In order to apply this technique, it is necessary to know how the hydraulic system behaves and, therefore, it must be modelled. The Chapter 4 will deal with this topic.

4 MATHEMATICAL MODELING OF HYDRAULIC ACTUATION SYSTEM

The following section will present the mathematical modeling of a generic hydraulic circuit according to the diagram shown in Figure 4.1. The mathematical model to be carried out in this section will only focus on the servovalve and the cylinder dynamics. Neither the hydraulic power unit nor the rest of components located before the valve will be considered in this modeling.

Figure 4.1 – Diagram of a generic hydraulic circuit showing the parts to be modelled.



Source: Personal collection.

Two kinds of mathematical models are presented in this chapter:

1. a nonlinear model, which is used specifically for simulation in order to obtain realistic force responses;
2. a linear model, for the controller design.

Both models are explained for each component present in the hydraulic circuit. It is noteworthy that this hydraulic circuit belongs to a test rig called Ybitú, which is used in the Laboratory of Hydraulic and Pneumatic Systems (LASHIP) of the Mechanical Engineering Department at Federal University of Santa Catarina. The technical data of each component is presented in Appendix A.

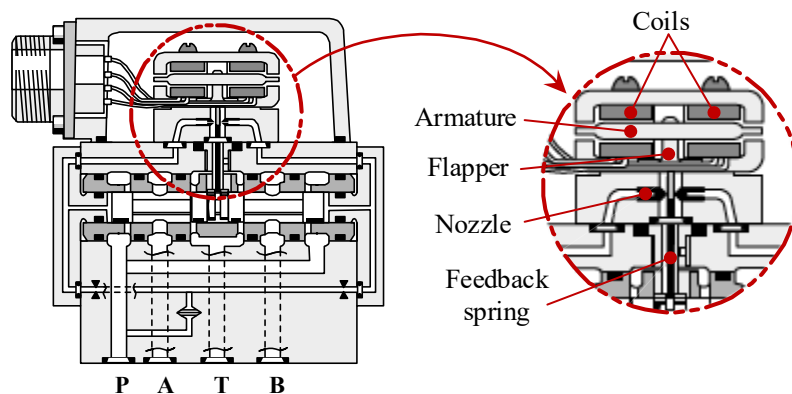
Some considerations need to be defined before initiate the mathematical modeling of the hydraulic system:

- the modeling procedure to be explained in this chapter is generic. Therefore, it can be applied to both symmetrical and asymmetrical combinations of valve and cylinders,
- the valve/cylinder combination used for experimental test in this thesis is symmetrical, i.e. the cylinder is symmetrical, both sides of the piston have identical area, and, consequently, the servovalve to be used has control orifices that are also matched and symmetrical,
- all the mathematical development will be described in a generic mode, and when necessary, it will be focused in the symmetrical case.

4.1 SERVOVALVE

The valve to be analyzed is a two-stage nozzle flapper torque motor servovalve. The hydraulic preamplifier of the valve, known as pilot stage or first-stage, is a symmetrical double-nozzle and flapper driven by a torque motor (see Figure 4.2).

Figure 4.2 – Nozzle flapper torque motor servovalve description (first stage).

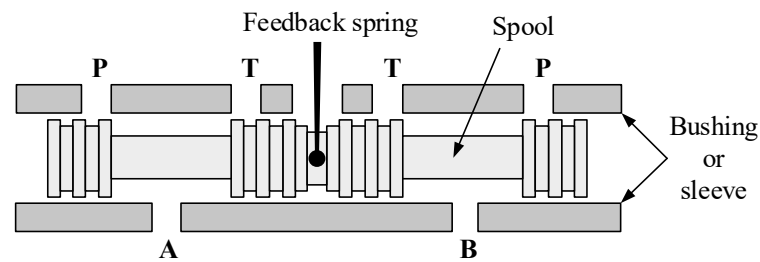


Source: Adapted from Moog (2001) and Moog (2007).

The output stage of the valve is 4-way with closed-center (see Figure 4.3). The two-stage valves are usually classified by the type of feedback used, which in this case is a mechanical spool position feedback provided by a cantilever spring.

In order to reproduce the dynamic behavior of a servovalve, the mathematical model should include two different dynamics, both of them related to each stage of the valve. The first stage model describes the spool motion dynamics analyzed from the control input signal to the spool position, and the second stage model is related to the flowrate dynamics as a consequence of the spool motion produced by the first stage.

Figure 4.3 – Second stage parts description at null position.



Source: Adapted from Moog (2001).

4.1.1 Nonlinear model

The first stage of the servovalve (hydraulic pre-amplifier) could include several dynamics of different domains such as:

- electromagnetics, related to the magnetic forces created by current induction in torque motor coils, which produces the rotation of the armature and the flapper;
- mechanics, since exists a mechanical torque produced during the flexible spring deflection;
- and hydraulics, referred to the hydraulic flowrates inside the nozzles and on the sides of the spool, which produce the motion of the latter.

However, in order to simplify the mathematical model of this first stage, the use of a generic second order function is proposed. This simplification is feasible since the natural frequency of the valve is usually much higher than the other components of the hydraulic circuit and does not affect the representativeness of the model as will be shown in Chapter 6.

The proposed function approximates the dynamic relationship between an input control signal (U_C) and the spool displacement, which is represented here by an equivalent voltage (U_{Csp}), such that:

$$U_C = \frac{1}{\omega_{nv}^2} \frac{d^2 U_{Csp}}{dt^2} + \frac{2\xi_v}{\omega_{nv}} \frac{dU_{Csp}}{dt} + U_{Csp}, \quad (4.1)$$

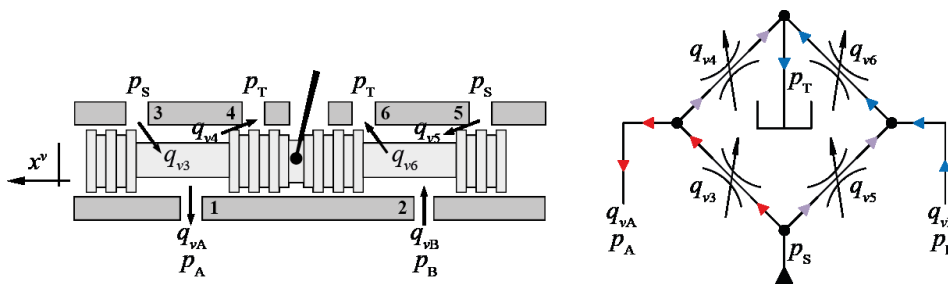
where ω_{nv} is the natural frequency of the valve and ξ_v represents the damping ratio of the valve.

The modeling of the second stage of the valve is focused on the influence of the spool motion on the flow dynamics. Different types of flows arise during the spool motion, which can be represented basically by laminar and turbulent flows. A laminar flow is expected during the overlapping stages of the spool and is related to the leakage flow due to the clearance between the spool and the sleeve. On the other hand, the turbulent flow occurs during the valve opening, or underlapping stages of the spool. Because each type of flow dynamics is represented by different equations, a continuity between them is needed in order to have a model that represent the hydraulic flow dynamics in the whole range of spool displacement.

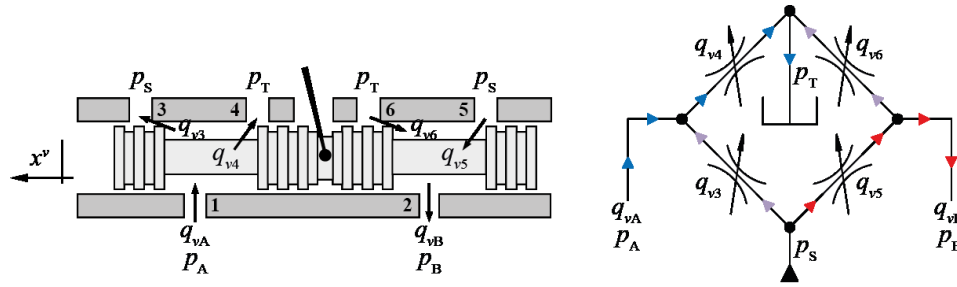
Some researchers have presented nonlinear models improving the representation of the flowrate dynamics within the valve (ERYILMAZ AND WILSON, 2000; FEKI AND RICHARD, 2005; MARÉ AND ATTAR, 2008; XU, 2013). However, the model complexity increases substantially as it becomes more representative of the experimental responses.

In order to maintain a simple model that describes correctly the fluid dynamics in the second stage of the valve, the following mathematical equations are described in equations (4.2) to (4.11) (PEREIRA, 2006; PEREIRA et al., 2008; SZPAK et al., 2010). For modeling purposes, a control voltage signal range of ± 10 V was assumed, where negative and positive voltages result in a corresponding spool displacement, as can be seen in figures 4.4 and 4.5.

Figure 4.4 – Flow rates during a positive displacement of the spool ($U_{Csp} \geq 0$).



Source: Personal collection.

Figure 4.5 – Flow rates during a negative displacement of the spool ($U_{Csp} < 0$).

Source: Personal collection.

Considering a positive spool displacement ($U_{Csp} \geq 0$), and according to Figure 4.4, the flowrates behavior within the valve can be described as:

$$q_{v3} = \text{sign}(p_S - p_A) \left(K_{v3} \frac{U_{Csp}}{U_{Cn}} + K_{vin3} \right) \sqrt{|p_S - p_A|}, \quad (4.2)$$

$$q_{v4} = \text{sign}(p_A - p_T) K_{vin4} \sqrt{|p_A - p_T|}, \quad (4.3)$$

$$q_{v5} = \text{sign}(p_S - p_B) K_{vin5} \sqrt{|p_S - p_B|}, \quad (4.4)$$

$$q_{v6} = \text{sign}(p_B - p_T) \left(K_{v6} \frac{U_{Csp}}{U_{Cn}} + K_{vin6} \right) \sqrt{|p_B - p_T|}. \quad (4.5)$$

where p_A and p_B are the pressures in lines A and B; p_S and p_T represent the supply and the reservoir pressures, respectively; and U_{Cn} is the nominal control voltage.

Since the servovalve is a four-way valve with critical center, symmetrical and matched orifices are usually considered for modeling the second stage. Considering the port number $i = 3$ to 6, $K_{vi} = K_{vp}$, where K_{vp} represents the partial flow coefficient of the valve. Likewise, $K_{vin i} = K_{vinp}$, such that K_{vinp} is the internal partial leakage coefficient (PEREIRA, 2006; PEREIRA et al., 2008; SZPAK et al., 2010).

In case of a negative spool displacement ($U_{Csp} < 0$), and according to Figure 4.5, the flowrates behavior can be described as:

$$q_{v3} = \text{sign}(p_S - p_A) K_{vin3} \sqrt{|p_S - p_A|}, \quad (4.6)$$

$$q_{v4} = \text{sign}(p_A - p_T) \left(K_{v4} \frac{|U_{Csp}|}{U_{Cn}} + K_{vin4} \right) \sqrt{|p_A - p_T|}, \quad (4.7)$$

$$q_{v5} = \text{sign}(p_S - p_B) \left(K_{v5} \frac{|U_{Csp}|}{U_{Cn}} + K_{vin5} \right) \sqrt{|p_S - p_B|}, \quad (4.8)$$

$$q_{v6} = \text{sign}(p_B - p_T) K_{vin6} \sqrt{|p_B - p_T|}. \quad (4.9)$$

In both cases, for $U_{Csp} \geq 0$ and $U_{Csp} < 0$, the following relationships are considered:

$$q_{vA} = q_{v3} - q_{v4}, \quad (4.10)$$

$$q_{vB} = -(q_{v5} - q_{v6}). \quad (4.11)$$

such that q_{vA} and q_{vB} represent the flowrates at ports A and B, respectively. It is important to highlight that the function *sign()* present in equations (4.2) to (4.9) is used to represent the effect of back-pressures in the lines between cylinder and the valve. This function was added in order to have a more realistic representation of the system.

The equations (4.2) to (4.11) presented above are already used at LASHIP due to its reliability. It is noteworthy that this modeling also includes the effects of internal leakage, which is dependent on the spool displacement direction, and have a relatively smooth transition between laminar and turbulent flow equations.

In practice, control signals sent to the servovalve under study are current signals (MOOG, 2007). However, the existence of a voltage/current signal conversion stage in between of the control equipment and the servovalve is considered. From here on after, this thesis assumes that the signal sent to the valve is in voltage. On the other hand, the partial flow coefficient (K_{vp}) and the internal partial leakage coefficient (K_{vinp}) can be, initially, obtained from catalog data using the following equations:

$$K_{vp} = \frac{q_{vn}}{\sqrt{2\Delta p_{tn}}}, \quad (4.12)$$

$$K_{vinp} = \frac{q_{vin}}{\sqrt{2p_{in}}}, \quad (4.13)$$

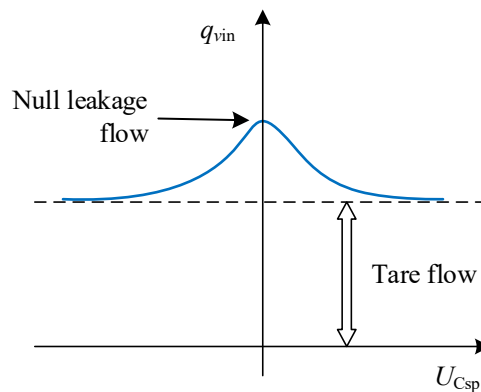
where q_{vn} represents the nominal flowrate at the maximum valve opening (100% command signal) measured at a nominal total valve pressure drop (Δp_{tn}). On the other hand, q_{vin} represents

the nominal internal leakage flowrate measured at a predefined pilot pressure (p_{in}). Both of these values can be obtained from the manufacturer catalog (MOOG, 2007).

Due to the natural high stiffness of the hydraulic transmission, if the actuator applies force over a relatively stiff environment of the same order of magnitude, high force peaks with a very low valve opening of the valve are expected. Therefore, in control force applications, the spool will move, most of the time, around the null position. Since the valve is almost always moving around the the null position, the leakage flowrate adopts an important role in the force control dynamics.

In practice, the leakage flowrate has a nonlinear behavior, being maximum at the null point position, which is the location where the valve supplies zero control flow at zero load pressure drop and decreasing constantly as the valve opens in both ways, as can be seen in Figure 4.6.

Figure 4.6 – Internal leakage flow around the null position.



Source: Personal collection.

The shape of the curve that defines the null leakage flow, which is the leakage flow at zero level of null position (MOOG, 2001), is more related to the edges of the spool and the bushing (sleeve). Its peak increase as the edges of the spool, and the lands of the sleeve, become rounded due to wear and abrasion, or due to some geometrical imperfection in the spool during its manufacturing. On the other hand, the hydraulic amplifier flow, known as tare flow, represents all of the other leakage flows different from the null leakage inside the valve (THAYER, 1962; MOOG, 2001). This additional leakage is unavoidable, but extremely necessary since it is used to supply hydraulic fluid to the first stage, lubricate, and maintain the spool centered with the sleeve as a laminar leakage flow.

Considering Figure 4.6, in order to represent the behavior of the total leakage flowrate (q_{vinT}) within the valve, the following hyperbolic equation is proposed:

$$q_{\text{vinT}} = q_{\text{tare}} + q_{\text{vin}} = q_{\text{tare}} + K_{\text{vinp}} \operatorname{sech}\left(\lambda\left(U_{\text{Csp}}/U_{\text{Cn}}\right)\right)\sqrt{2p_{\text{in}}}, \quad (4.14)$$

where q_{tare} is the tare flow and K_{vinp} value comes from Equation (4.13); q_{vin} is maximum at $U_{\text{Csp}} = 0$, and λ represents a curve-shape coefficient. This last coefficient is used for shaping the simulated leakage flow curve where larger values produces wider curve-shapes and vice versa. From experiments (see Chapter 5), it was observed that λ assumes values near to 100.

It is important to highlight that the values of q_{tare} and K_{vinp} can be, initially, obtained from manufacturer's data, but in practice, K_{vinp} is variable and in function of U_{Csp} . In order to obtain a more realistic representation of the flowrate behavior during the simulations, different values of $K_{\text{vin}i}$ and K_{vi} are required. These coefficients can be obtained through experiments, which will be detailed in Chapter 5.

4.1.2 Linear model

Considering the following assumptions:

Assumption 4.3. All of the valve coefficients K_{vi} and $K_{\text{vin}i}$ are identical and equal to the nominal values K_{vp} and K_{vinp} , respectively. Such that:

$$K_{\text{v3}} = K_{\text{v4}} = K_{\text{v5}} = K_{\text{v6}} = K_{\text{vp}}, \quad (4.15)$$

and

$$K_{\text{vin3}} = K_{\text{vin4}} = K_{\text{vin5}} = K_{\text{vin6}} = K_{\text{vinp}}. \quad (4.16)$$

Assumption 4.4. The control flowrate (q_{vC}) is the average value between q_{vA} and q_{vB} , then:

$$q_{\text{vC}} = \frac{q_{\text{vA}} + q_{\text{vB}}}{2}. \quad (4.17)$$

The control flowrate (q_{vC}) can be represented as:

$$q_{\text{vC}} = \operatorname{sign}(U_{\text{Csp}}) \left(K_{\text{vp}} \frac{|U_{\text{Csp}}|}{U_{\text{Cn}}} + K_{\text{vinp}} \right) \sqrt{\frac{p_{\text{S}} - p_{\text{T}} - \operatorname{sign}(U_{\text{Csp}})p_{\text{L}}}{2}} - \operatorname{sign}(U_{\text{Csp}}) K_{\text{vinp}} \sqrt{\frac{p_{\text{S}} - p_{\text{T}} + \operatorname{sign}(U_{\text{Csp}})p_{\text{L}}}{2}}, \quad (4.18)$$

where $p_L = p_A - p_B$ represents the load pressure. As can be seen in this equation, the control flowrate (q_{vC}) is a function of U_{Csp} and p_L .

Expressing Equation (4.18) as a Taylor' series around a particular operating point i , in order to linearize it, results in:

$$q_{vC} = q_{vCi} + \left. \frac{\partial q_{vC}}{\partial U_{Csp}} \right|_i \Delta U_{Csp} + \left. \frac{\partial q_{vC}}{\partial p_L} \right|_i \Delta p_L + \dots \quad (4.19)$$

Analyzing near to the vicinity of the operating point, the higher order infinitesimals of the Taylor's series are significantly small and can be neglected (MERRIT, 1967). Therefore, Equation (4.18) can be written as:

$$q_{vC} - q_{vCi} \equiv \Delta q_{vC} = K_{qUi} \Delta U_{Csp} - K_{ci} \Delta p_L, \quad (4.20)$$

where:

$$K_{qUi} = \left. \frac{\partial q_{vC}}{\partial U_{Csp}} \right|_i = \frac{K_{vp}}{U_{Cn}} \sqrt{\frac{(p_S - p_T - \text{sgn}(U_{Cspi}) p_{Li})}{2}}, \quad (4.21)$$

and

$$K_{ci} = \left. \frac{\partial q_{vC}}{\partial p_L} \right|_i = \frac{K_{vp}}{\sqrt{8}} \frac{|U_{Cspi}|}{U_{Cn}} \sqrt{\frac{1}{p_S - p_T - \text{sgn}(U_{Cspi}) p_{Li}}} + \frac{K_{vimp}}{\sqrt{8}} \left(\sqrt{\frac{1}{p_S - p_T - \text{sgn}(U_{Cspi}) p_{Li}}} + \sqrt{\frac{1}{p_S - p_T + \text{sgn}(U_{Cspi}) p_{Li}}} \right), \quad (4.22)$$

such that K_{qUi} is the flow-voltage gain at operating point i ; and K_{ci} is the flow-pressure coefficient at operating point i .

According to Merrit (1967), the null position ($U_{Csp} = p_L = 0$) is the most critical from a stability viewpoint and the system should be stable at all operating points if it is stable at this null point. The valve coefficients evaluated at this point are called null valve coefficients. Therefore, applying the Laplace transform in Equation (4.20) and considering the null valve coefficients, results in:

$$Q_{vC}(s) = K_{qU0} U_{Csp}(s) - K_{c0} P_L(s). \quad (4.23)$$

In the same way, Equation (4.1) can be described in terms of the Laplace domain, giving:

$$U_{Csp}(s) = \frac{\omega_{nv}^2}{s^2 + 2\xi_v \omega_{nv} s + \omega_{nv}^2} U_C(s). \quad (4.24)$$

4.2 CYLINDER

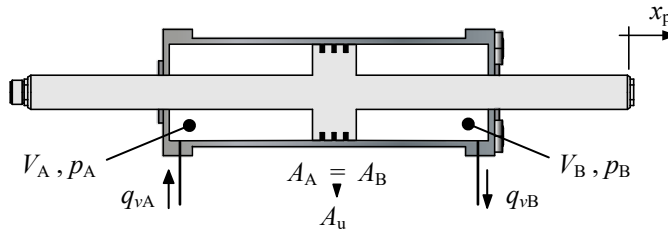
The dynamic behavior of this component can be described based on two main dynamics: hydraulic and mechanical, respectively. The hydraulic dynamics inside the cylinder chambers is described using the continuity equation, which is based on the mass conservation principle. Moreover, the mechanical dynamics uses the motion equation, which is based on the second Newton's law, to describe the motion of cylinder rod.

It is important to highlight that the cylinder used during the experiments and modelled in this section is a double acting and double rod type, which simplifies the mathematical modeling, especially during the process for obtaining the linear model.

4.2.1 Nonlinear model

Considering the Figure 4.7:

Figure 4.7 – Detail of flowrates and pressures inside the cylinder.



Source: Personal collection.

and based on the mass conservation principle, we have:

$$q_{vA} = \frac{dV_A}{dt} + \frac{V_A}{\beta_e} \frac{dp_A}{dt}, \quad (4.25)$$

$$q_{vB} = \frac{dV_B}{dt} - \frac{V_B}{\beta_e} \frac{dp_B}{dt}, \quad (4.26)$$

where V_A and V_B represent the volume inside the chamber A and B, respectively; and, β_e is the effective bulk modulus of the system.

The volumes V_A and V_B vary linearly with the (x_p) and are described as:

$$V_A = V_{A0} + A_A x_p \quad (4.27)$$

$$V_B = V_{B0} + A_B (L - x_p) \quad (4.28)$$

where V_{A0} and V_{B0} are called dead volumes and they are associated with the volume of fluid inside pipes or hoses that are coupled to each cylinder chamber; and L represents the cylinder stroke. On the other hand, $A_A = A_B = A_u$ represents the area of each side of the piston, which in this case, and due to the cylinder symmetry is called useful piston area (A_u).

The piston dynamics can be calculated using the Newton's second law as follows:

$$A_A p_A - A_B p_B = A_u (p_A - p_B) = M_t \frac{d^2 x_p}{dt^2} + F_{fr} \left(x_p, \frac{dx_p}{dt} \right) + F_e \quad (4.29)$$

such that M_t represents the total mass displaced by the piston; F_{fr} is related to the friction forces; and F_e is the measured force or the applied force. As can be seen in Equation (4.29), F_{fr} is a function of the position (x_p) and velocity (dx_p/dt) of the piston, and also it has a nonlinear behavior, whose modeling is discussed below.

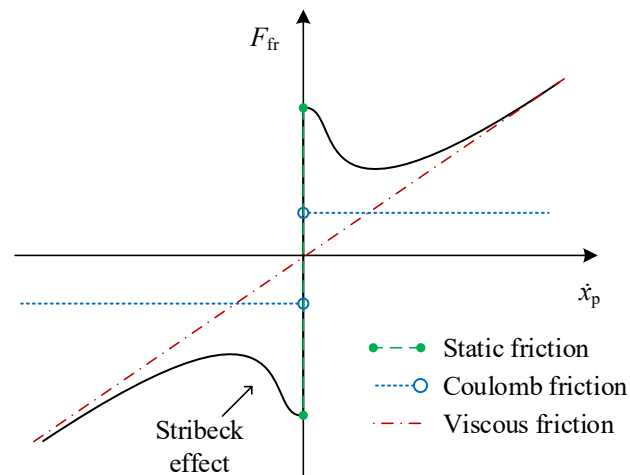
4.2.1.1 Friction force model

Friction is a complex phenomenon that exhibits many nonlinear features that affect the overall system performance and it is difficult to describe analytically (BARAHANOV AND ORTEGA, 2000; VALDIERO, 2005). Friction forces in hydraulic actuators appears mainly due to the contact between the piston seals and the cylinder body, but also can be increased by the presence of friction forces in external guides (PERONDI, 2002). The characteristics of friction forces depend on several factors, such as piston position and velocity, oil temperature in the chambers, fluid viscosity, load pressure, roughness of contact surfaces, seal forms and materials (PERONDI, 2002; VALDIERO, 2005; YANADA AND SEKIKAWA, 2008; TRAN et al., 2012).

Understanding friction, its modeling and identification, is a topic of several researches since the 18th century (ARMSTRONG-HÉLOUVRY et al., 1994). There is no universal friction model. Nevertheless, there are two modeling approaches widespread in the literature: the static and the dynamic friction models. Static models try to represent the friction considering the relationship between the frictional force, in steady-state, and the piston velocity, which is commonly represented by a static friction map. On the other hand, dynamic models aim to represent the instantaneous change in frictional force due to an instantaneous change in velocity.

A static friction model is usually represented as the combination of Coulomb friction, static friction, viscous friction, and Stribeck effect (see Figure 4.8).

Figure 4.8 – Typical static friction model with different phenomena, such as Coulomb friction, static friction, viscous friction and Stribeck effect.



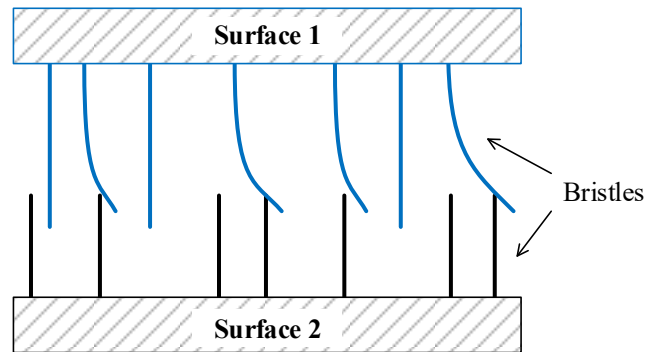
Source: Personal collection of Author.

Dynamic friction models, instead, gain more interest along the years because the classical static model cannot describe the hysteretic behavior of a system during nonstationary velocities, neither the variations in the break-away forces nor small displacements that occur at the contact interface during static friction (stiction) (CANUDAS DE WIT et al., 1995).

The dynamic friction model used in this dissertation is the LuGre model (CANUDAS DE WIT et al., 1995). This model is based on the Dahl model, which describes the friction dynamics as a spring-like behavior (DAHL, 1968). According to Canudas de Wit *et.al.* (1995), the Dahl model is basically the Coulomb friction with a lag every time that the direction of motion changes, but without including the Stribeck effect. As the Dahl model, the LuGre model describes the friction considering the interaction between two rigid bodies that make contact

through elastic bristles, as can be seen in Figure 4.9. Whenever exists a relative motion between the surfaces, a deflection of the bristles will occur. If the force is large enough, some of the bristles deflect so much that they will slip, reducing the reaction force.

Figure 4.9 – LuGre model assumption of the friction interface between two surfaces considering it as the contact between bristles.



Source: Adapted from Canudas De Wit et al. (1995).

However, the LuGre model introduces an additional state variable (z), related to the average deflection of the bristles, which can be modeled as:

$$\frac{dz}{dt} = v - \frac{|v|}{g(v)} z, \quad (4.30)$$

$$g(v) = F_C + (F_S - F_C) e^{-(v/v_s)^\alpha}, \quad (4.31)$$

where v represents the relative velocity between the surfaces; F_C , the Coulomb friction; F_S , the stiction; v_s , the Stribeck velocity; and α , which defines the Stribeck curve. Originally, the value proposed for α was 2 (CANUDAS DE WIT et al., 1995), however in order to generalize the Equation (4.31) several authors proposed to maintain α as another parameter to be obtained (LAMPAERT et al., 2002; YANADA AND SEKIKAWA, 2008; TRAN et al., 2012).

The first term of Equation (4.30) is related to the deflection of the bristles, and the second term is related to the Stribeck effect (CANUDAS DE WIT et al., 1995). Thus, the LuGre friction force expression is:

$$F_{fr} = \sigma_0 z + \sigma_1 \frac{dz}{dt} + \sigma_2 v, \quad (4.32)$$

where σ_0 represents the stiffness of the bristles; σ_1 , the bristle's damping coefficient; and σ_2 , the viscous friction coefficient.

At this point, it is important to notice that the LuGre model depends basically on $g(v)$ function, and σ_0 , σ_1 , and σ_2 parameters. The parameters σ_0 and σ_1 are related with the bristle dynamics. On the other hand, the parameters σ_2 , F_C , F_S , and α are static parameters, which can be obtained by measuring the steady-state friction force (F_{frSS}) when the velocity is held constant. In case of steady-state motion, the relationship between the friction force and the velocity is described by (CANUDAS DE WIT et al., 1995):

$$F_{\text{frSS}} = \text{sign}(v) \left(F_C + (F_S - F_C) e^{-(v/v_s)^\alpha} \right) + \sigma_2 v. \quad (4.33)$$

4.2.2 Linear model

Since the cylinder is symmetric, the linear model of the continuity equation can be represented as:

$$Q_{vC}(s) = A_u s X_p(s) + \frac{V_T}{4\beta_e} s P_L(s) \quad (4.34)$$

such that V_T represents the. Equation (4.34) strictly occurs when the rod cylinder is located at the center of the total stroke, so $V_A = V_B = V_T/2$. This equation is traditionally considered as the linear model of a symmetric cylinder (MERRIT, 1967).

In case of motion equation, considering only a viscous friction (B), its linear model results in:

$$A_u P_L(s) = (M_t s^2 + Bs) X_p(s) + F_e(s) \quad (4.35)$$

In Chapter 6 some considerations will slightly modify these linear cylinder equations.

4.3 HOSE

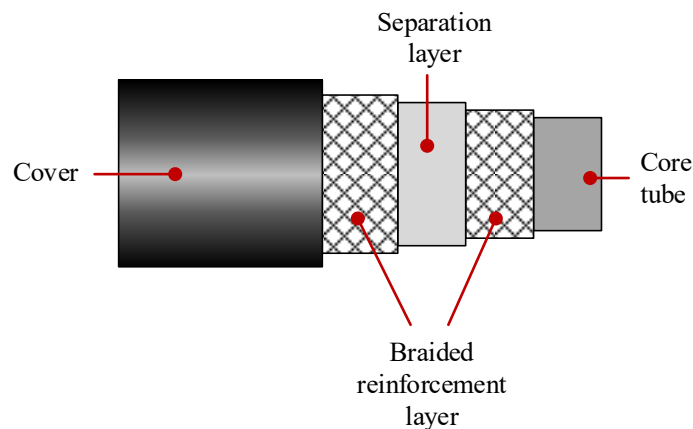
The effects of flexible hoses on the dynamics of hydraulic systems is well known. Beside the mechanical flexibility of hoses, allowing a fast installation in a hydraulic circuit, maybe the main perceptible dynamic effect is the reduction of effective bulk modulus and, consequently, the reduction of the hydraulic stiffness of the system. This allows to use hoses in

applications that require to reduce the pressure fluctuation in the line, and consequently the structural vibration and noise inside a hydraulic system, e.g. power steering (DREW et al., 1997; 1998; WAY, 2004).

Hoses have two main intrinsic characteristics: elasticity (compliance) and viscoelasticity. The hose elasticity allows to store fluid energy as the pressure inside the hose increases, affecting the magnitude of the effective bulk modulus. The viscoelasticity, instead, is more related with a dissipative behavior, providing a damping effect. This latter behavior is strongly frequency-dependent, ratifying the complex behavior of the hose (HÖLCKE, 2002).

All of the characteristics discussed before are related to the different constituent materials of hoses. An industrial hose is made of different materials disposed in many layers. Each material layer affects the fluid dynamics inside the hose in a particular manner (see Figure 4.10).

Figure 4.10 – Generic layers found in a braided hose.



Source: Personal collection.

The dynamic behavior of braided hoses has been studied by years. The researches about this topic include several kinds of analysis such as the elastic strains in the braid thread materials, the effect of braid angles, hose materials, storage and dissipative characteristics, lag times and filter dynamic effects (ENTWISTLE AND WHITE, 1977; ENTWISTLE, 1981; HÖLCKE, 2002).

Entwistle and White (1977) proposed a method for achieving effective load transfer between the inner and outer layers of a two-layer braided high-pressure hydraulic hose. Their analysis demonstrated the influence of the braid angles at load-sharing compatibility between

the layers of a braided high-pressure hose and how it is geometrically possible to improve this load-sharing by laying the braids at different angles.

Entwistle (1981) presented an analysis related to the expansion in hose length and in the strain of the braid wire when the system is under pressure, and how these expansions affect the dynamic behavior of the hose.

Hölcke (2002) focused his study into the development of a method for measuring the volumetric expansion in hoses as a dynamic response to frequency of the input pressure, and also in propose dynamic models that describe the behavior of rubber hydraulic hoses.

In order to determine the hose volumetric expansion and its modeling, Hölcke (2002) considered the influence of several intrinsic characteristics or factors when the hose is under pressure, such as:

- compression of the oil in the hose,
- compression of the rubber in the inner tube itself,
- bulging of the rubber between the threads in the steel cording,
- strain on the threads in the steel cording, and
- movement in the steel cording.

The sum of all factors indicated before contribute into the hose volumetric expansion.

Drew et al. (1998) presented a theoretical model of flexible hose containing a tuner, which is used to minimize the pressure ripple in hoses used in automotive power steering systems. Their model was used to derive a frequency-dependent impedance matrix that defines the relationships between pressure and flow ripples at both ends. However, the model also considered:

- the interaction between the hose wall and the fluid motion,
- the leakage through the walls of the tuner, and
- the frequency-dependent viscous effects.

Their experimental validation had shown an excellent agreement up to 1 kHz of frequency range. Besides the fact that their analysis was made for a particular kind of hose and application, the mathematical foundation were useful for a most recent researches, such as Johnston (2006) and Johnston et al. (2010).

In Johnston (2006), a dynamic model of a liquid-filled hose is presented. The model, developed by the author, is a time-domain model that can successfully represent the dynamic pressure and flow characteristics in flexible hoses. This model was mainly focused to represent rapid transients; however, it can also represent steady state characteristics.

In Johnston et al. (2010), a method for measuring the impedance matrix and the dynamic properties of a liquid-filled flexible hose is described. The results of experimental tests included several different hose types. Some important conclusions were that the dynamic bulk modulus and the axial stiffness values were found to be considerably higher than the statically measured values. The results shown in the paper provide also representative values that can be used in system modeling.

The hose model used in this thesis is the time-domain model presented by Johnston (2006). This model is loosely based on the transmission line method (TLM) and a recursive method is used to obtain a faster numerical approximation. Before explaining in detail, the hose modeling used in this thesis, some concepts and methods used for dynamic modeling in pipelines are described below.

The most widespread techniques found in literature for dynamic modeling of the laminar flow in pipelines are (WATTON AND TADMORI, 1988; SOUMELIDIS et al., 2005; JOHNSTON, 2012):

- *Method of Characteristics (MOC)*. In this method, the characteristic lines are analyzed, which are related to the motion of waves travelling at sound speed in both directions along the pipe (FOX, 1977). It is an accurate method usually suitable for fixed time-step solvers, when constant properties are considered. However, variable time-step solvers can be used if it is combined with an interpolation technique (WYLIE AND STREETER, 1978).
- *Lumped-element method (LEM)*. This method tries to describe the dynamic behavior of the transmission line by a series of lumped parameter such as resistor/inductor/capacitor (RLC). This simplification produces a simplified mathematical model with acceptable accuracy (RABIE, 2009).
- *Finite-element method (FEM)*. This method consists in mathematically discretizing the region of interest and replacing state variables with simple approximations (TAYLOR, 1998). The finite-element method has the advantage over the MOC because it is possible to use variable time-step numerical integration scheme. In

addition, the properties may vary along the line and over time, being easily incorporated (SANADA et al., 1993).

- *Modal approximation (MA)*. This method proposes the use of distributed-parameter model in order to represent the fluid transmission line dynamics (SOUMELIDIS et al., 2005).
- *Transmission Line Method (TLM)*. This method is similar to the MOC, with the difference that TLC method calculates the power variables (pressure and flow) at both ends of the pipeline and not at any internal nodes such as MOC method.

According to Johnston (2006), if the hose downstream pressure (p_{dw}) and the upstream flowrate (q_{up}) are set, the upstream pressure (p_{up}) and downstream flowrate (q_{dw}) can be approximated by:

$$p_{up}(t) = Z_1(f_1(t) - g_1'(t)) + Z_2(f_2(t) - g_2'(t)), \quad (4.36)$$

$$q_{dw}(t) = A_{ho}(f_1'(t) + g_1(t) + f_2'(t) + g_2(t)), \quad (4.37)$$

such that:

$$Z_i = \rho c_i, \quad (4.38)$$

$$f_1(t) = q_{up}(t) / (A_{ho}(1 - N_2 / N_1)) - g_1'(t), \quad (4.39)$$

$$f_2(t) = q_{up}(t) / (A_{ho}(1 - N_1 / N_2)) - g_2'(t), \quad (4.40)$$

$$g_1(t) = \frac{-p_{dw}(t) + 2Z_2 f_2'(t) + (Z_1 + (N_1 / N_2)Z_2) f_1'(t)}{Z_1 - (N_1 / N_2)Z_2}, \quad (4.41)$$

$$g_2(t) = \frac{-p_{dw}(t) + 2Z_1 f_1'(t) + (Z_2 + (N_2 / N_1)Z_1) f_2'(t)}{Z_2 - (N_2 / N_1)Z_1}, \quad (4.42)$$

where Z_i represents the hose characteristic impedance; ρ , the fluid density; c_i , the speed of wave i ; A_{ho} , the cross-sectional area of the fluid passageway in the hose; N_i , the modal ratio between the wall and fluid velocity for wave i ; f_i and g_i are the waves travelling in the forward and reverse direction; and finally, $f_1'(t)$ and $g_1'(t)$ are the delayed and attenuated waves, which can be obtained using the convolution theorem.

In the recursive method, proposed by Johnston (2006), the convolution integral is replaced by:

$$h'_i(t) = \sum_{n=1}^N w_{i,n}(t - T_i), \quad (4.43)$$

where $h'_i(t)$ represents the functions $f'_1(t)$ or $g'_1(t)$, N is the number of exponential weighting functions, T_i represents the time delay, and $w_{i,n}$ can be obtained from the numerical solution of:

$$dw_{i,n}(t)/dt = a_{i,n}h_i(t) - b_{i,n}w_{i,n}(t), \quad (4.44)$$

such that, $a_{i,n}$ and $b_{i,n}$ are coefficients calculated from non-dimensional values presented in (JOHNSTON, 2006)¹.

4.4 FORCE SENSOR

The force applied (F_e) can be calculated using:

$$X_L F_e(s) = K_S (X_p(s) - X_L(s)), \quad (4.45)$$

where K_S is the load cell stiffness, and X_L represents the position of the load or environment.

4.5 CHAPTER CONCLUSIONS

This chapter presented the mathematical modeling of a hydraulic force control system. The main components of the system were modeled, such as the servovalve, the cylinder, hoses, and the environment. Nonlinear and linear models were described throughout this chapter, and each of them is designed for different purposes. The nonlinear model was made in order to simulate the behavior of the plant in a realistic way and the linear model is proposed for the controller design. In order to validate the mathematical model proposed in this chapter, it is necessary to carry out experimental tests, which are described in Chapter 5.

¹ The hose simulation model implemented in Matlab/Simulink and used in this thesis is available at <http://people.bath.ac.uk/ensdnj/models/hose.html>.

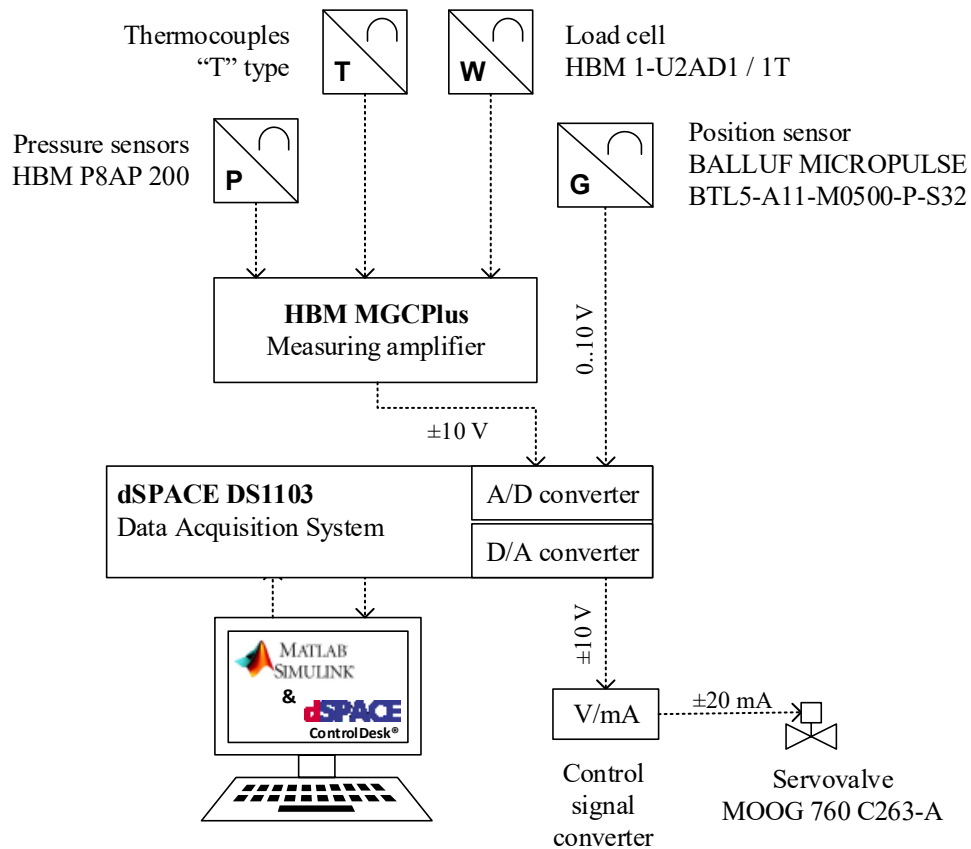
5 TEST RIG AND MODEL VALIDATION

5.1 DESCRIPTION OF TEST RIG

The experimental setup used for this thesis is called Ybitú and belongs to the Laboratory of Hydraulic and Pneumatic Systems (LASHIP), which is part of the Mechanical Engineering Department at the Federal University of Santa Catarina (UFSC).

Figure 5.1 shows the schematic of the data acquisition system in the test rig.

Figure 5.1 – Schematic of the data acquisition system of the test rig Ybitú.

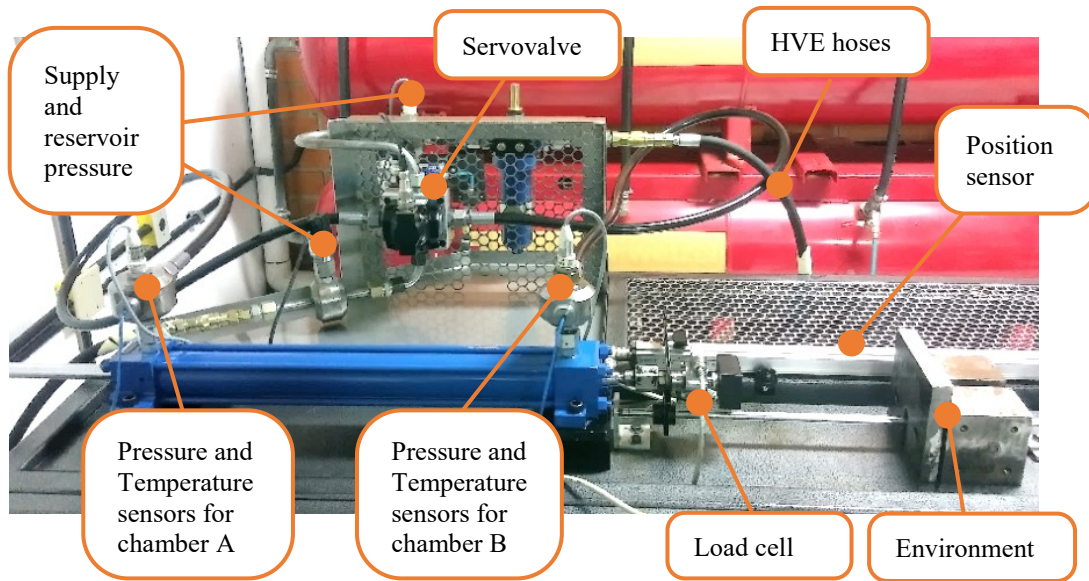


Source: Personal collection.

Additionally, Table A.1 (see Appendix A) summarizes the technical data of all components used for the experimental tests.

Furthermore, Figure 5.2 shows the test rig with the hydraulic system under analysis including the location of all sensors that were used for experimental tests.

Figure 5.2 – Picture of the hydraulic test rig Ybitú used for the study.



Source: Personal collection.

5.2 EXPERIMENTAL TESTS

Two experimental tests were carried out on the valve MOOG 760 C263-A of the Ybitú test rig. Both tests were based on standard ISO 10770-1, which describes methods for determining the performance characteristics of hydraulic flow control valves that are 4-way directional and electrically modulated (INTERNATIONAL ORGANIZATION FOR STANDARDIZATION, 2009).

The following subsections will explain in detail the tests performed in the test rig, along with some considerations taken into account. It is noteworthy that the experimental tests carried out and explained in this section are mainly performed to determine the valve coefficients to be used for simulations.

5.2.1 Internal leakage test

This experimental test allowed obtaining the internal leakage curve and was performed based on ISO 10770-1, item 8.1.3 - Internal leakage test (INTERNATIONAL ORGANIZATION FOR STANDARDIZATION, 2009).

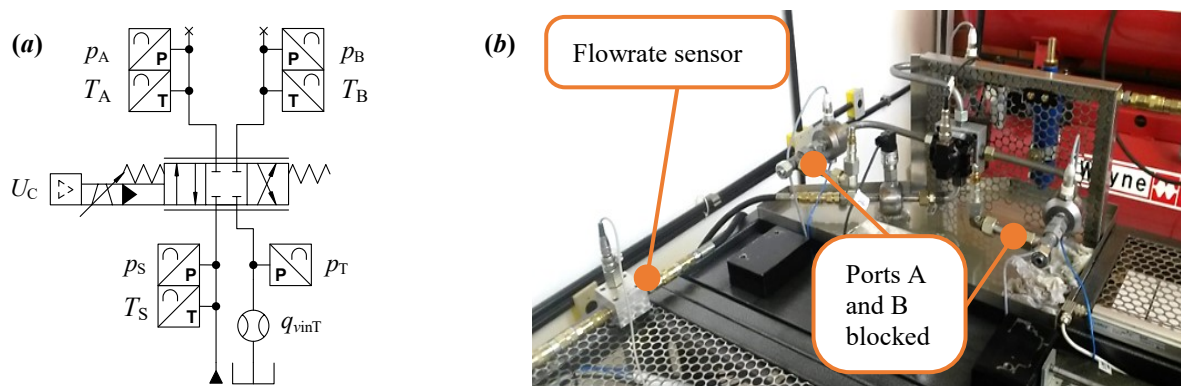
During this test, some considerations were taken into account:

- the oil temperature was maintained around 37°C (see Figure 5.4(a));

- the supply pressure was regulated to 7×10^6 Pa;
- the standard ISO 10770-1 indicates to send a triangular waveform signal of 0.02 Hz or lower to the servovalve for the measurements. However, a sinusoidal waveform signal with a period of 240 s (0.00417 Hz) was sent to the valve, aiming to have a smooth behavior during the change of direction in the spool motion and also trying to avoid any dynamic effect which could influence the results;
- on the other hand, because the nominal flowrate of hydraulic power unit (q_{pn}) is 1.6×10^{-4} m³/s (9.8 L/min) and the nominal flowrate of the valve (q_{vn}) is 6.30×10^{-4} m³/s at 7×10^6 Pa (10 gal/min at 1000 psi), a maximum variation of ± 30 % of the nominal control signal was selected (± 3 V). This decision was made in order to maintain the total pressure drop constant.

Figure 5.3 shows the hydraulic circuit and the test rig arrangement used to perform this test.

Figure 5.3 – (a) Hydraulic circuit and (b) test rig arrangement used for internal leakage test.

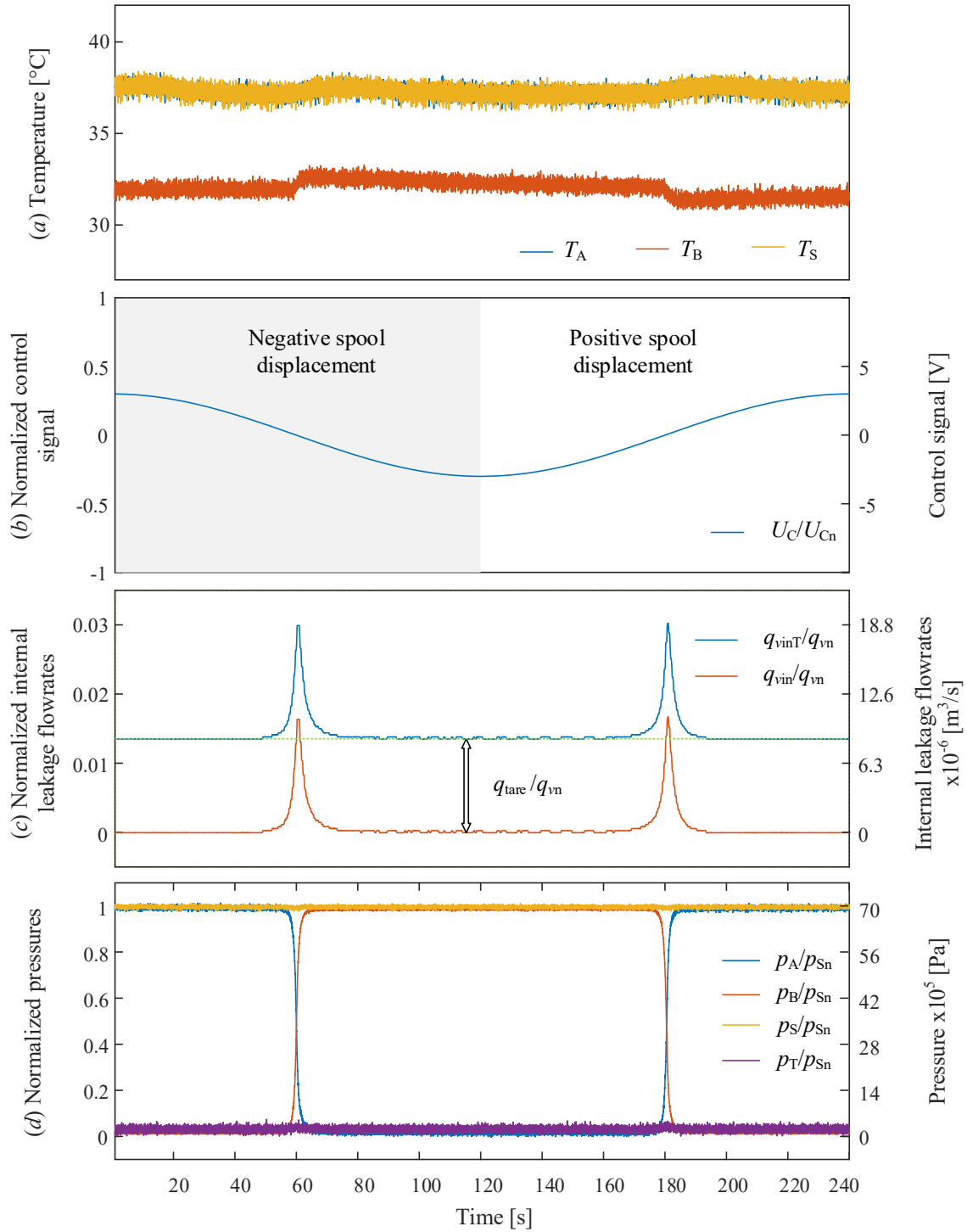


Source: Personal collection.

The experimental test measurements are plotted in Figure 5.4. In order to simplify future comparisons, all plot curves were normalized.

The value of the total internal leakage flowrate (q_{vinT}) increases whenever the spool position is near to the null position ($U_C = 0$). However, the measured value also includes the tare flow and the internal flowrate. The tare flow (q_{tare}) can be extracted from the total leakage flowrate considering the average value at the base of the curve (offset) (see Figure 5.4(b)). The resultant tare flow was $q_{tare} = 7.55 \times 10^{-6}$ m³/s at 70×10^5 Pa.

Figure 5.4 – Internal leakage test measurements using WEBTEC LT5 flowmeter. (a) Temperature of the oil, (b) normalized control signal sent to the servovalve, (c) normalized internal leakage flowrates, and (d) normalized pressures.



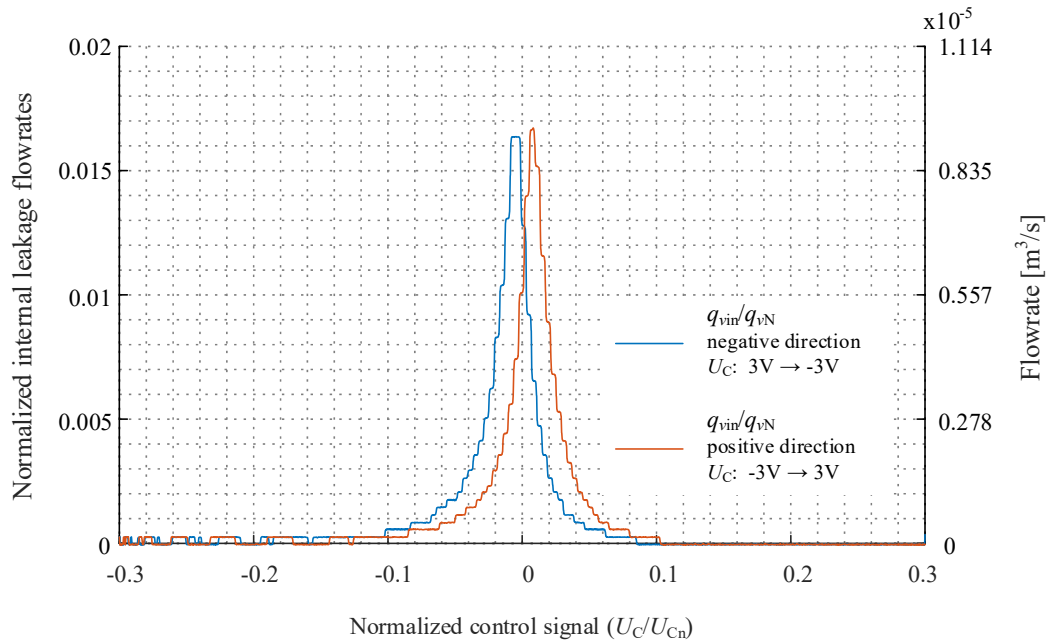
Source: Personal collection.

Figure 5.5 shows both internal leakages curves when the spool motion is in negative and positive direction, respectively. As can be seen in Figure 5.5, similar curve-shapes of the

leakage flow can be found in both motion directions. However, there is an offset of 0.5% (-0.05 V) in the negative direction and 0.78% (0.078 V) in the positive direction. This offset can be possibly related to the hysteresis of the valve.

Based on the experimental measurements, shown in Figure 5.4(b), the peak value of q_{vin} is 1.67% of the nominal flowrate of the valve (q_{vN}), resulting in $q_{vin} = 9.31 \times 10^{-6} \text{ m}^3/\text{s}$ at $70 \times 10^5 \text{ Pa}$. Afterwards, the value of K_{vinp} can be calculated using Equation (4.13), resulting in $K_{vinp} = 2.488 \times 10^{-9} \text{ m}^3/(\text{s} \cdot \text{Pa}^{0.5})$.

Figure 5.5 – Internal leakage curves in positive and negative spool directions.



Source: Personal collection.

Based on the catalog data provided by the manufacturer, the ratio q_{tare}/q_{vin} varies from 42.62% to 65%, and the ratio obtained via experimental tests was 44.77%. Therefore, the value obtained is within the range indicated by the manufacturer.

5.2.2 Metering test

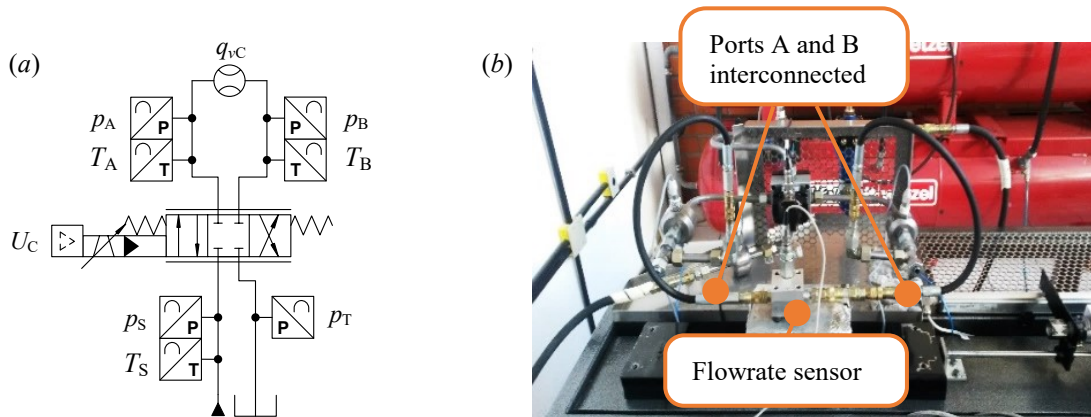
According to the standard ISO 10770-1, item 8.1.4 – Metering test, a steady-state test is proposed to determine the metering characteristics of each metering path at a constant pressure drop (INTERNATIONAL ORGANIZATION FOR STANDARDIZATION, 2009).

The main reason to perform this test was to obtain the flow gain coefficient of the valve. The considerations taken into account during this test are similar to the previous case and are listed below:

- the oil temperature was maintained between 40°C and 44°C;
- the supply pressure (p_s) was regulated to 7×10^6 Pa;
- the same sinusoidal waveform signal used in Subsection 5.2.1 was sent to the valve for this test;
- moreover, a range of ± 30 % of the nominal control signal ($U_{Cn} = \pm 10$ V) was used during the tests performed with the flowmeter WEBTEC CT60, and a range of ± 13 % with the flowmeter WEBTEC LT5;
- the ISO standard advises to use two different flowrate sensors (flowmeter) for this test, one used for higher flows and the other for low flows. Considering the previous advice, two different flowrate measures were performed using two different flowmeters (CT60 and LT5).

Figure 5.6 shows the test rig arrangement and the hydraulic circuit used for this particular test.

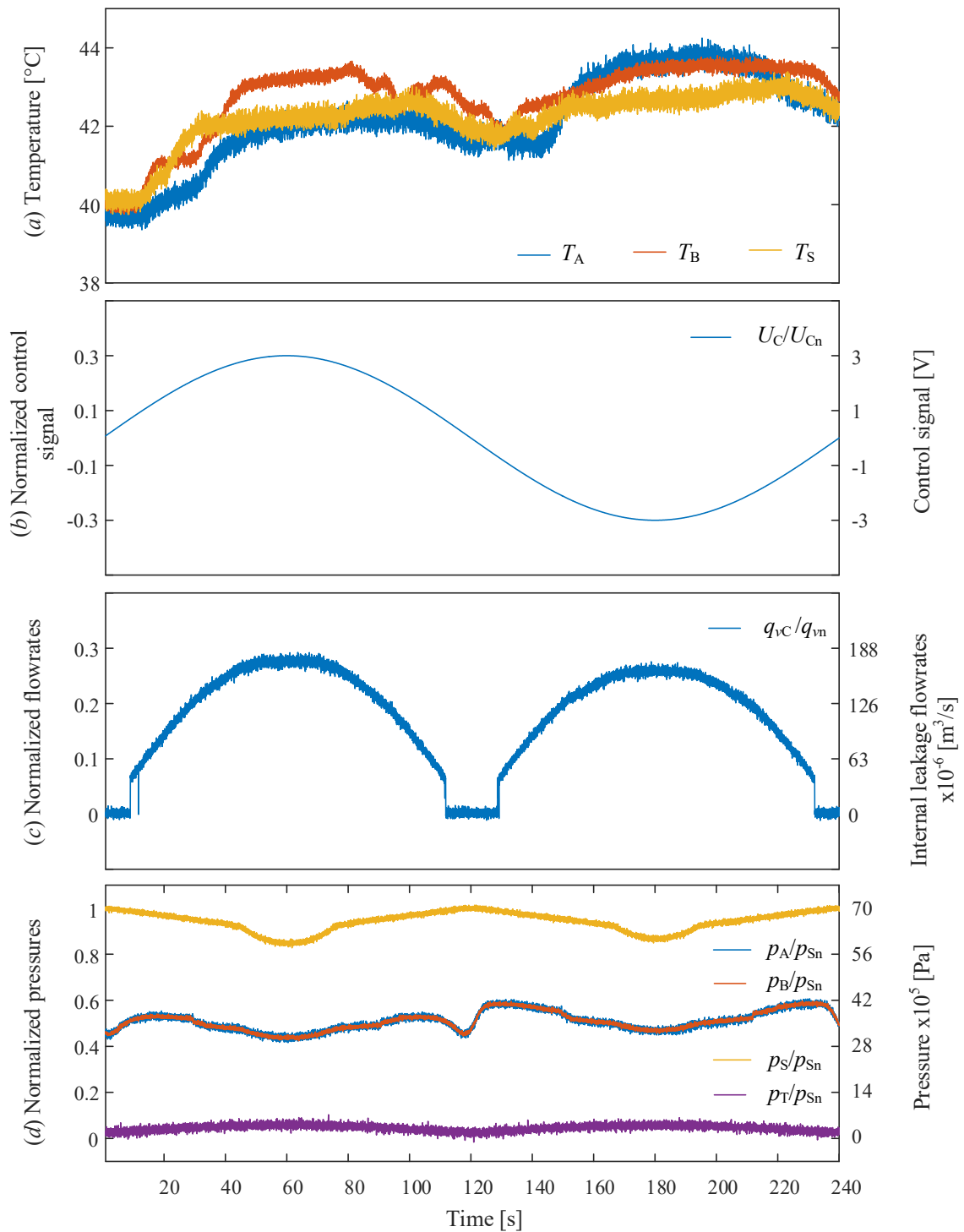
Figure 5.6 – (a) Hydraulic circuit and (b) test rig arrangement used for metering test.



Source: Personal collection.

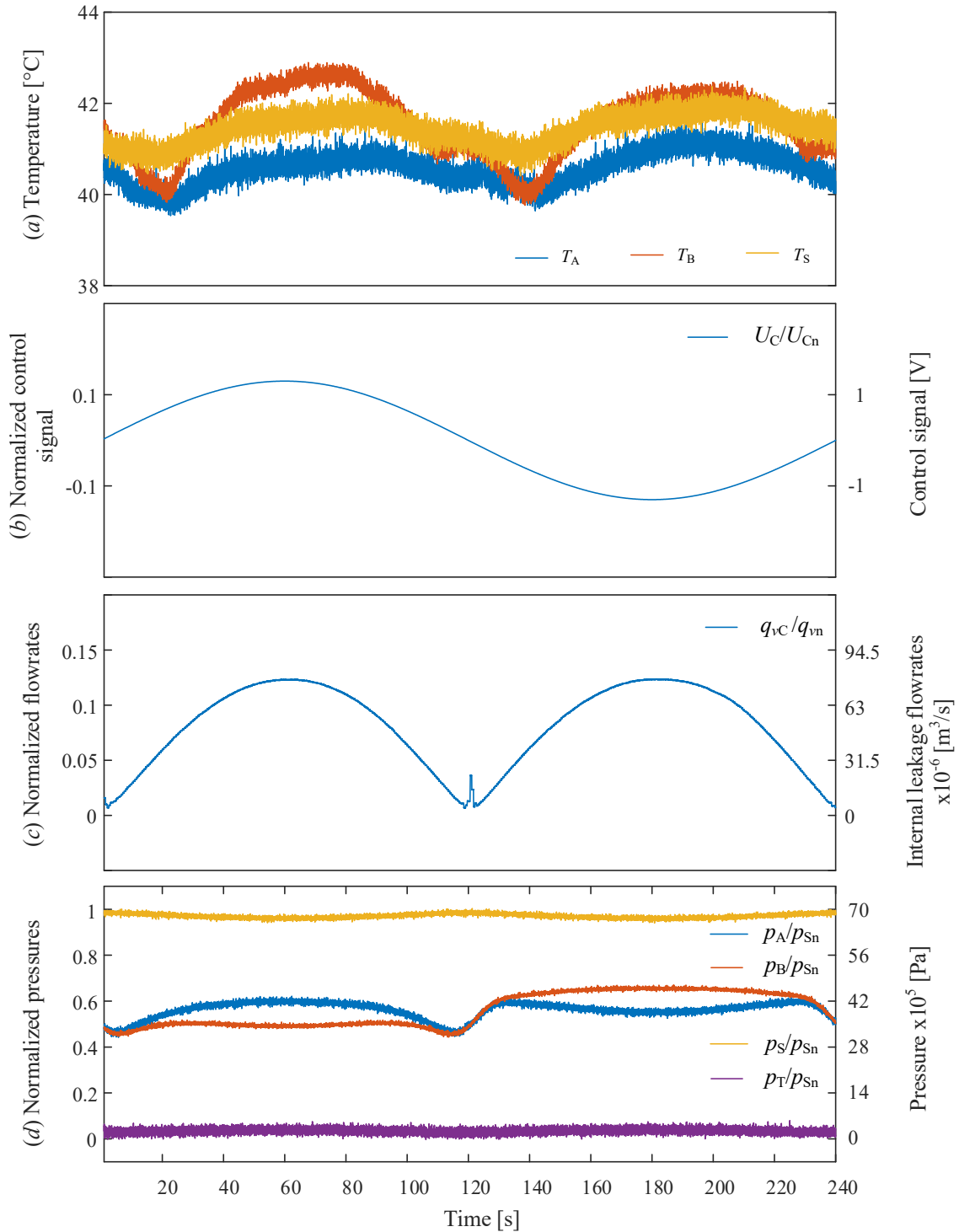
Figure 5.7 shows the experimental measurements obtained with a 1×10^{-3} m³/s (60 L/min) flowmeter (WEBTEC CT60). As can be seen in Figure 5.7(b), the sensor has limitations in the measurement of lower flowrates, which is the main reason to use a second flowmeter with smaller metering range (Figure 5.8) to try to fill this gap in measure.

Figure 5.7 – Metering test measurements using WEBTEC CT60 flowmeter. (a) oil temperature, (b) normalized control signal sent to the servovalve, (c) normalized internal leakage flowrates, and (d) normalized pressures.



Source: Personal collection.

Figure 5.8 – Metering test measurements using WEBTEC LT5 flowmeter. (a) Oil temperature, (b) normalized control signal sent to the servovalve, (c) normalized internal leakage flowrates, and (d) normalized pressures.



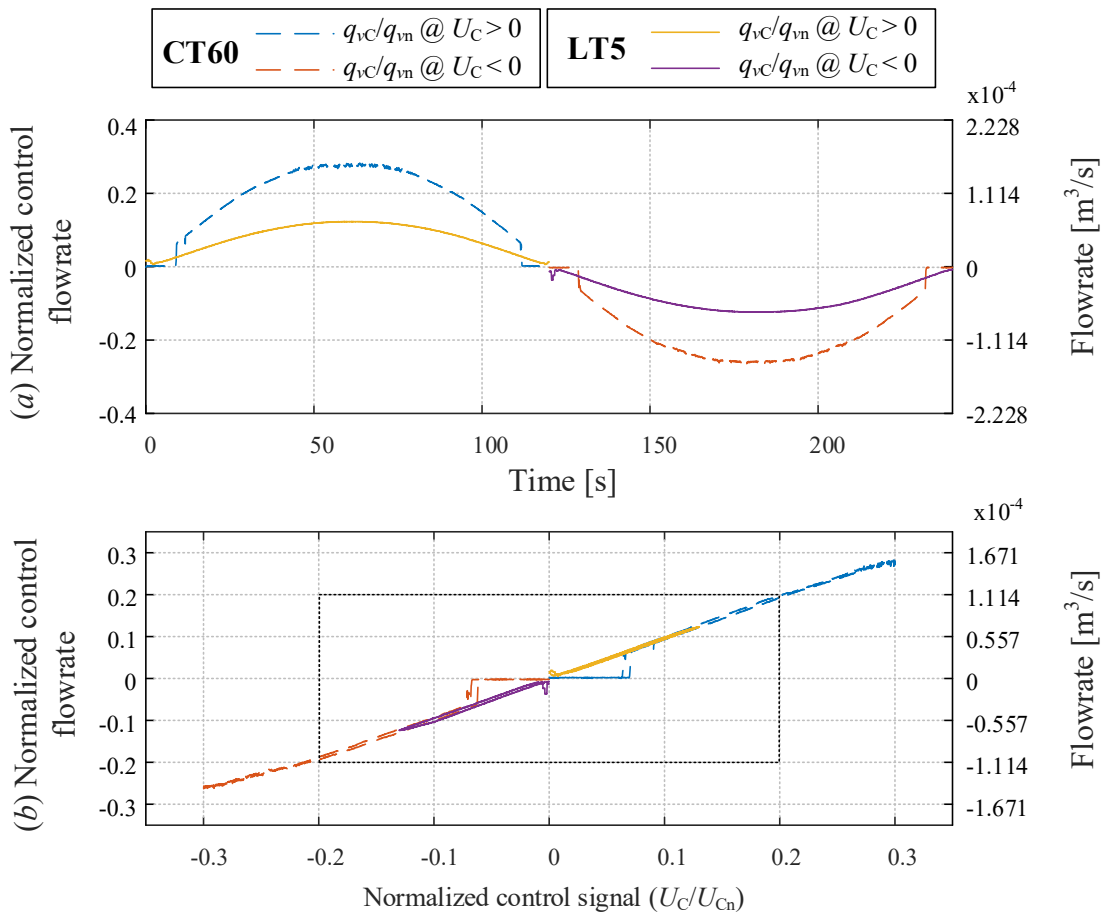
Source: Personal collection.

From Figure 5.7(d), it is possible to see that the supply pressure cannot be maintained constant because it reduces as the valve opening increases. This situation occurs due to the

increment in the flowrate as a result of larger opening valves. Notwithstanding, the main reason could be that the unit power pump has a smaller flowrate than the valve, forcing to have a limitation in the maximum valve opening value for the experiments in order to maintain a constant supply pressure

Comparing figures 5.7(d) and 5.8(d), it is possible to see that the flowmeter LT5 produce higher pressure drops than the other during the flowrate measurements. This effect occurs because of the difference between the dimension of flowmeter orifice in both sensors. Since the small flowmeter (LT5) has a small orifice compared to the other (CT60), the pressure drop is greater. Because both of the flowmeters are turbine type, the flowrate values measured were always positive disregarding the direction of the fluid flow, as seen in figures 5.7(c) and 5.8(c). Figure 5.9, shows an adaptation of the plots mentioned previously, but considering also the direction of the flow. It is possible to notice that in Figure 5.9 (b) the measuring of both flowmeters results in a similar overlap in both directions. This can be observed in Figure 5.10.

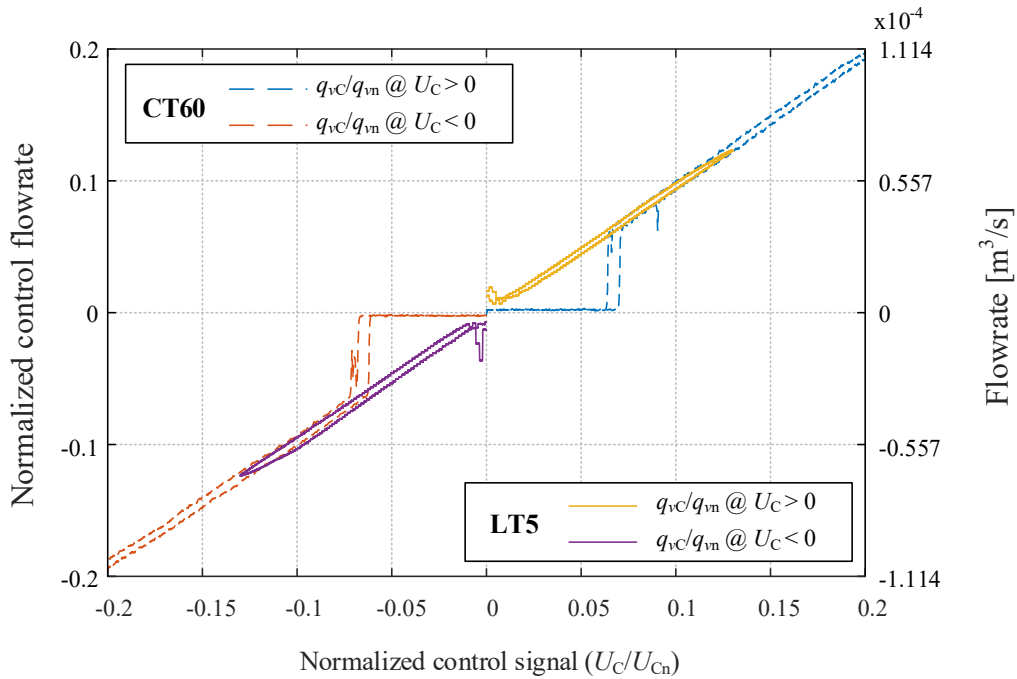
Figure 5.9 – (a) Normalized control flowrate measurements using flowmeters CT60 and LT5, and (b) Normalized control flowrate vs normalized control signal.



Source: Personal collection.

It is noteworthy that Figure 5.9(b) is known as flow-gain curve in the literature. The slope of this curve shows how much flowrate the servovalve allows to pass to the system at every increment of the opening valve. In normalized terms, ideally, the slope of this curve should be unitary, because the valve should be closed at null position (0% of flowrate) and gives the nominal flowrate of the valve at 100% of opening valve.

Figure 5.10 – Zoom-in of area remarked in Figure 5.9(b).



Source: Personal collection.

The results shown in Figure 5.9, and after a few calculations, the valve tested has an 88% of the nominal flowrate of the catalog. The results shown in figures 5.9(b) and 5.10 can be used to calculate the value of K_{vp} using Equation (4.12), which resulted in a value of $2.97 \times 10^{-7} \text{ m}^3/(\text{s} \cdot \text{Pa}^{0.5})$. Additionally, the slope of the curve can also be used to calculate the flow gain value for the linearized model of the valve. Moreover, based on Figure 5.10, it is possible to notice the existence of a hysteresis in the valve.

5.3 MODEL VALIDATION

Particular simulation models were used to represent both test procedures of subsections 5.2.1 and 5.2.2, aiming to obtain similar response to validate the nonlinear model (see Chapter 4).

The first approach was to use the coefficients calculated directly from the plots and consider $K_{vi} = K_{vp}$, for $i = 3$ to 6, where K_{vp} represents the partial flow coefficient of the valve. In the same way, one considered $K_{vin i} = K_{vinp}$, for $i = 3$ to 6, such that K_{vinp} is the internal partial leakage coefficient (see Table 5.1). However, the experimental results and the simulation results did not present a similar behavior, and a nonlinear optimization algorithm was used to find the valve coefficients, which values are listed in Table 5.1. The main task of this algorithm was to find the minimum value of a nonlinear function based on a cost function. In this case, the objective was to minimize the quadratic error between the experiments and the simulation results.

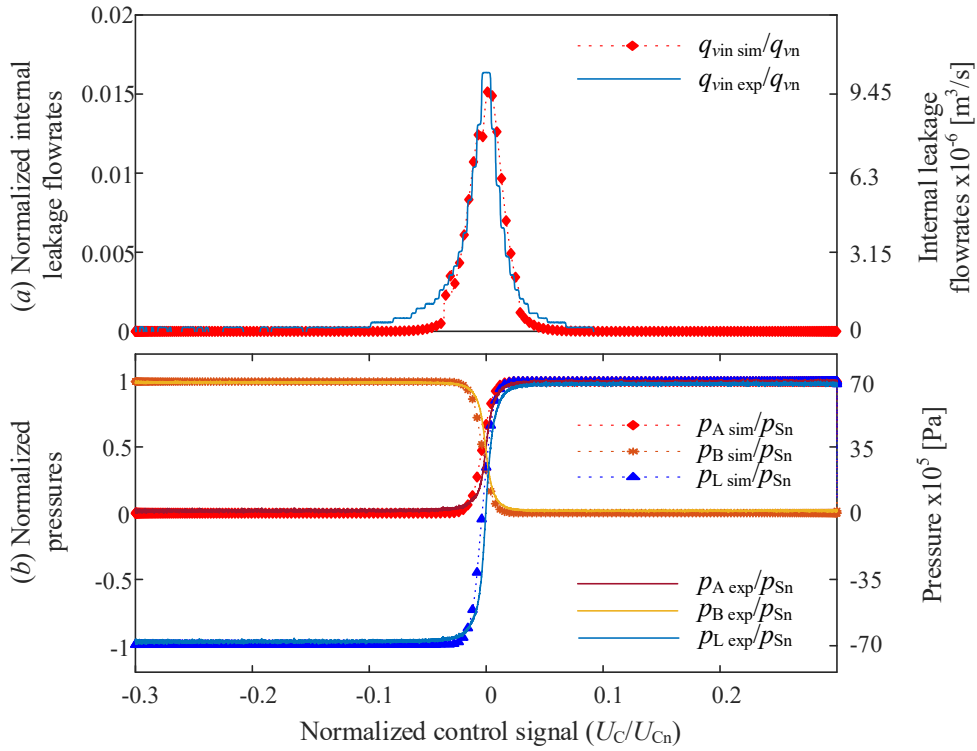
Table 5.1 – Valve coefficients obtained using a nonlinear optimization algorithm and based on experimental test results.

Parameter	Units	Values obtained through calculation	Values obtained via optimization
K_{v3}	$\text{m}^3/(\text{s} \cdot \text{Pa}^{0.5})$	2.97×10^{-7}	3.2×10^{-7}
K_{v4}	$\text{m}^3/(\text{s} \cdot \text{Pa}^{0.5})$	2.97×10^{-7}	2.5×10^{-7}
K_{v5}	$\text{m}^3/(\text{s} \cdot \text{Pa}^{0.5})$	2.97×10^{-7}	2×10^{-7}
K_{v6}	$\text{m}^3/(\text{s} \cdot \text{Pa}^{0.5})$	2.97×10^{-7}	3.85×10^{-7}
K_{vin3}	$\text{m}^3/(\text{s} \cdot \text{Pa}^{0.5})$	2.48×10^{-9}	2.35×10^{-9}
K_{vin4}	$\text{m}^3/(\text{s} \cdot \text{Pa}^{0.5})$	2.48×10^{-9}	2.2×10^{-9}
K_{vin5}	$\text{m}^3/(\text{s} \cdot \text{Pa}^{0.5})$	2.48×10^{-9}	1.7×10^{-9}
K_{vin6}	$\text{m}^3/(\text{s} \cdot \text{Pa}^{0.5})$	2.48×10^{-9}	2.35×10^{-9}

Source: Personal collection of Author.

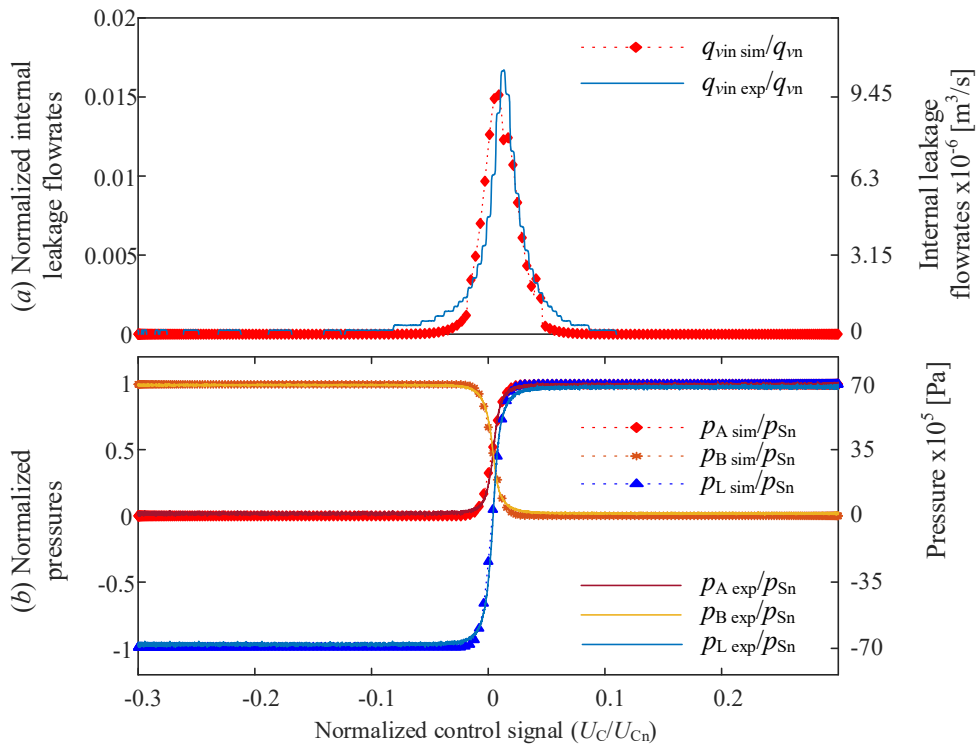
The results of the new valve coefficient values produced better results and their comparison can be observed in Figures 5.11 and 5.12. It is important to note that each plot represents the spool motion in negative and positive direction, respectively. On the other hand, Figure 5.11(b) and Figure 5.12(b) show the behavior of the pressure at the ports A and B during the spool motion. In the literature, this curve is known as the pressure sensitivity, and its slope can be also used for the calculation of the flow-pressure coefficient, which is useful for the linear model of the valve. Considering the comparison results between the experiments and the simulation results, it is possible to conclude that the nonlinear model, proposed in Chapter 4, is representative of the real system when considering the coefficient values shown in Table 5.1.

Figure 5.11 – Comparison of experimental and simulation results for (a) normalized internal leakage flowrates and (b) normalized pressures during a negative displacement of the spool.



Source: Personal collection.

Figure 5.12 – Comparison of experimental and simulation results for (a) normalized internal leakage flowrates and (b) normalized pressures during a positive displacement of the spool.



Source: Personal collection.

5.4 CHAPTER CONCLUSIONS

This chapter deals with the experimental validation process of the mathematical models presented in the previous chapter (Chapter 4). Considering that the servovalve is one of the most critical components in hydraulic force control, a detailed analysis trying to validate the model is presented. Two experimental tests were presented: internal leakage test, based on ISO 10770-1 (item 8.1.3), which allows to obtain the internal leakage curve in the valve; and the metering test, based on ISO 10770-1 (item 8.1.4), used to obtain the flow gain coefficient of the valve. The comparative results shown a good correspondence between the simulation and the experimental responses, highlighting the validity of the mathematical modeling proposed in Chapter 4.

The next chapter will introduce the Pure Hydroelastic Actuator (PHEA) as a type of actuator whose hydraulic stiffness is purposely modified using specially selected capacitive hydraulic components for force control applications.

6 PURE HYDROELASTIC ACTUATOR

6.1 DESCRIPTION

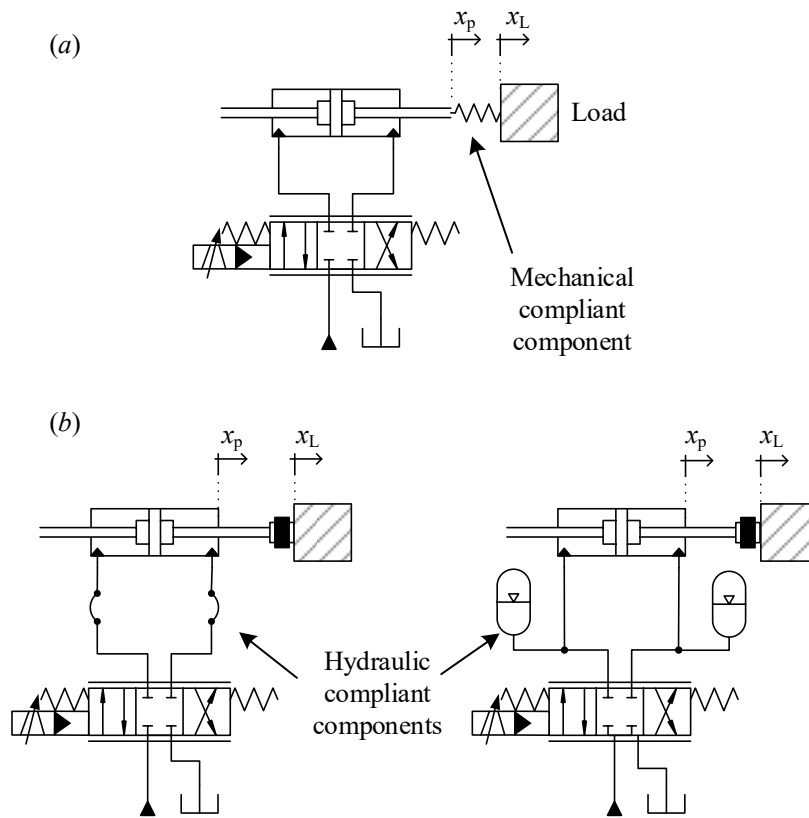
Several researches can be found in the literature related to the force control using hydraulic actuators. Most of them use a spring as a representation of the load (or environment) in order to simplify the mathematical model and the analysis. Nevertheless, they did not consider the filtering effect provided by the compliant element and, using particular control techniques, good force responses were obtained (XU et al., 1995; NIKSEFAT AND SEPEHRI, 1999; ALLEYNE AND LIU, 2000; AHN, K. K. et al., 2008; NAKKARAT AND KUNTANAPREEDA, 2009; KARPENKO AND SEPEHRI, 2012).

On the other hand, other studies highlight the use of spring in series with the actuator and its influence on force control since this mechanical component increases the system compliance and improves the system performance (ROBINSON AND PRATT, 2000; SIVASELVAN et al., 2008). The SEA is a classic example of the inclusion of a passive compliant element (spring) that aims to reduce the effect of the environment dynamics over the actuation system, making possible to control the applied forces in a stable and robust way. In addition, Plummer (2007) and Lamming et al. (2010) emphasize the inclusion of the load motion measurements in the control loop trying to cancel this disturbance characteristic and obtain a better force tracking. This approach results very effective but requires more sensing hardware, being possible to use as a complement for the present work.

The fact of achieving the same behavior through purely hydraulic components is something that has not yet been clearly explored within the state of the art of hydraulic force control and it is the main purpose of this thesis. Figure 6.1 shows the hydraulic counterpart for the SEA, and henceforward-denominated Pure Hydroelastic Actuator (PHEA). The main characteristic of PHEA is to have a compliant behavior like the SEA, however using hydraulic means. In this sense, it is also possible to obtain a reduction of the impedance at the interaction port reducing the hydraulic transmission stiffness value by using HVE hoses or accumulators.

Notwithstanding, some considerations need to be taken into account before the analysis and they will be discussed in the following sections.

Figure 6.1 – Hydraulic force control system using: (a) mechanical compliant component (SEA) and (b) hydraulic compliant components.



Source: Adapted from Ledezma et al. (2018).

6.2 INCREASING PASSIVE COMPLIANCE THROUGH HYDRAULIC STIFFNESS VALUE

This section will describe the mathematical background and the procedure used to define which should be the transmission stiffness value required to increase the compliance of the system in a predefined way.

As commented along this thesis, the main objective of this research is to analyze how to make the hydraulic actuation more compliant through hydraulic means. However, it is not only related to increase the compliance without any limits, but also doing it in a controllable way that allows to achieve performance and disturbance rejection requirements.

The hydraulic stiffness is an intrinsic characteristic of the hydraulic transmission and is defined as (WATTON, 2009):

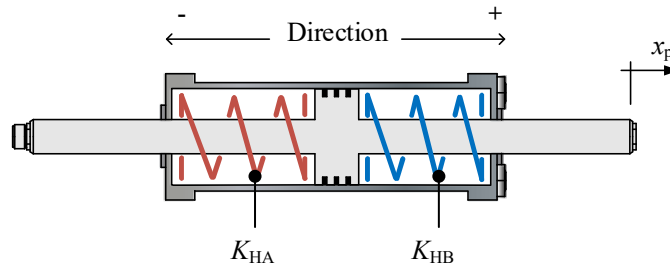
$$K_H = K_{HA} + K_{HB} = \frac{\beta_c A_A^2}{V_A} + \frac{\beta_c A_B^2}{V_B}. \quad (6.1)$$

Since the cylinder under analysis is symmetric ($A_A = A_B = A_u$), Equation (6.1) can be rewritten as:

$$K_H = \beta_c A_u^2 \left(\frac{1}{V_A} + \frac{1}{V_B} \right). \tag{6.2}$$

According to Equation (6.1), the hydraulic stiffness of an actuator is composed by the interactions of two internal stiffness related to each cylinder chamber (K_{HA} and K_{HB}) (see Figure 6.2). It is known that the oil inside each chamber introduce a behavior equivalent to a spring, when the ports A and B are closed (STRINGER, 1976).

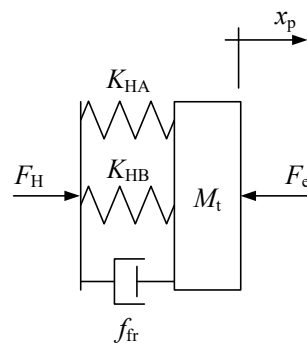
Figure 6.2 – Schematic representation of the hydraulic stiffness of each cylinder chamber.



Source: Personal collection.

For better understanding, a homologous mechanical model of the hydraulic cylinder is shown in Figure 6.3.

Figure 6.3 – Schematic representation of the hydraulic cylinder in the mechanical domain.



Source: Personal collection.

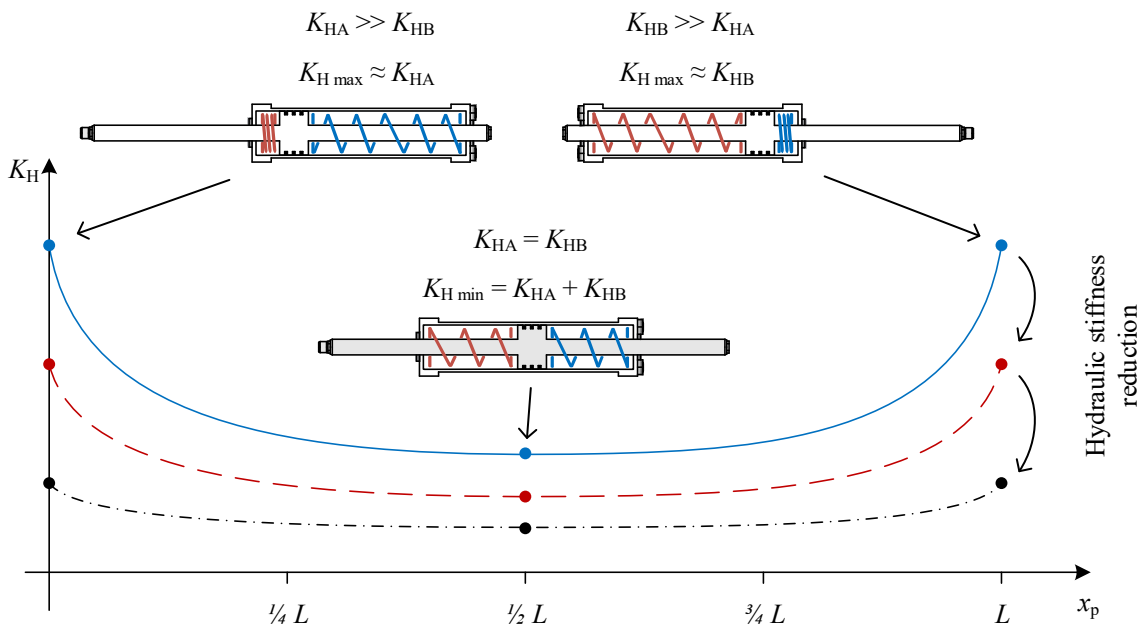
Substituting equations (4.27) and (4.28) in Equation (6.2), and considering that due to the symmetry of the cylinder, both V_{A0} and V_{B0} are also equal to V_0 , results in:

$$K_H = \beta_e A_u^2 \left(\frac{1}{A_u x_p + V_0} + \frac{1}{A_u (L - x_p) + V_0} \right). \tag{6.3}$$

Every time that the piston moves, the value of each chamber hydraulic stiffness changes. As it can be seen in Figure 6.4, considering the symmetry of the cylinder, both of stiffness (K_{HA} and K_{HB}) are equal at the center, where the total hydraulic stiffness (K_H) is minimum.

However, as the piston is near to one of the extremes of the cylinder, i.e. when $x_p = 0$ or $x_p = L$, one of the chamber hydraulic stiffness dominates the value of the sum in Equation (6.1) and the total hydraulic stiffness assumes its maximum value. As it can be seen, the value of K_H is a nonlinear function that depends of the piston position, cylinder size and the fluid bulk modulus. Figure 6.4 also shows examples of changes in the hydraulic stiffness curve if some of its internal parameters modify the compliance of the actuator, decreasing it. As can be seen, the more hydraulic stiffness reduction, the flatter the hydraulic stiffness will be. Consequently, the actuation system becomes more compliant.

Figure 6.4 – Hydraulic stiffness in function of the piston position considering a symmetrical cylinder. The blue line is an example of the initial hydraulic stiffness values depending on the piston position. The red dashed line and the black dashed line with dots represent how the hydraulic stiffness changes as the compliance increases.



Source: Personal collection.

Observing Equation (6.3), several useful insights can result in order to reduce the hydraulic stiffness of the actuator. Nevertheless, all possible solutions are about the modifications of three parameters:

- The effective bulk modulus (β_e), which can be altered according to other internal parameters, such as the oil, the container (volume or stiffness), and the quantity of entrapped air inside the fluid line;
- the useful area of the piston ($A_u = A_A = A_B$), which can be considered fixed, since it depends on the cylinder size. However, if we consider a special telescopic piston where the useful area changes along the stroke of the cylinder, it can also modify the hydraulic stiffness;
- due to the symmetry of the cylinder, $V_{A0} = V_{B0} = V_0$, which is related to the oil volume trapped in the line between the valve and the cylinder. Consequently, the container of this oil trapped can be a tube, a hose, or any other capacitive device coupled between the valve and the cylinder. This parameter and the effective bulk modulus are intrinsically linked, i.e. if V_0 changes, β_e also changes. This relationship will be explained later.

The following subsections will establish the mathematical background including some considerations taken into account for sizing the hydraulic components required for the PHEA.

6.2.1 Modifications in the linear model of the system

As can be seen in Figure 6.4, since the hydraulic stiffness has a nonlinear behavior, it will be necessary to make some considerations in order to simplify the analysis.

Taking into account that this thesis will use a robust control technique (QFT), which can work with parametric uncertainties, it is also possible consider some parameters as an uncertainty for simplification purposes. One of them is the volume of oil inside each one of the chambers (V_A and V_B), which varies every time there is a piston motion. Since the total variation of V_A is equal to the total variation of V_B , both of them can be substituted by an uncertain parameter called V . This new parameter can incorporate all possible variation in the chamber volumes and not only a small variation in the vicinity of the operating point, what is done in the traditional linearization approach. Moreover, the Equation (6.1) can be modified to:

$$K_H = \frac{2\beta_c A_u^2}{V}. \quad (6.4)$$

On the other hand, Equation (4.34) shown the traditional linear model of the continuity equation for symmetrical cylinders. However, after some mathematical operations with equations (4.25) and (4.26), and considering the assumption expressed in Equation (6.4), Equation (4.34) becomes:

$$Q_{vC}(s) = A_u s X_p(s) + \frac{A_u^2}{K_H} s P_L(s). \quad (6.5)$$

Finally, based on Equation (4.29), the friction force (F_{fr}), which is a nonlinear function of piston velocity (dx_p/dt), can be described by an uncertain parameter (f_v). Therefore, this assumption allows the linear motion equation shown in Equation (4.35) to become:

$$A_u P_L(s) = (M_t s^2 + f_v s) X_p(s) + F_e(s). \quad (6.6)$$

Considering Figure 6.1(a), where K_S is the load cell stiffness, and combining the equations (4.23), (4.24), (4.45), (6.5), and (6.6), the open-loop (OL) transfer function that relates the output force (F_e) with the input control signal (U_C) and the load displacement (x_L) is:

$$F_e(s) = \frac{c_0 U_C(s) - K_S (b_4 s^4 + b_3 s^3 + b_2 s^2 + b_1 s + b_0) s X_L(s)}{a_5 s^5 + a_4 s^4 + a_3 s^3 + a_2 s^2 + a_1 s + a_0}, \quad (6.7)$$

where:

$$\begin{aligned} a_0 &= \omega_{nv}^2 K_{c0} K_H K_S, \\ a_1 &= \omega_{nv}^2 A_u^2 (K_H + K_S) + K_{c0} K_H (2\zeta_v \omega_{nv} K_S + \omega_{nv}^2 f_v), \\ a_2 &= 2\zeta_v \omega_{nv} A_u^2 (K_H + K_S) + \omega_{nv}^2 A_u^2 f_v + K_{c0} K_H (2\zeta_v \omega_{nv} f_v + \omega_{nv}^2 M + K_S), \\ a_3 &= 2\zeta_v \omega_{nv} A_u^2 f_v + \omega_{nv}^2 A_u^2 M + K_{c0} K_H (2\zeta_v \omega_{nv} M + f_v) + A_u^2 (K_H + K_S), \\ a_4 &= 2\zeta_v \omega_{nv} A_u^2 M + A_u^2 f_v + K_{c0} K_H M, \\ a_5 &= A_u^2 M, \\ b_0 &= \omega_{nv}^2 A_u^2 K_H + \omega_{nv}^2 f_v K_{c0} K_H, \\ b_1 &= 2\zeta_v \omega_{nv} A_u^2 K_H + \omega_{nv}^2 A_u^2 f_v + K_{c0} K_H (2\zeta_v \omega_{nv} f_v + \omega_{nv}^2 M), \\ b_2 &= 2\zeta_v \omega_{nv} A_u^2 f_v + \omega_{nv}^2 A_u^2 M + A_u^2 K_H + K_{c0} K_H (2\zeta_v \omega_{nv} M + f_v), \\ b_3 &= 2\zeta_v \omega_{nv} A_u^2 M + A_u^2 f_v + K_{c0} K_H M, \\ b_4 &= A_u^2 M, \\ c_0 &= A_u K_H K_{qU0} K_S \omega_{nv}^2. \end{aligned}$$

Equation (6.7) shows two different dynamics interacting when the system is coupled and applying force to a load or an environment. The first one is related to the effect of the $U_C(s)$ over the applied force ($F_e(s)$), and the second one represents the effect of the load motion ($sX_L(s)$) on $F_e(s)$. As it can be seen, the load motion denotes the natural feedback velocity, discussed during the literature review (see Chapter 2), and it is indeed intrinsic to the system since it appears only when the cylinder is coupled to the load.

By considering the Equation (6.7) and expressing the input control signal as $G(s)(F_{\text{ref}}(s) - F_e(s))$, where $G(s)$ and $F_{\text{ref}}(s)$ represent the controller transfer function and the reference force, respectively, the closed-loop (CL) transfer function results in:

$$F_e(s) = \frac{G(s)N_1(s)}{D(s) + G(s)N_1(s)} F_{\text{ref}}(s) - \frac{N_2(s)}{D(s) + G(s)N_1(s)} sX_L(s), \quad (6.8)$$

where:

$$\begin{aligned} N_1(s) &= c_0, \\ N_2(s) &= K_S(b_4s^4 + b_3s^3 + b_2s^2 + b_1s + b_0), \\ D(s) &= a_5s^5 + a_4s^4 + a_3s^3 + a_2s^2 + a_1s + a_0. \end{aligned}$$

As before, Equation (6.8) comprises two parts: the first one is related to the *force control performance*, which defines the system behavior characteristics and is in function of the force reference ($F_e(s)$) and the controller ($G(s)$). The second part describes how the system behaves with respect to a disturbance input motion ($sX_L(s)$). It is also noticeable that this part is also affected by the controller. This second part is related to the output impedance and it can be considered as a measure of the *disturbance rejection capability*. Therefore, in order to have a compliant behavior during a force control task, two different approaches are possible:

1. design a force controller in order to obtain a virtual compliant behavior, which is the main purpose of active compliance force control method;
2. modify the physical transmission of the actuation, which is the objective of passive compliance force control method, and also the main objective of this thesis.

Independently of the method type to be selected, it is important to highlight that it will always exist a trade-off between performance and disturbance rejection capability. A force

control system cannot have an excellent compliant behavior without damaging the performance, and the opposite case also happens.

Therefore, the following subsections will show the mathematical background that allows to calculate the hydraulic stiffness required to increase, passively, the compliance of the system based on the performance and disturbance rejection analysis.

6.2.2 Disturbance rejection based on the output impedance

The output impedance of the system is described by the transfer function $F_e(s)/sX_L(s)$ of Equation (6.8) and interesting insights can be obtained after analyzing this term.

Reasoning mathematically and considering the load displacement ($X_L(s)$) instead of the load motion or velocity ($sX_L(s)$), the mere presence of the zero at the origin introduces a natural disturbance rejection for step-type disturbances. This assertion is demonstrated in Proposition 6.2.

Assumption 6.1. The load displacement ($X_L(s)$) represents a disturbance in the force control system under analysis defined in Equation (6.8).

Proposition 6.2. *The zero at origin in the second half of Equation (6.8) guarantees a natural step-disturbance rejection.*

Proof. Let $G(s)$ be a unitary gain controller in order to analyze the behavior of the system without the influence of the controller function.

Under the Assumption 6.1, and isolating the second half of Equation (6.8), the relationship between $F_e(s)$ and $X_L(s)$ can be defined as:

$$F_e(s) = \frac{sK_s (b_4s^4 + b_3s^3 + b_2s^2 + b_1s + b_0)}{a_5s^5 + a_4s^4 + a_3s^3 + a_2s^2 + a_1s + a_0 + c_0} X_L(s). \quad (6.9)$$

Assuming a stable system, the steady-state value of the force (F_{ess}) for a step disturbance $X_L(s) = x_{L0}/s$, can be obtained applying the final-value theorem (OGATA, 2010), as follows:

$$F_{\text{ess}} = \lim_{s \rightarrow 0} sF_e(s) \left(\frac{x_{L0}}{s} \right). \quad (6.10)$$

Substituting Equation (6.9) in Equation (6.10), gives:

$$\begin{aligned}
 F_{eSS} &= \lim_{s \rightarrow 0} \frac{s^2 K_S (b_4 s^4 + b_3 s^3 + b_2 s^2 + b_1 s + b_0)}{a_5 s^5 + a_4 s^4 + a_3 s^3 + a_2 s^2 + a_1 s + a_0 + c_0} \frac{x_{L0}}{s} \\
 &= \lim_{s \rightarrow 0} \frac{s(K_S x_{L0} b_0)}{a_0 + c_0} \\
 &= 0
 \end{aligned} \tag{6.11}$$

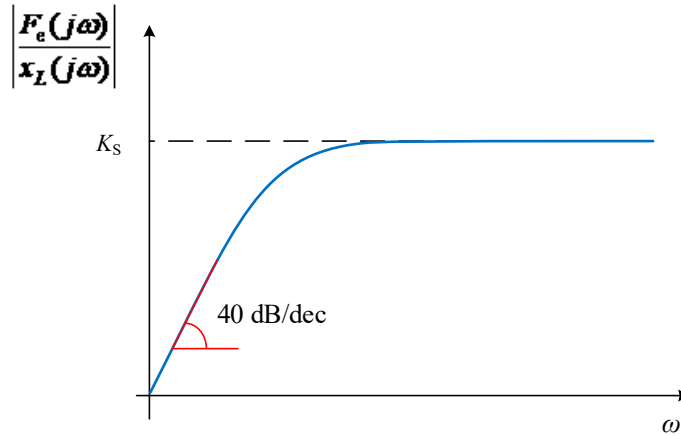
Therefore, the force response in steady-state is zero in front of a step disturbance. Since this zero at origin is intrinsic to the system, because it is related to the natural velocity feedback (DYKE et al., 1995), it is possible to conclude that this zero guarantees a *natural step-disturbances rejection*, demonstrating this proposition. □

On the other hand, the load displacement is, in fact, mechanically filtered by the system. This can be seen in the second half of Equation (6.8) where zeros and poles are dynamically affecting the input disturbance ($X_L(s)$).

The influence of the load motion on the force control system decreases as the value of the load cell stiffness (K_S) decreases. This is the main reasoning used by Williamson (1995) and Robinson (2000) during their presentation of the Series Elastic Actuator. The authors used a compliant spring, instead of a stiff load cell, that, indirectly, gives the measure of the force applied on the load. However, this comes from the fact that the cited authors did not consider the hydraulic stiffness during their research or assumed it as a very large value.

Robinson (2000) suggested, based on several simplifications, that in low frequencies the output impedance of the SEA turns to simulate an equivalent mass, i.e. the load considers the actuator as a translational mass. However, at high frequencies the load considers the actuator as a spring with a stiffness value equal to the load cell stiffness. Consequently, all of the high frequency disturbances such as load shocks and others are filtered through it (Figure 6.5). On the other hand, if this analysis made by (ROBINSON, 2000) is extended, highlighting the effects of the hydraulic stiffness variation at high frequencies, the output impedance tends, indeed, to have a constant value equals to $(K_H K_S / (K_H + K_S))$, which henceforth will be called equivalent stiffness (K_{eq}).

Figure 6.5 – Rough characterization of a hydro-elastic actuator impedance proposed by Robinson (2000), showing that the impedance is equal to an equivalent mass at low frequencies, and it tends to acts as a spring with a stiffness equal to the load cell stiffness at high frequencies.



Source: Adapted from Robinson (2000).

If the load dynamics is well known, theoretically the implementation of a feed-forward compensator should result advantageous for force control applications. However, this almost never happens and, in most of the cases, the load dynamics is unknown making difficult to implement a compensator. Even if the load dynamics is known, the compensator will be model-based and so the applicability of this control scheme will be too much dependable on the accuracy of the load dynamics model. Therefore, if one of the parameters in the load dynamics model change, it will affect the entirely force control dynamics. Based on that, reducing the output impedance (increasing the compliance) seems to be a better option due to the reduction of the system sensibility to load dynamics.

Since the load motion dynamics is commonly unknown, the measuring of load motion helps to implement a velocity compensation, reducing the output impedance and allowing a better force tracking. This velocity compensation is discussed in several researches available in the literature (EPPINGER AND SEERING, 1987; SERAJI AND COLBAUGH, 1993; ALLEYNE AND LIU, 1999; PLUMMER, 2007; LAMMING et al., 2010; BOAVENTURA et al., 2012). Another approach used to reduce the effect of load dynamics is to consider the load motion as a disturbance but maintaining a required performance (NIKSEFAT AND SEPEHRI, 2001), which is the approach used in this thesis. Some researches combine the advantages of reduce the output impedance (using a spring) with the load dynamics compensation (using load velocity measurements) (PLUMMER, 2007; LAMMING et al., 2010).

Considering all the previous discussion, it can be concluded that, to achieve a good disturbance rejection behavior against the load motion, the output impedance is required to be as low as possible. Since the output impedance is based on the stiffness transmission, this assertion implies that the hydraulic stiffness need to be as low as possible. Nevertheless, this value must be greater than or equal to the hydraulic stiffness required to achieve the required performance, which is discussed below.

6.2.3 Performance based on the desired tracking control ratio

Based on the linear modelling shown in Chapter 4, the hydraulic system behavior is defined by the interaction of three different kind of dynamics:

- electromagnetic dynamics related to the preamplifier stage of the valve (spool motion);
- hydraulic dynamics, which describes the behavior of the fluid through de valve and inside the pipes and cylinder chambers;
- mechanical dynamics related to the piston motion.

Equation (6.7) shows a Fifth order transfer function, which comprises the interaction between all of these dynamics including the load dynamics. However, it is difficult to evaluate the influence of each dynamic without simulating the entire system. For this reason, this thesis proposes to substitute Equation (6.7) by:

$$\frac{F_c(s)}{U_C(s)} = \left(\frac{K_{qU0}K_{eq} / A_u}{s + K_{c0}K_{eq} / A_u^2} \right) \left(\frac{d_0}{s^2 + d_1s + d_0} \right) \left(\frac{e_0}{s^2 + e_1s + e_0} \right), \quad (6.12)$$

where:

$$d_0 = (K_H + K_S)/M,$$

$$d_1 = f_v/M,$$

$$e_0 = \omega_{nv}^2,$$

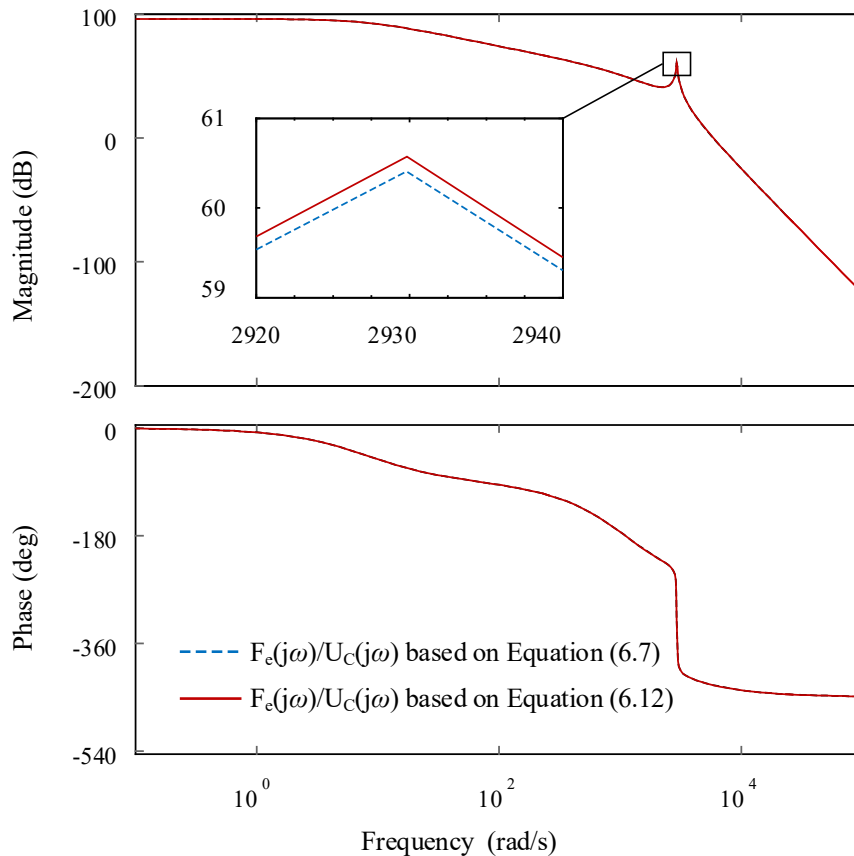
$$e_1 = 2\zeta_v\omega_{nv},$$

$$K_{eq} = K_S K_H / (K_S + K_H), \text{ representing the equivalent stiffness.}$$

The first term of Equation (6.12) defines the hydraulic dynamics inside the system. The middle term is related to the mechanical dynamics based on Newton's second law. Finally, the third term, on the right side, represents the servovalve dynamics.

Using the parameters presented in Table A.1, Figure 6.6 shows a frequency domain comparison between the first half part of Equation (6.7) and Equation (6.12). The figure demonstrates that the latter equation is a quasi-exact approximation of the first half of Equation (6.7), resulting in a maximum difference between curves of 0.2 dB in magnitude and 0.003° in phase.

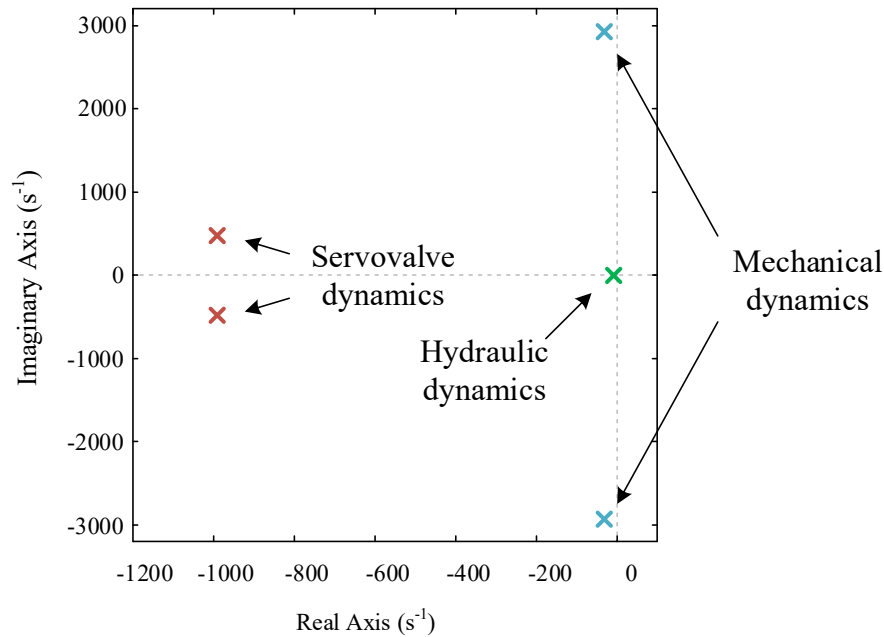
Figure 6.6 – Frequency response comparison between a complete linear model (Equation (6.7)) and a quasi-exact approximated linear model (Equation (6.12)).



Source: Personal collection.

Figure 6.7 shows the root locus of the approximated transfer function presented in Equation (6.12).

Figure 6.7 – Zero-pole map of the approximated linear model shown in Equation (6.12).



Source: Personal collection.

Table 6.1 presents the pole location for different hydraulic stiffness values.

Table 6.1 – Pole locations for different values of K_H .

K_H [N/m]	Hydraulic dynamics	Mechanical dynamics	Servovalve dynamics
	$\frac{K_{qU0}K_{eq} / A_u}{(s + K_{c0}K_{eq} / A_u^2)}$	$\frac{d_0}{(s^2 + d_1s + d_0)}$	$\frac{e_0}{(s^2 + e_1s + e_0)}$
$K_{Hn} = 1.5 \times 10^7$	- 2.963	- $11.6 \pm 2.93 \times 10^3i$	- $989 \pm 479i$
$0.1 K_{Hn}$	- 0.336	- $11.4 \pm 2.75 \times 10^3i$	- $989 \pm 479i$
$0.01 K_{Hn}$	- 0.034	- $11.4 \pm 2.73 \times 10^3i$	- $989 \pm 479i$

Source: Personal collection.

It is noteworthy that K_{Hn} corresponds to the nominal stiffness when using rigid pipes. The real pole related to the hydraulic subsystem is $-K_{c0}K_{eq}/A_u^2$ and it becomes dominant over the other two complex pair of poles as the value of K_H decreases. This fact is numerically noticeable in Table 6.1. The damped natural frequency of the mechanical subsystem is loosely influenced by the hydraulic stiffness variation.

Due to the dominance of the real pole, as can be seen in Table 6.1, the system represented in Equation (6.12) can be directly approximated by the first order hydraulic subsystem dynamics, yielding:

$$\frac{F_e(s)}{U_C(s)} = \frac{K_{qU0}K_{eq} / A_u}{s + K_{c0}K_{eq} / A_u^2}, \quad (6.13)$$

and the corresponding closed-loop transfer function results in:

$$\frac{F_e(s)}{F_{ref}(s)} = \frac{G(s)(K_{qU0}K_{eq} / A_u)}{s + (K_{c0}K_{eq} / A_u^2) + G(s)(K_{qU0}K_{eq} / A_u)}. \quad (6.14)$$

On the other hand, a performance specification, also known as a desired tracking control ratio, can be specified as:

$$\frac{F_e(s)}{F_{ref}(s)} = \frac{K_{SS}}{(\tau_d s + 1)}, \quad (6.15)$$

where K_{SS} is the steady state gain and τ_d is the desired time constant.

Considering a proportional controller for $G(s)$, with (K_p) as the proportional gain and based on the combination of Equation (6.14) and Equation (6.15), the desired hydraulic stiffness can be described as:

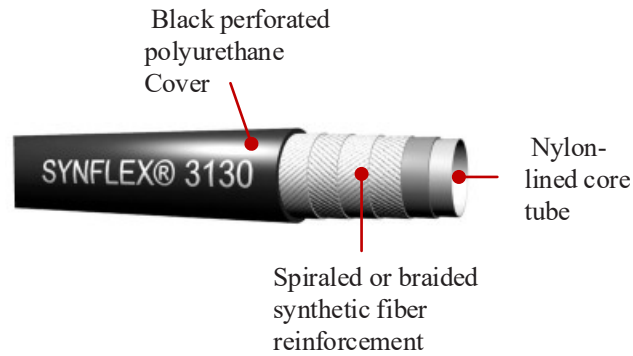
$$K_H = \frac{K_S A_u^2}{(K_S \tau_d (K_{c0} + A_u K_p K_{qU0}) - A_u^2)}. \quad (6.16)$$

6.3 SIZING AND SELECTION OF HIGH VOLUMETRIC EXPANSION HOSES

High volumetric expansion hoses (HVE) are special hoses characterized by their expansion capability, being more compliant than other kind of industrial hoses. This expansion capability is mainly related to the materials used for its construction, e.g. the hose EATON Synflex 3130 presented in Figure 6.8 has synthetic materials in every layer, allowing it to have greater volumetric expansion than metal braided hoses.

The supply pressure of Ybitú test rig is regulated to 70×10^5 Pa, which can be considered a low working pressure in a traditional hydraulic system. Considering this supply pressure, the range of possible HVE hoses for selection is relatively large.

Figure 6.8 – Constitutive layers of Synflex 3130 hoses provided by the manufacturer EATON.



Source: Adapted from Eaton (2008).

The supply pressure of Ybitú test rig is regulated to 70×10^5 Pa, which can be considered a low working pressure in a traditional hydraulic system. Considering this supply pressure, the range of possible HVE hoses for selection is relatively large.

6.3.1 Mathematical background for HVE hose sizing and selection

6.3.1.1 Hose diameter calculation

The hose diameter can be calculated based on the maximum flowrate (q_{\max}) expected inside the hydraulic system and a selected oil velocity inside the hose (v_{oil}) according to:

$$D_{\text{ho}} = \sqrt{4q_{v\max} / \pi v_{\text{oil}}} \quad (6.17)$$

The recommended mean velocity of the oil inside the line in hoses is within 2.1 to 4.6 m/s for pressure line and 0.6 to 1.2 m/s for the suction, return, and low pressure lines (RABIE, 2009). Hose manufacturers provide nomographs to simplify the selection of a commercial hose diameter (EATON, 2008; PARKER, 2012).

6.3.1.2 Hose length calculation

Given that $A_u = A_A = A_B$, the maximum and minimum values for the hydraulic stiffness (K_H) can be calculated from Equation (6.3), giving:

$$K_{H\max} = \frac{\beta_e A_u^2 (A_u L + 2V_{\text{ho}})}{V_{\text{ho}} (A_u L + V_{\text{ho}})} \Rightarrow \text{at } x_p = 0 \text{ or } x_p = L \quad (6.18)$$

and

$$K_{H\min} = \frac{4\beta_e A_u^2}{A_u L + 2V_{ho}} \Rightarrow \text{at } x_p = \frac{L}{2}, \quad (6.19)$$

where β_e is the effective bulk modulus, V_{ho} represents the volume of oil trapped in the hose coupled to each cylinder chamber, and L is the piston stroke. For simplification, henceforth Equation (6.19) will be used for the calculation of K_H . Following the use of a robust control technique, K_H can also be considered as an uncertain parameter that varies between two known limits.

Neglecting the presence of air in the system, the effective bulk modulus can be represented as:

$$\beta_e = \beta_0 \beta_{ho} / (\beta_0 + \beta_{ho}) = r_\beta \beta_0 \beta_{hoSS} / (\beta_0 + r_\beta \beta_{hoSS}), \quad (6.20)$$

where β_0 is the fluid bulk modulus and β_{ho} represents the dynamic bulk modulus of the hose. Hose bulk modulus have a different value during the system operation, i.e. dynamic hose bulk modulus (β_{ho}) is higher than static or steady state hose bulk modulus (β_{hoSS}) due an effect called dynamic hardening (JOHNSTON et al., 2010). Johnston et al. (2010) shows several experimental results for different kind of hoses and highlighted the fact that the dynamic hardening produces a ratio (r_β) between the dynamic bulk modulus and static bulk modulus of about 4 to 5 times for nylon braid hoses, which is the case of the HVE hoses analyzed in this thesis.

According to Johnston et al. (2010), the static hose bulk modulus (β_{hoSS}) can be expressed as:

$$\beta_{hoSS} = \left(1 + \frac{\Delta V_{ho}}{V_{0ho}} \right) \frac{dp}{d\left(\frac{\Delta V_{ho}}{V_{0ho}} \right)}, \quad (6.21)$$

where ΔV_{ho} represents the change in the hose volume, V_{0ho} is the initial volume of the hose, and p is the working pressure.

Equation (6.21) can be rewritten in order to calculate β_{hoSS} as a function of hose catalog data, yielding:

$$\beta_{hoSS} = \left(1 + \frac{\Delta V_{ho}}{V_{0ho}} \right) \frac{dp}{d\left(\frac{\Delta V_{ho}}{V_{0ho}} \right)} = \left(A_{ho} + \frac{\Delta V_{ho}}{L_{ho}} \right) \frac{dp}{d\left(\frac{\Delta V_{ho}}{L_{ho}} \right)}. \quad (6.22)$$

Based on the standard ISO 6801 (INTERNATIONAL ORGANIZATION FOR STANDARDIZATION, 1983), which is related to the procedure for determination the volumetric expansion of rubber or plastic hoses under hydrostatic pressure, it is possible to define the volumetric expansion (E), in a simplified way, as:

$$E = \frac{\Delta V_{ho}}{L_{ho}}, \tag{6.23}$$

where ΔV_{ho} represents the volumetric expansion of the hose and L_{ho} , the hose free length.

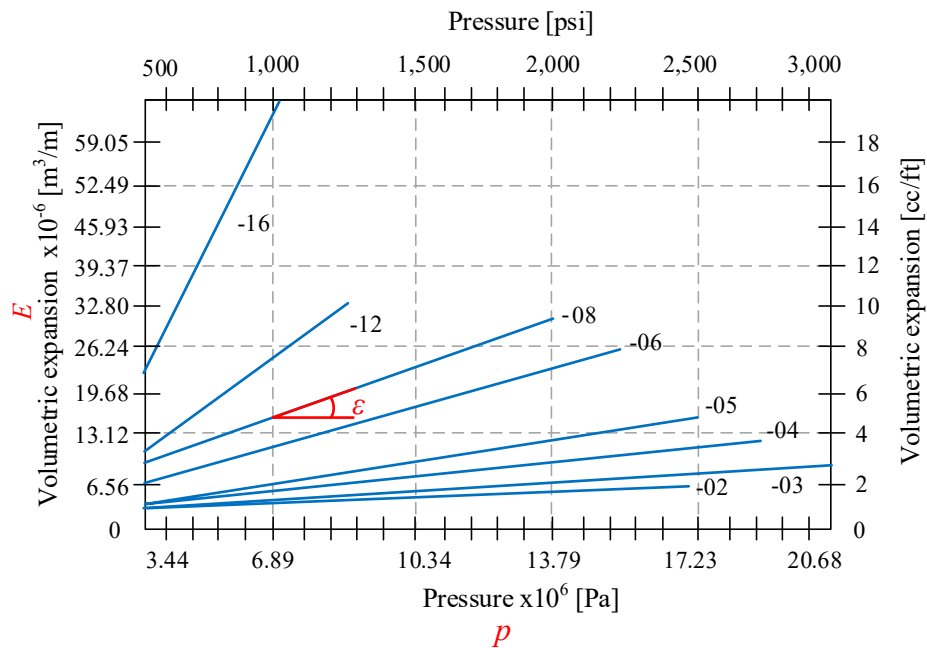
Substituting Equation (6.23) in Equation (6.22), gives:

$$\beta_{hoSS} = (A_{ho} + E) \frac{dp}{dE} = \frac{(A_{ho} + E)}{\varepsilon} = \frac{(\pi D_{ho}^2 + 4E)}{4\varepsilon}, \tag{6.24}$$

such that ε corresponds to the expansion slope of the hoses (dE/dp) and D_{ho} is the hose diameter.

E is a parameter determined at the working pressure (p) and ε can be assumed constant for a specific hose, corresponding to the slope of the straight lines in graphs of E versus p provided by manufacturers such as Eaton (EATON, 2008) (see Figure 6.9).

Figure 6.9 – Volumetric expansion data of Synflex 3130 hose model provided by the manufacturer EATON.



Source: Adapted from Eaton (2008).

Nevertheless, other manufacturers also present the volumetric expansion properties of their hoses as line equations, e.g. Parker manufacturer (PARKER, 2012). In the latter case, the values of E and ε can be easily extracted from the equations and no calculation nor approximation are required.

Combining equations (6.19), (6.20), and (6.24) yields:

$$L_{ho} = \frac{8A_u^2 r_\beta \beta_0 (\pi D_{ho}^2 + 4E)}{\pi D_{ho}^2 K_H (4\varepsilon \beta_0 + r_\beta (\pi D_{ho}^2 + 4E))} - \frac{2A_u L}{\pi D_{ho}^2}. \quad (6.25)$$

Equation (6.25) shows that to obtain smaller hydraulic stiffness K_H , longer hose L_{ho} is required. Furthermore, the greater the hose volumetric expansion, the lower the hose length to achieve the same hydraulic stiffness.

6.3.1.3 Hydraulic stiffness calculation based on hose length and diameter

If necessary, the process of hose selection using equation (6.16) and (6.25) can be iterative to avoid obtaining long hoses, which may not be suitable for implementation. For example, if a calculated hydraulic stiffness results in a long hose, the proportional gain can be decreased in (6.16), resulting in a higher K_H and smaller L_{ho} . Therefore, the final value of hydraulic stiffness is obtained from a trade-off between K_H , K_p , and L_{ho} .

By rewriting Equation (6.25) as:

$$K_H = \frac{8r_\beta \beta_0 A_u^2 (\pi D_{ho}^2 + 4E)}{(4\varepsilon \beta_0 + r_\beta (\pi D_{ho}^2 + 4E))(2A_u L + \pi D_{ho}^2 L_{ho})}. \quad (6.26)$$

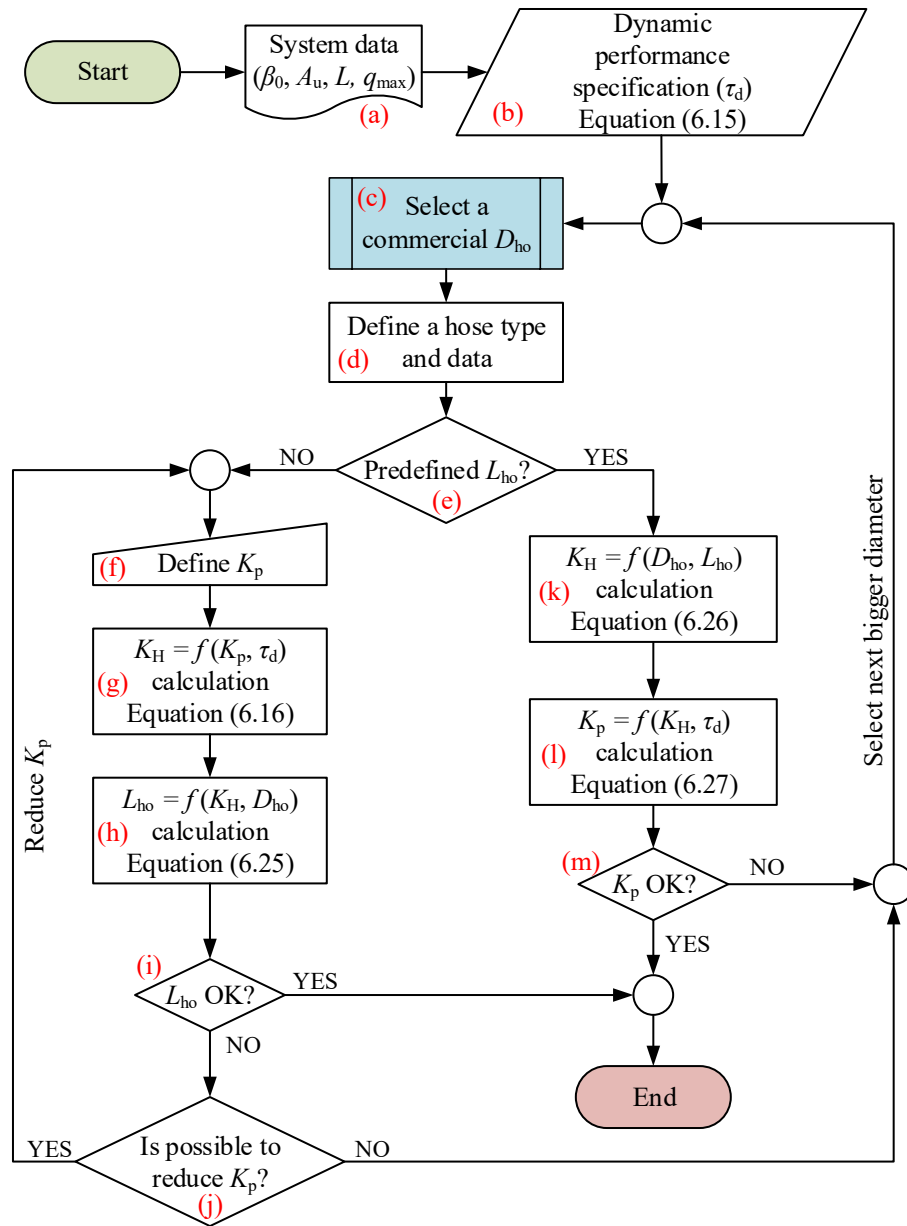
it is also possible to start the hose selection from a defined hose length. K_H can be calculated based on a pre-selected hose with the required D_{ho} (from (6.17)), and a desired L_{ho} . After that, the proportional gain to achieve the required closed loop response can be calculated by:

$$K_p = \frac{1}{K_{qU0}} \left(\frac{A_u (K_H + K_S)}{\tau_d K_H K_S} - \frac{K_{c0}}{A_u} \right). \quad (6.27)$$

6.3.2 High volumetric expansion hose selection flowchart

The procedure steps for sizing and select an HVE hose will be shown in Figure 6.10 and described below:

Figure 6.10 – High volumetric expansion hose sizing and selection flowchart.



Source: Personal collection.

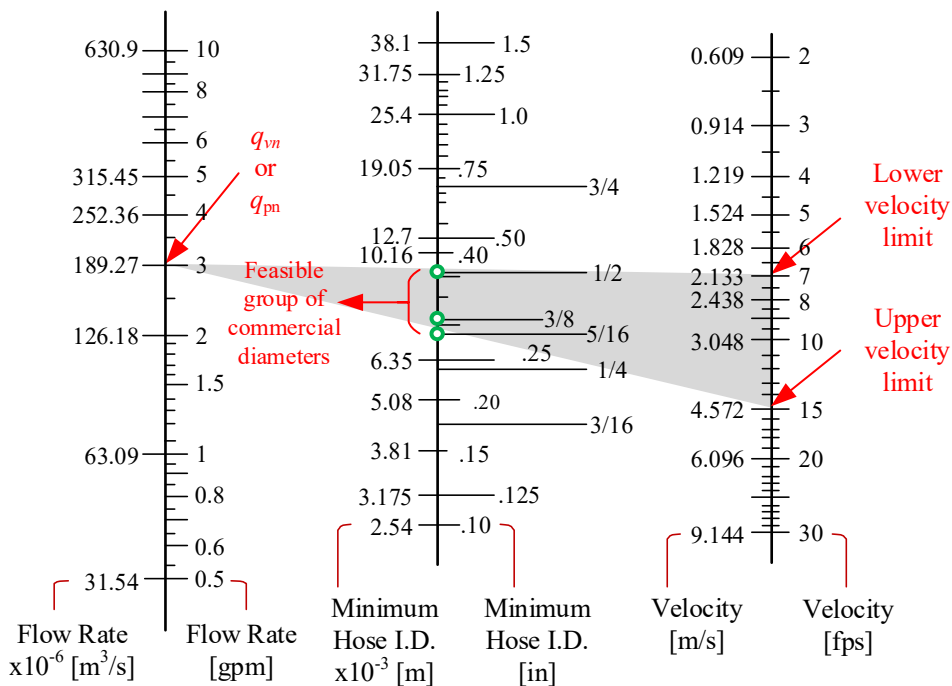
- (a) **System data.** It is related to the technical data of the cylinder (A_u, L), servovalve (K_{qU0}, K_{c0}, q_{vn}), power unit (q_{pn}), oil bulk modulus (β_0), and environment (K_S).
- (b) **Dynamic performance specification.** In this step, it is necessary to define a time constant (τ_d) considering that the hydraulic force control system behaves as a first order system according to Equation (6.15). Taken into account that the performance requirements are also used during the controller design process, it is possible to define an unique settling time (t_s) for both hose selection and

control design processes. The value of τ_d can be calculated from the value of t_s through the following relationship: $\tau_d = t_s / 4$ (OGATA, 2010).

(c) **Sizing and selection of commercial hose diameter.** This step is composed by internal substeps, which are described below:

- (c.1) *Next commercial D_{ho} required?* It is a decision block where the project designer decides if the next bigger commercial hose diameter is required or not.
- (c.2) *Define the acceptable v_{oil} range.* The literature recommends a mean oil velocity from 2.1 to 4.6 m/s (7 to 15 fps) for pressure lines (RABIE, 2009).
- (c.3) *Define the group of feasible commercial hose diameters.* This substep requires to consider the maximum flowrate that passes through the hydraulic system, which is defined as the minimum value between the nominal flowrate of the valve (q_{vn}) and the nominal flowrate of the pump (q_{pn}). After defining the flowrate inside the system, and the limits of the acceptable oil velocity for pressure lines (substep (c.2)), it is possible to define a region in a nomograph where a group of feasible commercial diameters can be determined (EATON, 2008; PARKER, 2012) (see example in Figure 6.11).

Figure 6.11 – Example of defining a feasible group of hose commercial diameters.

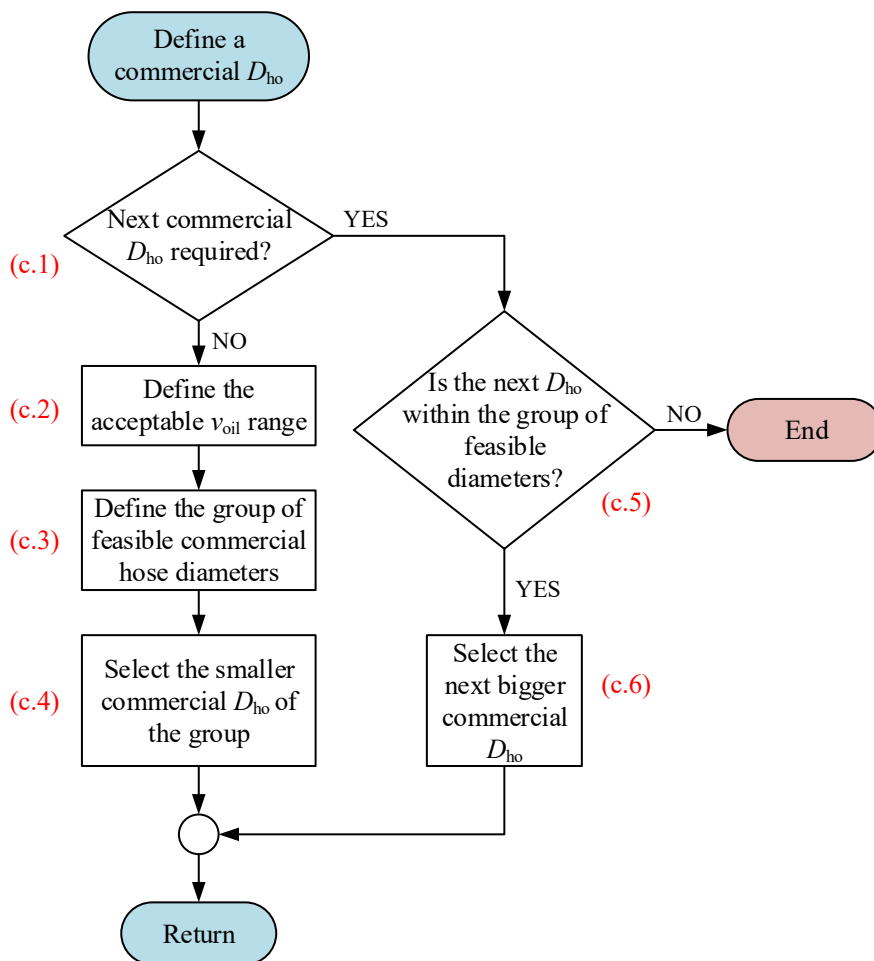


Source: Adapted from Eaton (2008).

- (c.4) *Select the smaller commercial D_{ho} of the group.* Based on the group of feasible hose diameters defined in Substep (c.3).
- (c.5) *Is the next D_{ho} within the group of feasible diameters?* In case of an affirmative answer, select the next bigger commercial diameter inside the group defined in Substep (c.3). Otherwise, the selection process ends here, which could imply that the HVE hoses of the selected brand (manufacturer) does not have the sufficient expansion capability or that the solution using HVE hoses indeed is not feasible.
- (c.6) *Select the next bigger commercial D_{ho} .* Based on the group of feasible hose diameters defined in Substep (c.3).

The flowchart that summarize the step (c) is shown in Figure 6.12.

Figure 6.12 – Internal description of the commercial hose diameter selection subprocess.



Source: Personal collection.

- (d) **Define a hose type and data.** This step is focused on defining the HVE hose model to be used in the system. Based on the manufacturers catalog, a hose model with the better volumetric expansion capability should be selected. The reason behind this recommendation is because greater volumetric expansion allows to increase the compliance of the system without requiring large hose lengths.
- (e) **Predefined L_{ho} ?** In some cases, physical restriction could limit the hose length within an admissible range. In that case, the procedure also permits two different possibilities or branches, which are explained below. Figure 6.10 shows two different possible ways to size and select the HVE hose required. The first way, or branch, tries to obtain a combination of K_H , K_p , and L_{ho} . On the other hand, the second way tries to obtain a combination of K_H , K_p , and D_{ho} . Both cases aim to achieve the performance specification defined at the beginning of the process selection.
- (f) **Define K_p .** Establish an initial value for this loop. A unitary value is recommended to initiate this iterative loop.
- (g) **K_H calculation.** Based on Equation (6.16).
- (h) **L_{ho} calculation.** Based on Equation (6.25).
- (i) **L_{ho} OK?** An affirmative answer finishes this process since the hose diameter and length seems to have a good dimension for future implementation in the system. Otherwise, it is necessary to advance to the next Step (j).
- (j) **Is possible to reduce K_p ?** A reduction in the value of K_p allows to have lower values of K_H and, consequently, it decreases the value of L_{ho} . The value of K_p can be continuously reduced until the value L_{ho} achieves practical values, i.e. the final hose length has a value such that allows it to be implemented without any problem in the system. However, too small values of K_p , e.g. $K_p < 1 \times 10^{-4}$, can lead to control problems during experimental implementation because the control signal sent to the valve can be too small or produce very conservative force responses. In case of the impossibility to reduce the value of K_p , it is necessary to select the next bigger diameter of the group of feasible commercial hose diameters.

- (k) **K_H calculation.** Based on Equation (6.26). In this case, the value of the hydraulic stiffness depends on the geometrical values of the hose (D_{ho} and L_{ho}).
- (l) **K_p calculation.** Based on Equation (6.27).
- (m) **K_p OK?** This decision block is almost similar to the decision block of Step (j). However, in this case K_p is considered acceptable if its value is not extremely small, in which case could be difficult for practical implementation.

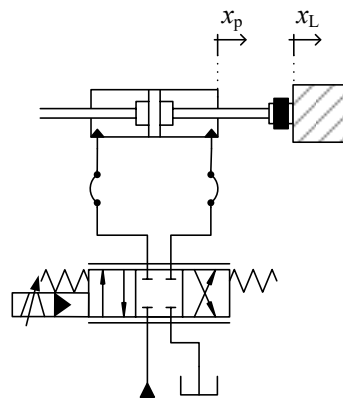
6.4 SIZING HVE HOSES AND DESIGNING A QFT-BASED CONTROLLER FOR PHEA: CASE OF STUDY

6.4.1 High volumetric expansion hose selection

Based on the Figure 6.10, the following example shows the applicability of the sizing and selection of HVE hose procedure proposed in this thesis. This case study considers a Pure Hydro-Elastic Actuator (PHEA) project, as shown in Figure 6.13.

A settling time ($t_{s1\%} = 200$ ms) is defined as a dynamic performance requirement for this study case. This selection of the settling time was based on the analysis of several other researches related to the force control in hydraulic actuators where the settling time used for their experiments varies from 100 ms to 800 ms, and the force reference varies from 500 N to 4000 N (NIKSEFAT AND SEPEHRI, 1999; ALLEYNE AND LIU, 2000; AHN, K. K. et al., 2008; SIVASELVAN et al., 2008; YANG et al., 2008; NAKKARAT AND KUNTANAPREEDA, 2009; KARPENKO AND SEPEHRI, 2012).

Figure 6.13 – Hydraulic circuit considered for the case of study of a PHEA.



Source: Personal collection.

Considering the settling time of 200 ms, the time constant value τ_d should have a value of 50 ms, based on the Step (b) at the sizing flowchart described in Subsection 6.3.2. All the system parameters are shown in Table A.1 (see Appendix A).

The maximum flowrate inside the hydraulic system is determined by the minimum value between the nominal flowrate of the pump and the valve. According to the Table A.1, the flowrate through the system comes defined by the pump ($q_{pn} = 1.6 \times 10^{-4} \text{ m}^3/\text{s}$) since it is smaller than the nominal flowrate of the valve ($q_{vn} = 6.31 \times 10^{-4} \text{ m}^3/\text{s}$).

After determining that the group of feasible commercial hose diameters at the nomograph, which includes hoses with gauge diameter of 5/16", 3/8", 1/2", it is possible to continue with the next step.

Two different brands of hose manufacturers were analyzed (EATON, 2008; PARKER, 2012). Specifically, the models PARKER Parflex® 510C/518C and EATON Synflex ® 3130 have the best volumetric expansion capabilities in each brand. It is important to highlight that the pressure supply used in this thesis was $7 \times 10^6 \text{ Pa}$ (70 bar), and since it is considered low pressure for hydraulic systems, the hose models selected for this analysis can effectively support that pressure.

A commercial hose diameter of 12.7 mm (1/2 in) was selected after a few iterations. Analyzing HVE hose catalogues, the EATON Synflex ® 3130-08 was selected, because it has more volumetric expansion capability than the PARKER Parflex® 510C-8/518C-8. The hose volumetric expansion value extracted from the catalog is $1.56 \times 10^{-5} \text{ m}^3/\text{m}$ at $7 \times 10^6 \text{ Pa}$ (4.7 cc/ft at 1000 psi), resulting in a static bulk modulus (β_{hoSS}) of $6.36 \times 10^7 \text{ Pa}$. Based on (JOHNSTON et al., 2010), a r_β value equal to 5 was considered since the selected hose is nylon braided.

As discussed in Subsection 6.3.2, the system performance can be achieved through a trade-off between K_H , K_p , and L_{ho} . Table 6.2 shows an example of an iteration considering the first branch (left side) of the HVE hose selection flowchart described in Subsection 6.3.2.

Due to its special features, this type of expandable hose is very difficult to obtain in small quantities in the domestic market. A small piece of 3 m of the required hose was found and purchased for the experiments, and in order to obtain the maximum benefit from that piece of hose, a L_{ho} equal to 1.5 m was specified as a constraint. Therefore, the second branch of the HVE hose selection flowchart was used. Using (6.26) and (6.27), the resulting K_H was $2.24 \times 10^6 \text{ N/m}$ and K_p , 2.7×10^{-4} .

Table 6.2 – Combinations of K_p , K_H , and L_{ho} to obtain the required dynamic performance assuming the HVE hose model EATON Synflex ® 3130-08.

K_p	K_H [N/m] using (6.16)	L_{ho} [m] using (6.25)
0.01	5.65×10^4	180
0.001	5.76×10^5	14.84
0.0005	1.175×10^6	5.66
0.00025	2.46×10^6	1.07

Source: Personal collection.

6.4.2 QFT-based controller design for PHEA

The objective of the QFT-based control design is to synthesize a prefilter ($F(s)$) and a controller ($G(s)$) such that the force responses of the system always fall within a predefined time-domain tolerance described by upper and lower limits (HOROWITZ, 1988; HOUPIS AND RASMUSSEN, 1999; YANIV, 1999; HOUPIS, 2002). For this case of study, the controller design was carried out using the QFT frequency domain control design toolbox for use with Matlab (BORGHESANI et al., 2003). For more information, Appendix A presents the fundamentals of the QFT methodology.

The upper and lower limits were defined as:

- Upper limit ($B_U(t)$): settling time ($t_{S1\%}$) of 0.1 s and maximum overshoot of 1%.
- Lower limit ($B_L(t)$): settling time ($t_{S1\%}$) of 0.3 s without overshoot.

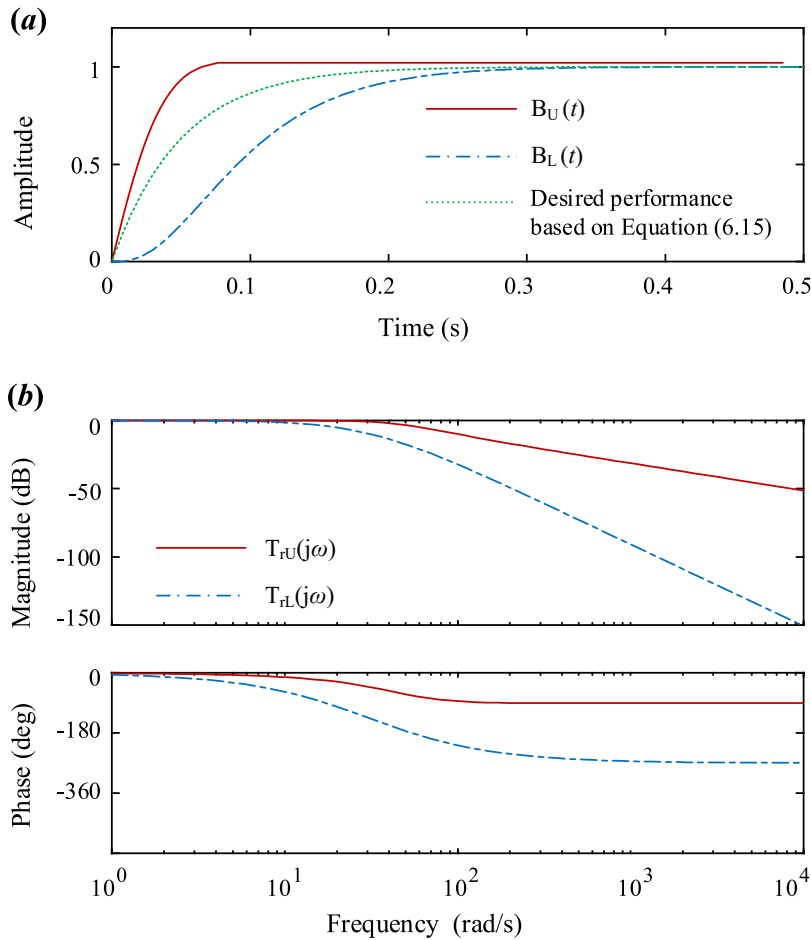
Translating the specifications from the time domain to the frequency domain yields:

$$B_U(s) = \left(\frac{2116}{s^2 + 73.6s + 2116} \right) \left(\frac{s + 75}{75} \right), \quad (6.28)$$

$$B_L(s) = \left(\frac{400}{s^2 + 40s + 400} \right) \left(\frac{50}{s + 50} \right). \quad (6.29)$$

The addition of a zero and a pole in equations (6.28) and (6.29), respectively, relax the requirements for the controller design in the frequency domain without affecting the responses in time domain (Figure 6.14).

Figure 6.14 – Upper and lower limits of performance specifications described in (a) time-domain and, posteriorly translated to, (b) frequency-domain.



Source: Personal collection.

Table 6.3 shows the parametric uncertainties assumed in the plant model described by Equation (6.7). To define the uncertainties, the following considerations were assumed:

- f_v varies from a minimum value related to the Coulomb friction to a maximum value representing the stiction, which were obtained experimentally;
- the range of parametric uncertainty for K_{qU} was calculated using Equation (4.21), assuming no load ($p_L=0$) and the operating point at the maximum power ($p_L=2p_S/3$). On the other hand, the nominal value was obtained based on the results of Section 5.3;
- the range for K_c was calculated using Equation (4.22). The nominal value was obtained based on the results of the internal leakage measurement test according to

ISO 10770-1 (see Chapter 5) (INTERNATIONAL ORGANIZATION FOR STANDARDIZATION, 2009);

- K_H varies from the minimum to maximum hydraulic stiffness calculated by equations (6.18) and (6.19),
- Finally, a $\pm 20\%$ variation around the nominal values extracted from catalog is assumed for ω_{nv} and ξ_v .

Table 6.3 – Parameter uncertainties of the plant.

Parameter	Units	Nominal value	Range
f_v	[Ns/m]	100	100 to 3×10^4
K_{qU}	[m ³ /(s·V)]	5.4×10^{-5}	3.23×10^{-5} to 5.61×10^{-5}
K_c	[m ³ /(s·Pa)]	6.42×10^{-13}	6.42×10^{-13} to 7×10^{-11}
K_H	[N/m]	2.24×10^6	2.24×10^6 to 4.11×10^6
ω_{nv}	[rad/s]	1099	879 to 1319
ξ_v	-	0.9	0.72 to 1.08

Source: Personal collection.

The other parameter values used for the controller design were shown in Table A.1 (see Appendix A), with exception of K_s that was changed in order to represent the equivalent stiffness instead of just the load cell characteristic. Based on measurement of the environment deflection, the resulting K_s was 2×10^7 N/m.

For the QFT boundary generation, robust stability, disturbance rejection and reference tracking criteria are considered in this study (see Chapter 3).

The robust stability bounds are defined through (HOUPIS AND RASMUSSEN, 1999):

$$|T_1(j\omega)| = \left| \frac{P(j\omega)G(j\omega)}{1+P(j\omega)G(j\omega)} \right| = \left| \frac{L(j\omega)}{1+L(j\omega)} \right| \leq \delta_1(\omega) = 1.3, \quad \omega \in \Omega_1, \quad (6.30)$$

where $P(j\omega)$ represents the plant, $G(j\omega)$ represents the controller, $L(j\omega)$ is known as the loop transmission function, and $\delta_1(\omega)$ is a constant constraint calculated assuming a gain margin of 5 dB. The set of frequencies of interest Ω_1 is [0.01, 0.1, 1, 5, 10, 50, 100, 150] rad/s.

For the disturbance rejection bounds, the constraint function $\delta_2(\omega)$ represents the disturbance control ratio:

$$|T_2(j\omega)| = \left| \frac{Y(j\omega)}{D(j\omega)} \right| = \left| \frac{1}{1+L(j\omega)} \right| \leq \delta_2(\omega) = \frac{j\omega}{j\omega+15}, \quad \omega \in \Omega_2, \quad (6.31)$$

where $Y(j\omega)$ represents the output, $D(j\omega)$ is the disturbance signal, and the set of frequencies for analysis is Ω_2 is [0.01, 0.1, 1, 5, 10] rad/s.

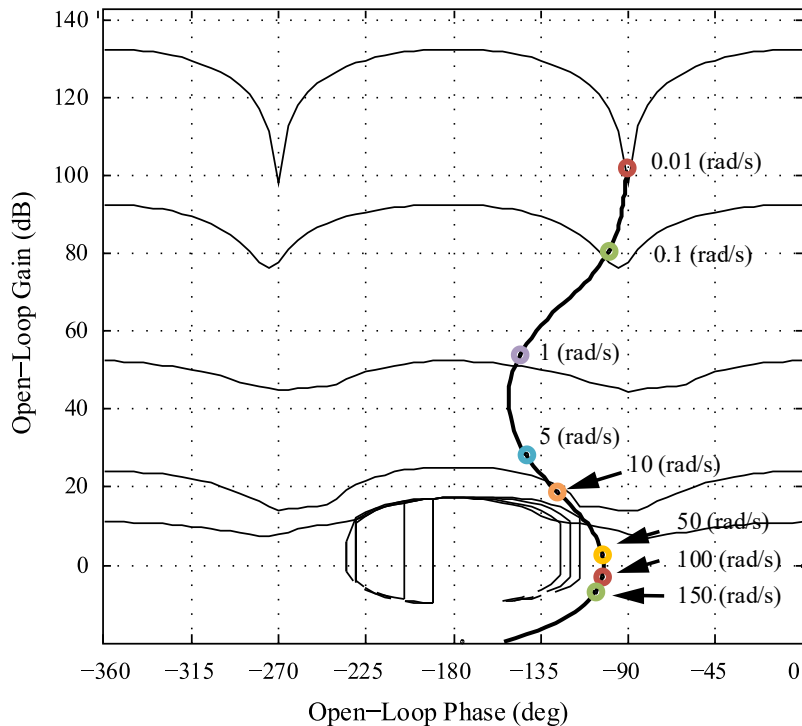
Finally, the reference tracking bounds are defined as:

$$\delta_{5\text{inf}}(\omega) \leq |T_5(j\omega)| = \left| \frac{Y(j\omega)}{R(j\omega)} \right| = \left| F(j\omega) \frac{L(j\omega)}{1+L(j\omega)} \right| \leq \delta_{5\text{sup}}(\omega), \quad \omega \in \Omega_5, \quad (6.32)$$

where $R(j\omega)$ is related to the reference signal, and the constraint functions $\delta_{5\text{sup}}(\omega)$ and $\delta_{5\text{inf}}(\omega)$ are the transfer functions $B_U(s)$ and $B_L(s)$ defined in equations (6.28) and (6.29), respectively. The set of frequencies of interest is Ω_5 is [0.01, 0.1, 1, 5, 10, 50, 100, 150] rad/s.

After the bound generation and intersection, the loop shaping process was carried out in order to obtain the controller function (see Figure 6.15) (HOUPIS AND RASMUSSEN, 1999).

Figure 6.15 – Loop shaping of the QFT-based controller.



Source: Personal collection.

The resulting controller is:

$$G_1(s) = (0.001s + 0.008) / s \quad (6.33)$$

The synthesis of the prefilter is similar to that of the controller, resulting on:

$$F_1(s) = 910 / (s^2 + 83s + 910) \quad (6.34)$$

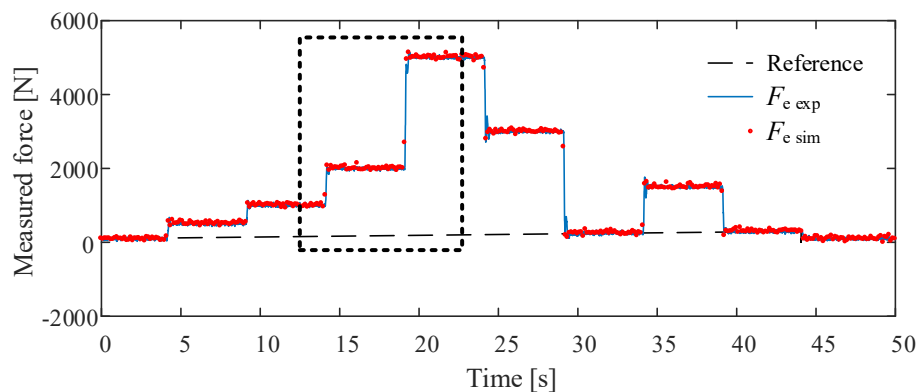
The hydraulic force control system, including the prefilter and controller, was implemented in Simulink.

6.5 SIMULATION AND EXPERIMENTAL RESULT ANALYSIS

Experimental tests and simulations were carried out using the selected HVE hose according to Section 6.3 and using the Ybitú test rig. A force tracking reference were defined as several force steps of different magnitudes (see Figure 6.16). In order to show that the model used for simulation has a good matching with the experimental results, an enlarged plot can be observed in Figure 6.17.

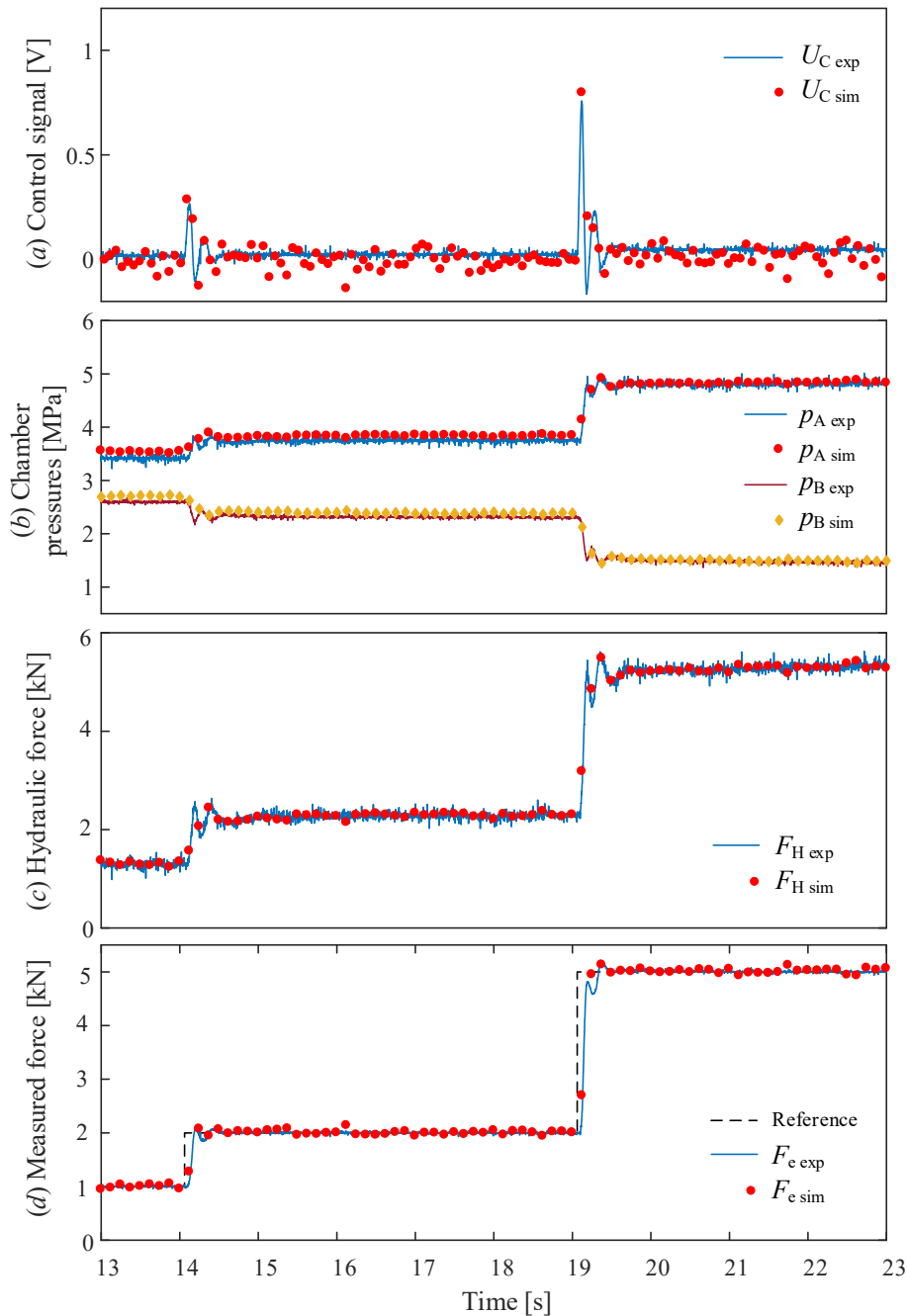
The hydraulic force (F_H), chamber pressures (p_A and p_B), and the control signal sent to the valve (U_C) also demonstrate the good representativeness of the nonlinear dynamic model. In both simulation and experiment, the QFT-based prefilter and controller were used. The systems parameters are those presented in the Chapter 4.

Figure 6.16 – Comparison between experimental and simulation force tracking responses based on a step force references using HVE hoses.



Source: Personal collection.

Figure 6.17 – Enlarged plot of the region marked in Figure 6.16, including: (a) control signal sent to the valve, (b) chamber pressures, (c) hydraulic force, and (d) measured force in the same range of time.



Source: Personal collection.

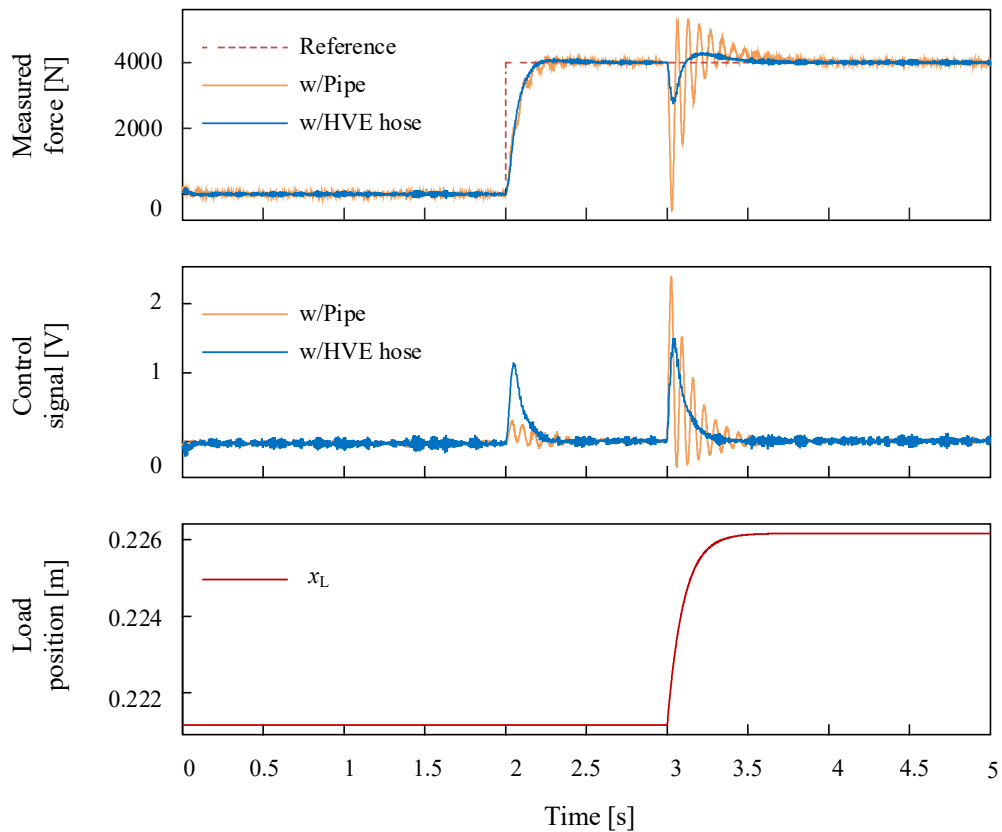
The advantages of using HVE hoses for adding compliance to the system for improving the force control performance can be observed when comparing with the system using rigid pipes.

The controller $G_2(s)$ and prefilter $F_2(s)$ were designed for the case when rigid pipes are used. An industrial steel pipe was considered for this case, with an inner diameter of $10,5 \times 10^{-3}$

m and an outer diameter of 16×10^{-3} m. Similar pipes with lengths of 0,35 m were considered between the valve and the cylinder.

Figure 6.18 shows the system force simulation responses using pipes and hoses. A 4 kN step reference force was applied at 2 s. The disturbance input was a filtered step, in order to reproduce a load movement disturbance, with 5 mm of magnitude at 3 s.

Figure 6.18 – Comparison between force responses using pipes or HVE hoses.



Source: Personal collection.

Therefore, assuming the same performance specifications applied to the system with hoses, but using pipes instead, the resultant controller and prefilter functions are:

$$G_2(s) = (0.0005s + 0.002) / s, \quad (6.35)$$

and

$$F_2(s) = 484 / (s^2 + 44s + 484) \quad (6.36)$$

The step response using rigid pipes was more oscillatory compared with the system with HVE hoses. The resulting overshoots were 3.87% and 2.15% and settling times ($t_{s1\%}$) equal to 0.33 s and 0.20 s, respectively. The settling time of the system with hoses is between the time domain specifications presented in Section 6.4, however the overshoot is higher than 1%. The system with pipes was not able to achieve strictly the specifications using the designed QFT controller. It is important to notice that the QFT controller was designed based on the linear model considering the parameter uncertainties. Therefore, some deviation from the specifications can be expected.

The main drawback on a force control system is the disturbance rejection. As can be seen in Figure 6.18, by reducing hydraulic stiffness through the use of HVE hoses, the output impedance is decreased, such that the load displacement causes small changes in the applied force. The control signal has higher amplitude and is more oscillatory when using pipes as expected since there is not a hydraulic or mechanical compliant element.

6.6 CHAPTER CONCLUSIONS

This chapter introduced the PHEA, which is a type of actuator whose hydraulic stiffness is purposely modified using high volumetric expansion hoses specially selected for force control applications. A set of equations is provided for sizing HVE hoses, considering the desired value of hydraulic stiffness, which in turn is aligned with the dynamic performance requirements.

A flowchart is presented to show the procedure for selecting commercial hoses focusing on force control applications. After applying the hose selection procedure in a case study performed in LASHIP, the experimental and simulation results demonstrate the applicability of the proposed procedure.

7 DISCUSSION AND CONCLUSIONS

Compliance, in a force control system, can be actively or passively added, and the focus of this thesis was the addition of purely hydraulic passive compliance. This is because it reduces the control effort and simplifies practical implementation. In addition, the linear hydraulic actuation system length is reduced compared to, for example, the Hydraulic Series Elastic Actuator (SEA) proposed by Robinson (2000) or any other type of SEA systems where there is an addition of a spring in series with the actuator.

A detailed mathematical analysis was carried out in order to demonstrate either through mathematical equations and experiments that it is possible to have a controlled reduction of the output impedance of a hydraulic actuator using hydraulic compliant components. Nonlinear mathematical models were developed, as well as linear models, of the hydraulic system. The focus of this thesis was to determine the mathematical background for the sizing procedure, establish it, and test it. Within the innovative mathematical equations presented in the thesis, it is possible to highlight the equation that models the behavior of the total leakage flowrate (q_{vinT}) within the valve (Equation(4.14)), as well as the simplified linear model, which results from the decomposition of the complete linear model of a hydraulic system (Equation (6.12)). With this decomposed model, it becomes simple to identify which of the internal dynamics of the system has the greater effect on the overall dynamic behavior of a hydraulic force control system. In addition, the hose sizing equations, proposed in Chapter 6, integrate force control performance requirements, as well as intrinsic hydraulic characteristics such as valve coefficients, hose sizes and volumetric expansion capabilities, and cylinder area and stroke, resulting in an innovative way of sizing specific HVE hoses to be applied in hydraulic force control systems.

In Chapter 6, it is also possible to see how the hose bulk modulus affects the system dynamics and increases the compliance of the system. From the mathematical analysis was found that the hose bulk modulus is directly proportional to the sectional area of the hose (A_{ho}), the volumetric expansion (E), which represents the amount of oil that can be accumulated during a hose expansion (ΔV_{ho}) per unit of hose length (L_{ho}), and the volumetric expansion slope (ϵ) (Equation (6.24)). Both of them are physical and intrinsic characteristics of the selected hose. Therefore, the hose bulk modulus value is affected by the sectional area of the hose and its mechanical characteristics, affecting the effective bulk modulus (Equation (6.20)) and, in consequence, modifying the hydraulic stiffness (Equation (6.19)). Equation (6.26) summarizes

the impact of the hose on the hydraulics stiffness of the system. As the area and length of the hose is larger, the lower the stiffness and the greater the added compliance of the system will be.

The applicability of HVE hoses was demonstrated during the experiments, obtaining promising force response behaviors. The performance requirements were achieved based on the HVE hose selection procedure and the QFT technique proposed and used in this thesis. The disturbances rejection capability also was analyzed considering a pipe line and an HVE hose line. The force responses show the advantage of using HVE hoses instead of pipes.

Nonlinear models were used to perform the simulations and, on the other hand, the linear models helped to design the QFT-based controllers. Since the compliance of the hydraulic system was increased due to the use of HVE hoses, it was possible to design a linear and robust controller capable of controlling a nonlinear system.

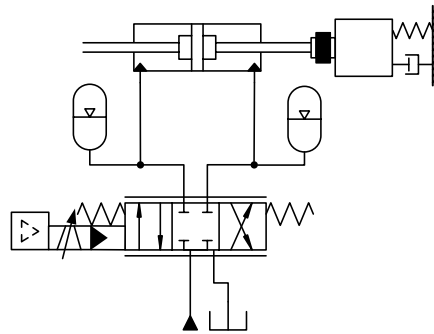
Regarding the control technique used in this thesis, the QFT was selected due to the parametric uncertainties of the hydraulic system. The QFT technique takes into account the possibility of including parametric uncertainty ranges during the controller design stage, as well as the inclusion of stability, disturbance rejection and reference tracking constraints. Therefore, the end result obtained is a tailor-made controller with a low order structure with constant gains that can meet the performance requirements defined by the designer. From the experimental results presented, it is clear that the controller designed by the proposed technique can well meet the desired performance requirements.

A gap in the scientific literature was identified during the elaboration of this thesis. It was related to the lack of a specific analysis of the use of hydraulic passive compliant components in force control systems. From the results obtained and shown in Chapter 6, it can be concluded that this gap can be considered filled.

7.1 FUTURE WORKS

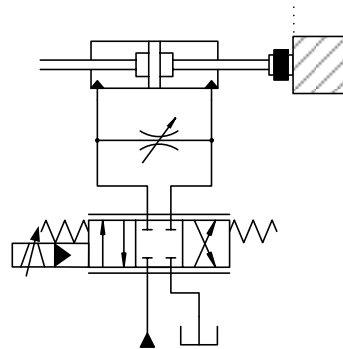
There are still several fields within the hydraulic force control systems to be explored as a product of this thesis. Considering the case of passive hydraulic compliant components, for example, it is possible to add other types of capacitive components such as accumulators (see Figure 7.1), but dissipative hydraulic components such as a flow control valve between chambers can also be used as they can also modify the output impedance of the actuation system (see Figure 7.2).

Figure 7.1 – Hydraulic force control system using accumulators.



Source: Adapted from Ledezma et al. (2018).

Figure 7.2 – Hydraulic force control system using a flow control valve between chambers.



Source: Adapted from Ledezma et al. (2018)

Both of the examples shown above can be considered as two different versions of PHEA, and the researches would be directed towards establishing the procedure for sizing both components.

Considering a dynamic modification of compliance, several new kinds of hydraulic components could be proposed such as variable accumulators, special flow control valves, new type of actuators with special rod or piston characteristics, among others, resulting in a Hydraulic Actuator with Variable Impedance (HAVI). It could be a really interesting research that would allow for much more advanced force control capabilities that could change according with the type of load or environment where the force will be applied.

Undoubtedly, there is still much to be explored in this line of research and the present thesis aims to collaborate and becomes a bibliographic reference basis for future researches.

REFERÊNCIAS

AHN, K. K. et al. Development of Hydraulic Load Simulator for Force Control with High Precision. In: 7th JFPS International Symposium on Fluid Power, 2008, Toyama, Japan. Japan: JFPS, 2008. p.189-194.

AHN, K. K. et al. Online self-tuning fuzzy porportional-integral-derivative control for hydraulic load simulator. **Proceedings of the Institution of Mechanical Engineers, Part I: Journal of Systems and Control Engineering**, v. 222, n. 2, p. 81-95, Mar. 2008. ISSN 0959-6518.

ALEXANDER, R. M. Three uses for springs in legged locomotion. **The International Journal of Robotics Research**, v. 9, n. 2, p. 53-61, 1990. ISSN 0278-3649.

ALLEYNE, A.; LIU, R. On the limitations of force tracking control for hydraulic servosystems. **Journal of Dynamic Systems, Measurement, and Control**, v. 121, n. 2, p. 184-190, June 1999. ISSN 0022-0434.

_____. A simplified approach to force control for electro-hydraulic systems. **Control Engineering Practice**, v. 8, n. 12, p. 1347-1356, Dec. 2000. ISSN 0967-0661.

ARMSTRONG-HÉLOUVRY, B.; DUPONT, P.; DE WIT, C. C. A survey of models, analysis tools and compensation methods for the control of machines with friction. **Automatica**, v. 30, n. 7, p. 1083-1138, 1994. ISSN 0005-1098.

BAILEY, F. N.; HUI, C.-H. A Fast Algorithm for Computing Parametric Rational Functions. **IEEE Transactions on Automatic Control**, v. 34, n. 11, p. 1209-1212, 1989. ISSN 0018-9286.

BARAHANOV, N.; ORTEGA, R. Necessary and sufficient conditions for passivity of the LuGre friction model. **IEEE Transactions on Automatic Control**, v. 45, n. 4, p. 830-832, 2000. ISSN 0018-9286.

BOAVENTURA, T. **Hydraulic Compliance Control of the Quadruped Robot HyQ**. 2013. 154 p. Ph.D. dissertation (Doctor of Philosophy). Dept. ADVR, University of Genova, Genova, Italy.

BOAVENTURA, T. et al. On the role of load motion compensation in high-performance force control. In: IEEE/RSJ International Conference on Intelligent Robots and Systems, 2012, Algarve, Portugal. **Proceedings...** 2012. p.4066-4071.

BORGHESANI, C.; CHAIT, Y.; YANIV, O. **The QFT Frequency Domain Control Design Toolbox: For use with Matlab**. Terasoft. California, USA, p.148. 2003

BUERGUER, S. P. **Stable, High-Force, Low-Impedance Robotic Actuators for Human-Interactive Machines**. 2005. 359 p. Doctoral Thesis (Doctor of Philosophy). Department of Mechanical Engineering, Massachusetts Institute of Technology, Cambridge, Massachusetts, USA.

CANUDAS DE WIT, C. et al. A new model for control of systems with friction. **IEEE Transactions on Automatic Control**, v. 40, n. 3, p. 419-425, 1995. ISSN 0018-9286.

COLGATE, J. E. **The control of dynamically interacting systems**. 1988. 299 pp. p. Doctoral Thesis (Doctor of Philosophy in Mechanical Engineering). Department of Mechanical Engineering, Massachusetts Institute of Technology, Cambridge, MA, USA.

CHEW, C.-M.; HONG, G.-S.; ZHOU, W. **Series damper actuator: a novel force/torque control actuator**. 4th IEEE/RAS International Conference on Humanoid Robots. Santa Monica, CA, USA: IEEE. 2: 533-546 p. 2004.

D'AZZO, J. J.; HOUPIS, H. C.; SHELDON, S. N. **Linear Control System Analysis and Design with Matlab**. Fifth Edition. USA: Marcel Dekker, 2003. 822 p. ISBN 0-8247-4038-6.

DAHL, P. R. **A solid friction model**. Air Force Systems Command. Los Angeles, LA, USA: May. 1968. (SAMSO-TR-77-131)

DE SCHUTTER, J. **A study of active compliant motion control methods for rigid manipulators based on a generic scheme**. IEEE International Conference on Robotics and Automation. Raleigh, North Carolina, USA: IEEE. 4: 1060-1065 p. 1987.

DÍAZ, J. M.; DORMIDO, S.; ARANDA, J. **QFT Robust Control Design by Interactive Approach**. 44th IEEE Conference on Decision and Control. Seville, Spain: IEEE. 44: 1301-1306 p. 2005.

DÍAZ, J. M.; DORMIDO, S.; ARANDA, J. **TIG: Generador interactivo de plantillas - Manual del Usuario**. Universidad Nacional de Educación a Distancia. Madrid, España. 2006

DÍAZ, J. M. et al. **Interactive Generation of Plant Templates for Robust Control**. American Control Conference. New York City, USA: IEEE: 212-217 p. 2007.

DIMIG, J. et al. Effective force testing: A method of seismic simulation for structural testing. **Journal of Structural Engineering**, v. 125, n. 9, p. 1028-1037, Sept. 1999. ISSN 0733-9445.

DREW, J. E.; LONGMORE, D. K.; JOHNSTON, D. N. Measurement of the longitudinal transmission characteristics of fluid-filled hoses. **Proceedings of the Institution of Mechanical Engineers, Part I: Journal of Systems and Control Engineering**, v. 211, n. 3, p. 219-228, 1997. ISSN 0959-6518.

_____. Theoretical analysis of pressure and flow ripple in flexible hoses containing tuners. **Proceedings of the Institution of Mechanical Engineers, Part I: Journal of Systems and Control Engineering**, v. 212, n. 6, p. 405-422, 1998. ISSN 0959-6518.

DYKE, S. J. et al. Role of control-structure interaction in protective system design. **Journal of Engineering Mechanics**, v. 121, n. 2, p. 322-338, 1995. ISSN 0733-9399.

EATON. **Synflex Hose and Fittings Master Catalog**. Hydraulic Hose Catalogue. EATON CO. Germany 2008.

ENTWISTLE, K. M. The behaviour of braided hydraulic hose reinforced with steel wires. **International Journal of Mechanical Sciences**, v. 23, n. 4, p. 229-241, 1981. ISSN 0020-7403.

ENTWISTLE, K. M.; WHITE, G. J. A method for achieving effective load transfer between the inner and outer layers of a two-layer braided high-pressure hydraulic hose. **International Journal of Mechanical Sciences**, v. 19, n. 4, p. 193-201, 1977. ISSN 0020-7403.

EPPINGER, S. D.; SEERING, W. P. **Understanding bandwidth limitations in robot force control**. IEEE International Conference on Robotics and Automation. Raleigh, North Carolina, USA: IEEE. 4: 904-909 p. 1987.

ERYILMAZ, B.; WILSON, B. H. **Modeling the internal leakage of hydraulic servovalves**. International Mechanical Engineering Congress and Exposition: ASME. 69: 337-343 p. 2000.

FEKI, M.; RICHARD, E. Including leakage flow in the servovalve static model. **International Journal of Modelling and Simulation**, v. 25, n. 1, p. 51-56, 2005. ISSN 0228-6203.

FOCCHI, M. **Strategies to improve the impedance control performance of a quadruped robot**. 2013. 172 p. Doctoral Thesis (Doctor of Philosophy). Department of Advanced Robotics, Università di Genova / Istituto Italiano di Tecnologia, Genova, Italy.

FOX, J. A. **Hydraulic analysis of unsteady flow in pipe networks**. England: The MacMillan Press, 1977. 216 p. ISBN 978-1-349-02792-7.

GARCÍA-SANZ, M. Control Robusto Cuantitativo QFT: Historia de una Idea. **Revista Iberoamericana de Automática e Informática Industrial**, v. 2, n. 3, p. 25-38, 2005. ISSN 1697-7912.

_____. Quantitative Robust Control Engineering: Theory and Applications. **Achieving Successful Robust Integrated Control System Designs for 21st Century Military Applications – Part II**, Neuilly-sur-Seine, France: RTO/NATO, 2006, p. 1-1 - 1-44

GARCÍA-SANZ, M.; HOUPIS, C. H. Quantitative feedback theory. In memoriam of Isaac Horowitz. **International Journal of Robust and Nonlinear Control**, v. 17, n. 2-3, p. 91-94, 2007.

HAM, R. V. et al. Compliant actuator designs. **IEEE Robotics & Automation Magazine**, v. 16, n. 3, p. 81-94, 2009. ISSN 1070-9932.

HOGAN, N. Impedance Control: An Approach to Manipulation: Part I - Theory. **Journal of Dynamic Systems, Measurement, and Control**, v. 107, n. 1, p. 1-7, 1985a.

_____. Impedance Control: An Approach to Manipulation: Part II - Implementation. **Journal of Dynamic Systems, Measurement, and Control**, v. 107, n. 1, p. 8-16, 1985b.

_____. Impedance Control: An Approach to Manipulation: Part III - Applications. **Journal of Dynamic Systems, Measurement, and Control**, v. 107, n. 1, p. 17-24, 1985c.

HOGAN, N.; BUERGUER, S. P. Impedance and Interaction Control. In: KURFESS, T. R. (Ed.). **Robotics and Automation Handbook**. United States of America: CRC Press, 2005. cap. 19, p.1-24.

HÖLCKE, J. **Frequency response of hydraulic hoses**. 2002. 88 p. Licentiate Thesis (Mechanical Engineer). Department of Machine Design, Royal Institute of Technology, KTH, Stockholm, Sweden.

HOROWITZ, I. M. **Quantitative Feedback Theory (QFT)**. American Control Conference. Atlanta, GA, USA: IEEE: 2032-2037 p. 1988.

_____. Survey of quantitative feedback theory (QFT). **International Journal of Robust and Nonlinear Control**, v. 11, n. 10, p. 887 - 921, 2001.

HOUPIS, C. H. Horowitz: bridging the gap. **International Journal of Robust and Nonlinear Control**, v. 12, n. 4, p. 295-302, 2002.

HOUPIS, C. H.; PACHTER, M. Application of QFT to Control System Design - An Outline for Engineers. **International Journal of Robust and Nonlinear Control**, v. 7, n. 6, p. 515-531, 1997. ISSN 1049-8923.

HOUPIS, C. H.; RASMUSSEN, S. J. **Quantitative Feedback Theory: Fundamentals and Applications**. USA: Marcel Dekker, 1999. 408 p. ISBN 0-8247-7872-3.

HURST, J. W.; RIZZI, A. A.; HOBBELEN, D. Series elastic actuation: Potential and pitfalls. In: 7th International Conference on Climbing and Walking Robots and the Support Technologies for Mobile Machines, 2004, Madrid, Spain. **Proceedings...** 2004.

INTERNATIONAL ORGANIZATION FOR STANDARDIZATION. ISO 6801. Rubber or plastics hoses - Determination of volumetric expansion. Switzerland: ISO, 1983.

_____. ISO 10770-1. Hydraulic fluid power — Electrically modulated hydraulic control valves — Part 1: Test methods for four-port directional flow-control valves. Switzerland: International Organization for Standardization, 2009.

IYER, S. **Modeling and testing of a series elastic actuator with controllable damping**. 2012. 99 p. Master Thesis (Master of Science in Mechanical Engineering). Department of Mechanical Engineering, Worcester Polytechnic Institute, Worcester, MA, USA.

JAFARI, A.; TSAGARAKIS, N. G.; CALDWELL, D. G. A novel intrinsically energy efficient actuator with adjustable stiffness (AwAS). **IEEE/ASME Transactions on Mechatronics**, v. 18, n. 1, p. 355-365, 2013. ISSN 1083-4435.

JOHNSTON, D. N. A time-domain model of axial wave propagation in liquid-filled flexible hoses. **Proceedings of the Institution of Mechanical Engineers, Part I: Journal of Systems and Control Engineering**, v. 220, n. 7, p. 517-530, Nov. 2006. ISSN 0959-6518.

JOHNSTON, D. N.; WAY, T. M.; CONE, K. M. Measured Dynamic Properties of Flexible Hoses. **Journal of Vibration and Acoustics**, v. 132, n. 2, p. 021011-1 - 021011-8, Mar. 2010. ISSN 0739-3717.

JOHNSTON, N. The transmission line method for modelling laminar flow of liquid in pipelines. **Proceedings of the Institution of Mechanical Engineers, Part I: Journal of Systems and Control Engineering**, v. 226, n. 5, p. 586-597, 2012. ISSN 0959-6518.

KARNOPP, D. C.; MARGOLIS, D. L.; ROSENBERG, R. C. **System Dynamics: Modeling, Simulation, and Control of Mechatronic Systems**. Fifth Edition. New Jersey, USA: John Wiley & Sons, 2012. 636 pp. p. ISBN 978-0-470-88908-4.

KARPENKO, M.; SEPEHRI, N. Electrohydraulic force control design of a hardware-in-the-loop load emulator using a nonlinear QFT technique. **Control Engineering Practice**, v. 20, n. 6, p. 598-609, June 2012. ISSN 09670661.

LAMMING, C. P. G.; PLUMMER, A. R.; HILLIS, A. J. Analysis of Robust Electrohydraulic Force Control. In: 7th IFK, 2010, Aachen, Germany. Germany: Apprimus, 2010. p.1-12.

LAMPAERT, V.; SWEVERS, J.; AL-BENDER, F. **Experimental comparison of different friction models for accurate low-velocity tracking**. Mediterranean Conference on Control and Automation 2002.

LAWRENCE, D. A. **Actuator limitations on achievable manipulator impedance**. IEEE International Conference on Robotics and Automation. Scottsdale, AZ, USA: IEEE: 560-565 p. 1989.

LEDEZMA, J. A.; DE NEGRI, V. J.; BARASUOL, V. **Interaction Analysis Between a Hydraulic Load Simulator and a Pneumatic Positioning System**. ASME/BATH Symposium on Fluid Power and Motion Control: American Society of Mechanical Engineers: V001T01A077-V001T01A077 p. 2017.

LEDEZMA, J. A.; DE NEGRI, V. J.; DE PIERI, E. R. New approach for hydraulic force control based on hydraulic compliance. In: International Conference on Fluid Power and Mechatronics (FPM), 2015: IEEE, 2015. p.454-459.

LEDEZMA, J. A.; DE PIERI, E. R.; DE NEGRI, V. J. Force control of hydraulic actuators using additional hydraulic compliance. **Strojniški vestnik - Journal of Mechanical Engineering**, v. 64, n. 10, p. 579-589, September 2018. ISSN 0039-2480.

LEE, Y.-F. et al. A Humanoid Robotic Wrist With Two-Dimensional Series Elastic Actuation for Accurate Force/Torque Interaction. **IEEE/ASME Transactions on Mechatronics**, v. 21, n. 3, p. 1315-1325, June 2016. ISSN 1083-4435.

LI, W. **Design and development of magneto-rheological actuators with application in mobile robotics**. 2014. 108 p. Master Thesis (Master of Engineering Science). The School of Graduate and Postdoctoral Studies, University of Western Ontario, London, Ontario, Canada.

LOSEY, D. P. et al. A Time Domain Approach to Control of Series Elastic Actuators: Adaptive Torque and Passivity-Based Impedance Control. **IEEE/ASME Transactions on Mechatronics**, v. 21, n. 4, p. 2085-2096, Aug. 2016. ISSN 1083-4435.

MARÉ, J.-C.; ATTAR, B. Enhanced model of four way valves characteristics and its validation at low temperature. **International Journal of Fluid Power**, v. 9, n. 3, p. 35-43, 2008. ISSN 1439-9776.

MARTÍN-ROMERO, J. J.; GIL-MARTÍNEZ, M.; GARCÍA-SANZ, M. **Analytical formulation to compute QFT templates for plants with a high number of uncertain parameters**. Mediterranean Conference on Control and Automation. Athens, Greece: IEEE: 1-6 p. 2007.

MASON, M. T. Compliance and force control for computer controlled manipulators. **IEEE Transactions on Systems, Man, and Cybernetics**, v. 11, n. 6, p. 418-432, 1981. ISSN 0018-9472.

MERRIT, H. E. **Hydraulic Control Systems**. USA: John Wiley & Sons, 1967. 358 p.

MOOG. **Electrohydraulic Valves... A Technical Look**. MOOG Industrial Controls Division. East Aurora, NY, USA, p.1-24. 2001. (CDL6566)

_____. **.760 Series - Servovalves - ISO 10372 Size 04**. MOOG. East Aurora, NY, USA. 2007. (CDL6335 Rev G 500-213 807)

NAKKARAT, P.; KUNTANAPREEDA, S. Observer-based backstepping force control of an electrohydraulic actuator. **Control Engineering Practice**, v. 17, n. 8, p. 895-902, Aug. 2009. ISSN 0967-0661.

NIKSEFAT, N.; SEPEHRI, N. **Robust force controller design for an electrohydraulic actuator based on nonlinear model**. IEEE International Conference on Robotics and Automation Detroit, MI, USA: IEEE. 1: 200-206 p. 1999.

_____. Designing Robust Force Control of Hydraulic Actuators Despite System and Environmental Uncertainties. **IEEE Control Systems Magazine**: IEEE, v. 21, n. 2, Apr. 2001, p. 66-77

NISE, N. S. **Control Systems Engineering**. Sixth Edition. USA: John Wiley & Sons, 2011. 926 p. ISBN 978-0470-54756-4.

OGATA, K. **Modern Control Engineering**. Fifth Edition. USA: Prentice-Hall, 2010. 894 p. ISBN 978-0-13-615673-4.

PAINE, N.; SENTIS, L. **A new prismatic series elastic actuator with compact size and high performance**. IEEE International Conference on Robotics and Biomimetics (ROBIO). Guangzhou, China: IEEE: 1759-1766 p. 2012.

PARKER. **Parflex® Thermoplastic & Fluoropolymer Products - Hose, Tubing, Fittings & Accessories**. PARKER HANNIFIN CORP. Ravenna, OH, USA 2012.

PAYNTER, H. M. **Analysis and design of engineering systems : class notes for M.I.T. course 1.751**. Cambridge, MA, USA: M.I.T. Press, 1961. 347 pp. p.

PEREIRA, P. I. I. **Theoretical and experimental analysis controllers for hydraulic systems (in portuguese)**. 2006. 163 p. M. S. thesis (M. Sc. in Mechanical Engineering). Postgraduate Prog. in Mech. Eng., Fed. Univ. Santa Catarina, Brazil.

PEREIRA, P. I. I.; GUENTHER, R.; DE NEGRI, V. J. Tracking control in hydraulic actuators using slow proportional directional valves. In: MIYAGI, P. E.; HORIKAWA, O., *et al* (Ed.). **ABCM Symposium Series in Mechatronics**. Brazil: ABCM, v.3, 2008. p.66-75.

PERONDI, E. A. **Controle Não-Linear em Cascata de um Servoposicionador Pneumático com Compensação do Atrito**. 2002. 196 pp. p. Tese de Doutorado (Doutor em Engenharia Mecânica). Programa de Pós-Graduação em Engenharia Mecânica, Universidade Federal de Santa Catarina, Florianópolis, SC, Brasil.

PETERSEN, N. R. **Loading assembly having a soft actuator**. United States of America: MTS Systems Corporation 2002.

PLUMMER, A. R. Robust electrohydraulic force control. **Proceedings of the Institution of Mechanical Engineers, Part I: Journal of Systems and Control Engineering**, v. 221, n. 4, p. 717-731, June 2007. ISSN 0959-6518.

PRATT, G. A. et al. Stiffness isn't everything. In: KHATIB, O. and SALISBURY, J. K. (Ed.). **Experimental Robotics IV**. Berlin, Germany: Springer, v.223, 1997. p.253-262. ISBN 978-3-540-76133-4.

RABIE, M. G. **Fluid Power Engineering**. USA: McGraw-Hill, 2009. 420 p. ISBN 978-0-07-162606-4.

ROBINSON, D. W. **Design and Analysis of Series Elasticity in Closed-loop Actuator Force Control**. 2000. 123 p. Ph.D. dissertation (Doctor of Philosophy in Mechanical Engineering). Dept. Mech. Eng., Massachusetts Institute of Technology, Massachusetts, USA.

ROBINSON, D. W.; PRATT, G. A. **Force Controllable Hydro-Elastic Actuator**. IEEE International Conference on Robotics and Automation. San Francisco, CA, USA: IEEE. 2: 1321-1327 p. 2000.

SANADA, K. et al. A finite element model of hydraulic pipelines using an optimized interlacing grid system. **Proceedings of the Institution of Mechanical Engineers, Part I: Journal of Systems and Control Engineering**, v. 207, n. 4, p. 213-222, 1993. ISSN 0959-6518.

SERAJI, H.; COLBAUGH, R. Force Tracking in Impedance Control. In: IEEE International Conference on Robotics and Automation, 1993, Atlanta, GA, USA. IEEE, 1993. p.499 - 506.

SHIELD, C. K.; FRENCH, C. W.; TIMM, J. Development and implementation of the effective force testing method for seismic simulation of large-scale structures. **Philosophical Transactions of The Royal Society A**, v. 359, n. 1786, p. 1911 - 1929, Sept. 2001.

SIDI, M. **Design of Robust Control Systems: From Classical to Modern Practical Approaches**. Malabar, FL, USA: Krieger Publishing Company, 2001. 504 pp. p. ISBN 1-57524-143-9.

SIVASELVAN, M. V. et al. Dynamic force control with hydraulic actuators using added compliance and displacement compensation. **Earthquake Engineering & Structural Dynamics**, v. 37, n. 15, p. 1785-1800, July 2008. ISSN 1096-9845.

SOUMELIDIS, M. I. et al. **A comparative study of modelling techniques for laminar flow transients in hydraulic pipelines**. Proceedings of the JFPS International Symposium on Fluid Power: The Japan Fluid Power System Society. 2005: 100-105 p. 2005.

STRINGER, J. D. **Hydraulic systems analysis: an introduction**. First Edition. London, England: The MacMillan Press Ltd., 1976. 185 p. ISBN 978-2-349-02599-2.

SZPAK, R.; RAMOS FILHO, J. R. B.; DE NEGRI, V. J. Theoretical and experimental study of the matching between proportional valves and symmetric and asymmetric cylinders. In: 7th IFK, 2010, Aachen, Germany. Germany: Apprimus, 2010. p.155-166.

TAYLOR, S. E. M. **Development of numerical models for hydraulic pipelines and flexible hoses**. 1998. Doctoral Thesis (PhD in Engineering). University of Bath

THAYER, W. J. **Specification Standards for electrohydraulic flow control servovalves**. MOOG. New York, USA, p.24. 1962

TOTTEN, G. E.; DE NEGRI, V. J. **Handbook of Hydraulic Fluid Technology**. Second Edition. United States: CRC, 2012. 944 p. ISBN 978-1-4200-8527-3.

TRAN, X. B.; HAFIZAH, N.; YANADA, H. Modeling of dynamic friction behaviors of hydraulic cylinders. **Mechatronics**, v. 22, n. 1, p. 65-75, 2012. ISSN 0957-4158.

TSAGARAKIS, N. G.; SARDELLITTI, I.; CALDWELL, D. G. **A new variable stiffness actuator (CompAct-VSA): Design and modelling**. IEEE/RSJ International Conference on Intelligent Robots and Systems (IROS). San Francisco, CA, USA: IEEE: 378-383 p. 2011.

VALDIERO, A. C. **Controle de Robôs Hidráulicos com Compensação de Atrito**. 2005. 177 pp. p. Tese de Doutorado (Doutor em Engenharia Mecânica). Programa de Pós-Graduação em Engenharia Mecânica, Universidade Federal de Santa Catarina, Florianópolis, SC, Brasil.

VANDEBORGHT, B. et al. Comparison of Mechanical Design and Energy Consumption of Adaptable, Passive-compliant Actuators. **The International Journal of Robotics Research**, v. 28, n. 1, p. 90-103, 2009. ISSN 0278-3649.

VON LISINGEN, I. **Fundamentals of Hydraulic Systems (in portuguese)**. 4th. Florianópolis, SC, Brazil: UFSC, 2013. 399 p. ISBN 85-328-00646-8.

VUKOBRATOVIĆ, M.; TUNESKI, A. Contact control concepts in manipulation robotics-an overview. **IEEE Transactions on Industrial Electronics**, v. 41, n. 1, p. 12-24, 1994. ISSN 0278-0046.

WATTON, J. **Fundamentals of Fluid Power Control**. USA: Cambridge University, 2009. 494 p. ISBN 978-0-511-60436-2.

WATTON, J.; TADMORI, M. J. A comparison of techniques for the analysis of transmission line dynamics in electrohydraulic control systems. **Applied mathematical modelling**, v. 12, n. 5, p. 457-466, 1988. ISSN 0307-904X.

WAY, T. M. **The use of hoses and hose inserts to reduce pressure ripple in hydraulic circuits**. 2004. 320 p. Doctoral thesis (PhD in Engineering). University of Bath, Bath, United Kingdom.

WELLS, D. L. et al. **An investigation of hydraulic actuator performance trade-offs using a generic model**. IEEE International Conference on Robotics and Automation. Cincinnati, OH, USA: IEEE: 2168-2173 p. 1990.

WHITNEY, D. **Historical perspective and state of the art in robot force control**. IEEE International Conference on Robotics and Automation. Missouri, USA: IEEE. 2: 262-268 p. 1985.

WILLIAMSON, M. M. **Series Elastic Actuators**. 1995. 83 p. M.S. thesis (Master of Science). Dept. Elect. Eng. and Comput. Sci., Massachusetts Institute of Technology, Massachusetts, USA.

WYLIE, E. B.; STREETER, V. L. **Fluid transients**. United States of America: McGraw-Hill, 1978. 384 p. ISBN 0-07-072187-4.

XU, Y. **Modelling and control of a high performance electro-hydraulic test bench**. 2013. 249 p. PhD Thesis (PhD of Science). Département Méthodes pour l'Ingénierie des Systèmes, University of Lyon, Lyon, France.

XU, Y.; HOLLERBACH, J. M.; MA, D. A Nonlinear PD Controller for Force and Control Transient Control. **IEEE Control Systems Magazine**, v. 15, n. 1, p. 15-21, Feb. 1995. ISSN 1066-033X.

YANADA, H.; SEKIKAWA, Y. Modeling of dynamic behaviors of friction. **Mechatronics**, v. 18, n. 7, p. 330-339, September 2008.

YANG, H.; XU, Y.; SUN, W. **New strategy of nonlinear PD controller for hydraulic force system under large variation of load stiffness**. IEEE/ASME International Conference on Advanced Intelligent Mechatronics. Xi'an, China: IEEE: 699-703 p. 2008.

YANG, J.-S.; LEVINE, W. S. Specification of Control Systems. In: LEVINE, W. S. (Ed.). **The Control Handbook**. Mumbai, India: Jaico (CRC & IEEE), v.1, 1999. cap. 10, p.158 - 169. ISBN 81-7224-785-0.

YANIV, O. **Quantitative feedback design of linear and nonlinear control systems**. USA: Kluwer Academic Publishers, 1999. 369 pp. p. ISBN 0-7923-8529-2.

ZOPPI, M. **Method for adapting stiffness in a variable stiffness actuator.** United States of America: Molfino, Rezia

Bo, Han

Zoppi, Matteo. GE2011A000096: 9 p. 2013.

APPENDICES

A TECHNICAL DATA OF HYDRAULIC COMPONENTS USED FOR EXPERIMENTAL TESTS

Table A.1 – Nominal parameters values of the components used for experimental tests based on manufacturer's catalog data.

(continue)

Hydraulic components	
Component	Description
Hydraulic power unit	Model: BOSCH – REXROTH ABMUP-10-20A AZPF005 N BKPV200 NMN $q_{pn} = 1.6 \times 10^{-4} \text{ m}^3/\text{s}$ (9.8 L/min)
Double rod and double acting cylinder	Model: BOSCH – REXROTH CGT3 MS2 50/22-500/Z1X/B1 $D_p = 0.05 \text{ m}$ $D_r = 0.022 \text{ m}$ $L = 0.5 \text{ m}$ $M_t = 13.1 \text{ kg}$
4/3 closed center servovalve	Model: MOOG 760 C263-A $q_{vn} = 6.31 \times 10^{-4} \text{ m}^3/\text{s}$ at $7 \times 10^6 \text{ Pa}$ (10 gpm at 1000 psi) $q_{vin} = 2.52 \times 10^{-5} \text{ m}^3/\text{s}$ to $3.84 \times 10^{-5} \text{ m}^3/\text{s}$ at $2.068 \times 10^7 \text{ Pa}$ (0.4 gpm to 0.61 gpm at 3000 psi) of pilot pressure or operating pressure $q_{tare} = 1.64 \times 10^{-7} \text{ m}^3/\text{s}$ at $2.068 \times 10^7 \text{ Pa}$ (0.26 gpm at 3000 psi) of pilot pressure or operating pressure $\omega_{nv} = 1099 \text{ rad/s}$ at $\pm 40\%$ (175 Hz at $\pm 40\%$) of opening valve $\zeta_v = 0.9$ at $\pm 40\%$ of opening valve
High volumetric expansion hose	Model: EATON Synflex ® 3130–08 $D_{ho} = 1.27 \times 10^{-2} \text{ m}$ (0.5 in) $L_{ho} = 1.5 \text{ m}$ $\varepsilon = 2.236 \times 10^{-12} \text{ m}^3/(\text{m} \cdot \text{Pa})$ (0.0047 cc/(ft·psi))

Sensors

Component	Description
Load cell	Model: HBM 1-U2AD1-1t Maximum capacity: 1000 Kg Maximum deflection at max. load: $< 1 \times 10^{-4}$ m Sensitivity: 2mV/V Hysteresis error: $< \pm 0.05\%$
Linear position transducer	Model: BALLUFF MICROPULSE BTL5-A11-M0500-P-S32 Measuring span: 0.5 m Repeatability: $< 2 \times 10^{-6}$ m (2 μ m) Hysteresis: 4×10^{-6} m (4 μ m)
Absolute pressure transducer	Model: HBM P8AP-200 Measuring span: 2×10^7 Pa (200 bar) Sensitivity: 2mV/V $\pm 2\%$ Repeatability: $\pm 0.1\%$
Positive displacement flowmeters	Model: WEBTEC LT5 Flow range: 1.67×10^{-6} m ³ /s – 8.33×10^{-5} m ³ /s (0.1 lpm – 5 lpm) Accuracy: $\pm 1\%$ of full scale Repeatability: $\pm 0.2\%$ Model: WEBTEC CT60 Flow range: 5×10^{-7} m ³ /s – 1×10^{-3} m ³ /s (3 lpm – 60 lpm) Accuracy: $\pm 1\%$ of indicating range Repeatability: $\pm 0.2\%$
Temperature sensors	Sensor type: Thermocouple “T” Temperature range: -200 °C to 200 °C Accuracy: ± 1 °C or $\pm 0.75\%$ (whichever is greater)

(conclusion)

Data acquisition, amplifier and conversion systems

Component	Description
Data Acquisition system	Model: dSPACE DS1103 with CLP1103 Connector panel Channels: 16 multiplexed channels ADC converter: Resolution: 16-bits I/O Voltage: $\pm 10\text{V}$ with $\pm 5\text{mV}$ of offset error
Measuring Amplifier System	Model: HBM MGCPlus with AB22A display and control panel Amplifier modules: ML801B multichannel amplifiers with AP809 and AP810i connectors I/O module: ML78B multichannel with AP809 and AP78 connectors
Signal converter module	Model: MOOG Z123-507 020 Signal conversion: from $\pm 10\text{V}$ to $\pm 20\text{mA}$ and vice versa

Source: Catalogues of the manufacturers.